

Colloids and Surfaces A: Physicochemical and Engineering Aspects

The zeta potential of quartz. Surface complexation modelling to elucidate high salinity measurements

--Manuscript Draft--

Manuscript Number:	COLSUA-D-22-01501R1
Article Type:	Research Paper
Keywords:	Zeta potential; Quartz; streaming potential; high salinity; shear plane location
Corresponding Author:	Philippe Leroy FRANCE
First Author:	Philippe Leroy
Order of Authors:	Philippe Leroy Alexis Mainault Shuai Li Jan Vinogradov
Abstract:	<p>The zeta potential is a measurable electrical potential of paramount importance to understand the electrochemical properties of rocks. However, the zeta potential remains poorly understood because it takes place at the nanoscale of the electrical double layer on the mineral surface. Streaming potential measurements on quartz-rich Fontainebleau and Lochaline sandstones carried out at high salinity (above 0.1 M NaCl) yield surprisingly high zeta potential values, which cannot be correctly reproduced by a traditional surface complexation model considering that the shear plane is located at the beginning of the diffuse layer. We found that placing the shear plane, where the zeta potential is defined, slightly closer to the mineral surface than the Stern plane significantly improves the predictions of the zeta potential and surface charge density of quartz at high salinity as well as the values of the equilibrium constant describing sodium adsorption in the Stern layer and Stern layer capacitance. Therefore, there may be a non-zero flow of water and counter-ions within the Stern layer of quartz in contact with NaCl solution. Our results have strong implications for the modelling of the electrochemical properties of minerals in contact with highly saline solutions.</p>

[Click here to view linked References](#)

1 **The zeta potential of quartz.**
2 **Surface complexation modelling to elucidate high salinity measurements**

3

4 Philippe Leroy¹, Shuai Li², Alexis Maineult³, and Jan Vinogradov⁴

5 ¹ BRGM, French Geological Survey, 45100 Orléans, France.

6 ² Hubei Subsurface Multi-scale Imaging Key Laboratory, Institute of Geophysics and Geomatics,
7 China University of Geosciences, Wuhan 430074, China.

8 ³ Sorbonne Université, CNRS, EPHE, UMR 7619 METIS, 75005 Paris, France.

9 ⁴ School of Engineering, University of Aberdeen, AB24 3UE, Aberdeen, United Kingdom.

10

11 Corresponding author: Dr. Philippe Leroy (p.leroy@brgm.fr)

12

13

14

15

16

17 *Intended for publication in Colloids and Surfaces A: Physicochemical and Engineering Aspects*

18 **Abstract**

19 The zeta potential is a measureable electrical potential of paramount importance to understand the
20 electrochemical properties of rocks. However, the zeta potential remains poorly understood
21 because it takes place at the nanoscale of the electrical double layer on the mineral surface.
22 Streaming potential measurements on quartz-rich Fontainebleau and Lochaline sandstones carried
23 out at high salinity (above 0.1 M NaCl) yield surprisingly high zeta potential values, which cannot
24 be correctly reproduced by a traditional surface complexation model considering that the shear
25 plane is located at the beginning of the diffuse layer. We found that placing the shear plane, where
26 the zeta potential is defined, slightly closer to the mineral surface than the Stern plane significantly
27 improves the predictions of the zeta potential and surface charge density of quartz at high salinity
28 as well as the values of the equilibrium constant describing sodium adsorption in the Stern layer
29 and Stern layer capacitance. Therefore, they may be a non-zero flow of water and counter-ions
30 within the Stern layer of quartz in contact with NaCl solution. Our results have strong implications
31 for the modelling of the electrochemical properties of minerals in contact with highly saline
32 solutions.

33

34 Key words: zeta potential, quartz, streaming potential, high salinity, shear plane location

35 **1. Introduction**

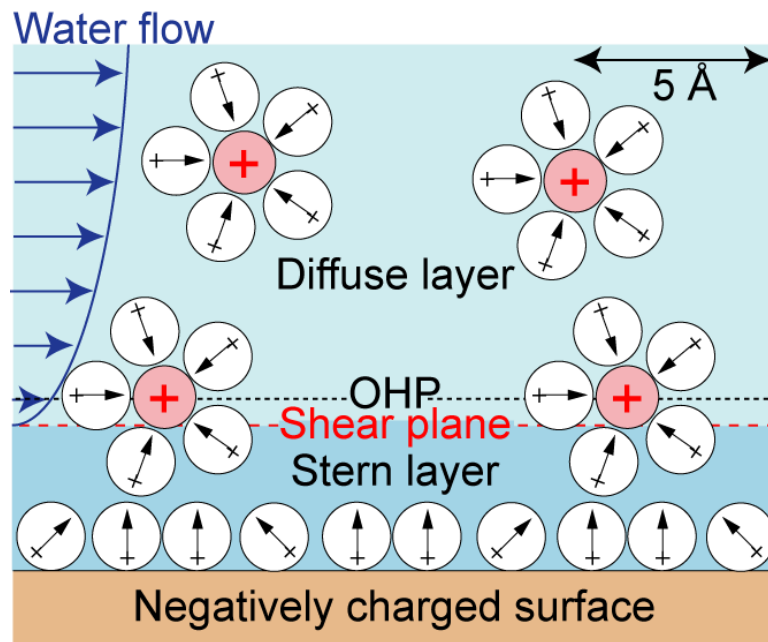
36 Quartz is a mineral that is particularly interesting to study because of its natural abundance and
37 usefulness in the development of new technologies [1]. In contact with water, quartz develops a
38 surface charge attracting counter-ions and repelling co-ions, thus forming the so-called electrical
39 double layer (EDL), usually represented by a “compact” Stern layer and a diffuse layer [2, 3].
40 Investigating the electrochemical properties of quartz is of great interest in many applications in
41 physics, chemistry and Earth sciences because these properties control adsorption and
42 dissolution/precipitation reactions, and wettability on the quartz surface [4-6]. The EDL of quartz
43 is also the source of electrokinetic and geophysical electrical (e.g., self-potential, resistivity,
44 induced polarization) measurements that are used to map for instance geological fluid flows or
45 biogeochemical reactions [7-12]. Studying quartz electrochemical properties, notably when quartz
46 is in contact with highly saline brines, has a high potential in many geo-environmental and
47 engineering applications including geo-sequestration of CO₂ in deep saline aquifers and enhanced
48 hydrocarbon recovery [13-16].

49 Exploring the electrochemical properties of quartz is very challenging because of their nanoscopic
50 nature [1, 17, 18]. Indeed, surface complexation reactions between surface sites and ions in the
51 aqueous solution occur at the nm-scale [3, 19-21]. In addition, natural quartz has a low specific
52 surface area (typically below 0.1 m² g⁻¹), which considerably complicates the direct experimental
53 characterization of its EDL compared to minerals with a large specific surface area such as
54 montmorillonite [2, 3, 22, 23]. Only few methods exist to probe the properties of the EDL on the
55 surface of minerals in contact with brines. Among them, there is the streaming potential method,
56 which implies application of a water pressure difference across the sample while measuring the
57 resulting voltage, the streaming potential, due to the displaced excess counter-ions in the EDL [24-

58 29]. From the measured streaming potential it is possible to obtain some relevant information on
59 the electrochemical properties of minerals through the calculation of the electrokinetic zeta
60 potential (ζ), which is defined as the electrical potential at the shear (or slip) plane [24, 26]. The
61 zeta potential determined experimentally can be interpreted in terms of mineral electrochemical
62 properties by matching observed and simulated zeta potential using a relevant surface complexation
63 model [20, 29, 30]. However, this approach relies on the assumption that the exact location of the
64 shear plane from the mineral surface is known, which is obviously not the case because of the lack
65 of experimental information at the molecular level [31-34]. Moreover, the zeta potential is, most
66 of the times, the only physico-chemical quantity available to validate the predictions of electrostatic
67 surface complexation models for low specific surface area minerals such as quartz or calcite [3, 29,
68 35]. In addition, the zeta potential is inferred from electro-hydrodynamic measurements while
69 surface complexation models rely on electrostatics at thermodynamic equilibrium [24, 34, 36, 37].
70 Therefore, these limitations contribute to additional uncertainties when investigating mineral
71 electrochemical properties from zeta potential measurements.

72 When water flow relative to the mineral surface takes place, it is widely accepted that the shear
73 plane is located between the “stagnant” Stern layer bounded by the outer Helmholtz plane (OHP)
74 and the diffuse layer because high water viscosity in the Stern layer prevents water flow within it
75 [3, 24, 38]. The Stern layer of silica-based materials such as amorphous silica and quartz in contact
76 with a NaCl solution is traditionally represented by a hydration layer followed by a layer containing
77 hydrated sodium counter-ions [17, 20, 39]. Some molecular dynamic (MD) simulations (e.g.,
78 Zhang et al. [32]), spectroscopy measurements (e.g., Lis et al. [40]) and microfluidic studies (e.g.,
79 Saini et al. [41] and Werkhoven et al. [42]) have demonstrated that there could be a non-zero flow
80 of water within the Stern layer of amorphous silica because some counter-ions form outer sphere

81 surface complexes. This implies that there may be some water displacement within the Stern layer
82 of amorphous silica and quartz. Therefore, the effective shear plane of these materials may be
83 located closer to the mineral surface than the outer Helmholtz plane (Figure 1), in disagreement
84 with the assumption accepted by most that the shear plane is located at the OHP (e.g., Sverjensky
85 [3]) or beyond it (e.g., Alizadeh and Wang [43]).



86
87 **Figure 1.** Sketch showing water flow and ion distribution at the interface between a silica mineral
88 and a NaCl aqueous solution (modified, from Brown et al. [39]). Circles with arrows inside
89 represent water molecules. The shear plane is denoted by the red dashed line. Counter-ions
90 adsorbed as outer sphere complexes form the outer Helmholtz plane.

91
92 The quartz (0001) crystal face is the most stable plane with the lowest surface energy and is often
93 considered as a “model surface”, convenient for modelling SiO₂ materials and hydrophilic surfaces
94 in general [34]. With the improved accuracy of the streaming potential method, it is now possible
95 to accurately measure extremely small voltages due to the displacement of the ions in the EDL of

96 quartz [14]. Published studies of Jaafar et al. [8], Vinogradov et al. [13], and Walker and Glover
97 [15] observed, that at high salinities (NaCl concentrations above 0.4 M, M means mol L⁻¹), the zeta
98 potential of sandstones appears to level off at a small constant negative value between -30 and -10
99 mV or even to increase slightly in magnitude (i.e. become more negative) with salinity. They noted
100 that the zeta potential of sandstones stabilizes at a salinity of about 0.4 M NaCl that corresponds to
101 a Debye length characterizing the diffuse layer thickness of approximately 0.47 nm, which is
102 similar to the size of a hydrated sodium ion. This observation led them to suggest that the constant
103 zeta potential of sandstones at high salinities reflected the maximum charge density in the diffuse
104 layer which was reached when the diffuse layer thickness approached the diameter of the counter-
105 ions. However, Jaafar et al. [8], Vinogradov et al. [13], and Walker and Glover [15] did not
106 explicitly explain this behavior through a surface complexation model describing their zeta
107 potential measurements on sandstones.

108 In our study, we used a surface complexation model named basic Stern model (BSM) and
109 considered that the shear plane is at the OHP or closer to the mineral surface than the OHP to
110 describe the zeta potential and the electrochemical properties of quartz at varying NaCl
111 concentrations. In our model we described the effective location of the OHP and the shear plane
112 (i.e., the average distances from topologically complex grains surfaces), hence modelling the
113 effective zeta potential. Therefore, the developed surface complexation model accurately replicated
114 the experimental conditions under which the streaming potential measurements on intact rock
115 samples comprising grains of various shape and roughness were conducted. The model predictions
116 were compared with the existing experimental zeta potential data on Fontainebleau and Lochaline
117 rocks measured over a broad salinity range (from around 10⁻⁴ M NaCl up to around 5.5 M NaCl).
118 The values of the optimized model parameters were finally discussed. Our findings shed light on

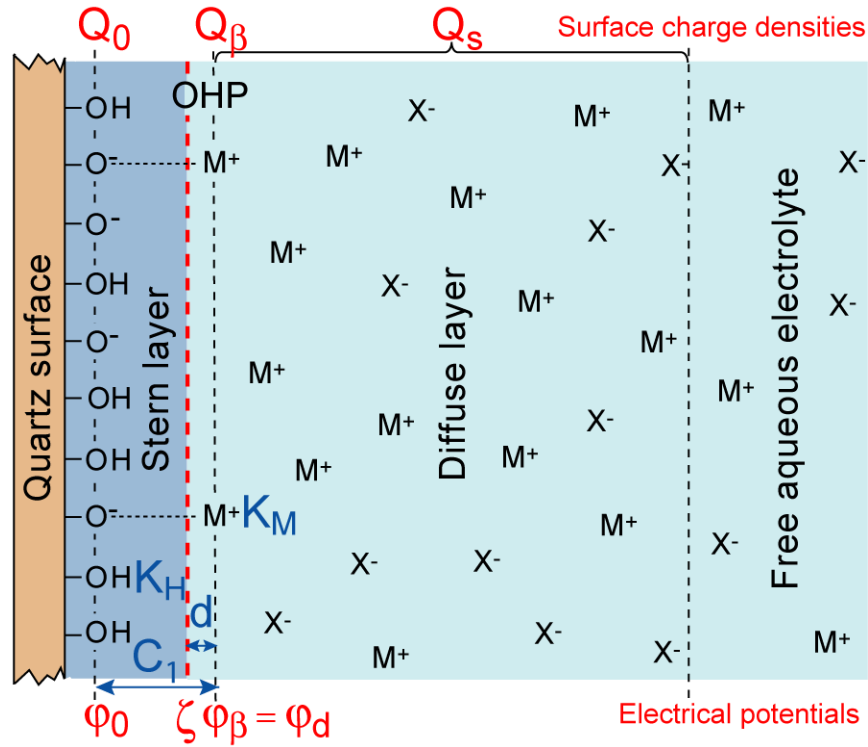
119 the electrochemical properties of quartz and on the likelihood of non-zero water flow within the
120 Stern layer.

121

122 **2. Theoretical background**

123 *2.1. Surface complexation model for quartz*

124 Our basic Stern model, BSM, [36, 44] describes proton (H^+) adsorption onto >SiO^- surface sites at
125 the 0-plane (defining the mineral surface) and sodium cation (Na^+) adsorption by these surface sites
126 at the β -plane (Stern plane and OHP) (Figure 2) [3, 6, 19, 20, 22]. The BSM considers that the β -
127 plane coincides with the d -plane defining the start of the diffuse layer (not the shear plane). This
128 model only needs one Stern layer capacitance as an input parameter to model the electrical potential
129 distribution between the mineral surface and the Stern plane. Recent studies utilizing atomic force
130 microscopy (AFM) (e.g., Siretanu et al. [45]) and X-ray photoelectron spectroscopy (XPS) (e.g.,
131 Brown et al. [39]) used BSM to model the electrochemical properties of amorphous silica in contact
132 with a NaCl aqueous solution and demonstrated that BSM could accurately reproduce the
133 experimental data. García et al. [6] also used BSM to match the measured electrochemical
134 properties of quartz in contact with a NaCl aqueous solution thus confirming the validity of the
135 approach.



136
 137 **Figure 2.** Sketch of our basic Stern model to describe the electrochemical properties of the interface
 138 between quartz and a 1:1 electrolyte like NaCl electrolyte. The model input parameters are shown
 139 in blue and the model output parameters, including the zeta potential (ζ), are shown in red.

140
 141 In our BSM we used four adjustable parameters, namely the logarithms of the two adsorption
 142 equilibrium constants K_H and K_{Na} , the Stern layer capacitance C_1 ($F\ m^{-2}$), and the distance d
 143 between the shear plane (where the zeta potential is defined) and the β -plane (Figure 2). It should
 144 be noted that we considered that the doubly coordinated surface groups ($>Si_2O^0$) are inert [19] and
 145 that the protonated silanol sites ($>SiOH_2^+$) are not expected to form at close-to-neutral pH of the
 146 streaming potential measurements on sandstones (pH varied between 6.4 and 7.3 in Walker and
 147 Glover [15]). Therefore, these surface sites were excluded from the model. For detailed information
 148 on our BSM, the reader can refer to Appendixes A and B, and to Leroy et al. [20].

149 2.2. Zeta potential computation

150 All calculations were performed by combining the geochemical software IPhreeqc for the surface
151 complexation modelling [46] with an in-house code implemented in Matlab for the calculation of
152 the zeta potential and the optimization procedure [47]. The zeta potential (V) defined at the shear
153 plane located at a distance d from the β -plane was determined from the computed by IPhreeqc φ_0
154 and φ_β electrical potentials by considering a linear, capacitor-like variation of the electrical
155 potential within the Stern layer [24]

$$\zeta = \varphi_\beta - \left(\frac{\varphi_\beta - \varphi_0}{x_\beta - x_0} \right) d, \quad (1)$$

156 where x is the distance from the mineral surface (defined by the 0-plane, in m). Combining equation
157 (1) with the following equation for the Stern layer capacitance [17]

$$C_1 = \frac{\varepsilon_1}{x_\beta - x_0}, \quad (2)$$

158 where ε_1 is the water permittivity in the Stern layer (F m^{-1} ; we used $\varepsilon_1 = 43\varepsilon_0$, where ε_0 is the
159 vacuum permittivity, in accordance with the study of Sverjensky [3]), we finally obtain an
160 expression for the zeta potential as a function of the modelled electrochemical properties

$$\zeta = \varphi_\beta - (\varphi_\beta - \varphi_0) \frac{C_1}{\varepsilon_1} d. \quad (3)$$

161 We did not consider the presence of a stagnant diffuse layer (also named buffer layer), which
162 implies that the shear plane is located further away from the mineral surface, as suggested in
163 Alizadeh and Wang [43]. To the best of our knowledge, the stagnant diffuse layer existence has

164 never been directly confirmed experimentally. To the contrary, Předota et al. [34], Brkljača et al.
 165 [18], and Biriukov et al. [33] predicted no such stagnant diffuse layer from their molecular dynamic
 166 simulations of the zeta potential of the hydroxylated (110) rutile (TiO₂) and (0001) quartz surfaces.
 167 Furthermore, Leroy and co-workers (e.g., Leroy et al. [48], Leroy et al. [49], Leroy et al. [20], Li
 168 et al. [29]) attributed the assumption of the presence of a stagnant diffuse layer in previous studies
 169 to the misinterpretation of the zeta potentials from electrokinetic (e.g., electrophoretic mobility,
 170 streaming potential) measurements due to disregard of surface conductivity effects. Indeed, surface
 171 conductivity decreases the magnitude of the measured electrokinetic signal hence implying smaller
 172 apparent zeta potentials, the effect that can be attributed to a shift of the shear plane further away
 173 from the mineral surface when modelling the zeta potential from a surface complexation model.

174 The parameters of our surface complexation model ($\log K_H$, $\log K_{Na}$, C_1 , d) were optimized by
 175 minimizing the following cost function [50]:

$$y = 1 - R^2 = \frac{\sum_{i=1}^N (\zeta_{mes}^i - \zeta_{mod}^i)^2}{\sum_{i=1}^N (\zeta_{mes}^i - \langle \zeta_{mes} \rangle)^2}, \quad (4)$$

176 where R^2 is the coefficient of determination, N is the number of zeta potential measurements, ζ_{mes}^i
 177 is the i -th measured zeta potential, $\langle \zeta_{mes} \rangle$ is the arithmetic mean of the measured zeta potentials,
 178 and ζ_{mod}^i is the i -th modelled zeta potential. The fitting procedure was realized by using the
 179 simulated annealing algorithm to find the global minimum of the cost function (equation (4)), with
 180 a refinement using the simplex method at the end of the process [47].

181

182 **3. Comparison with experimental data and discussion**

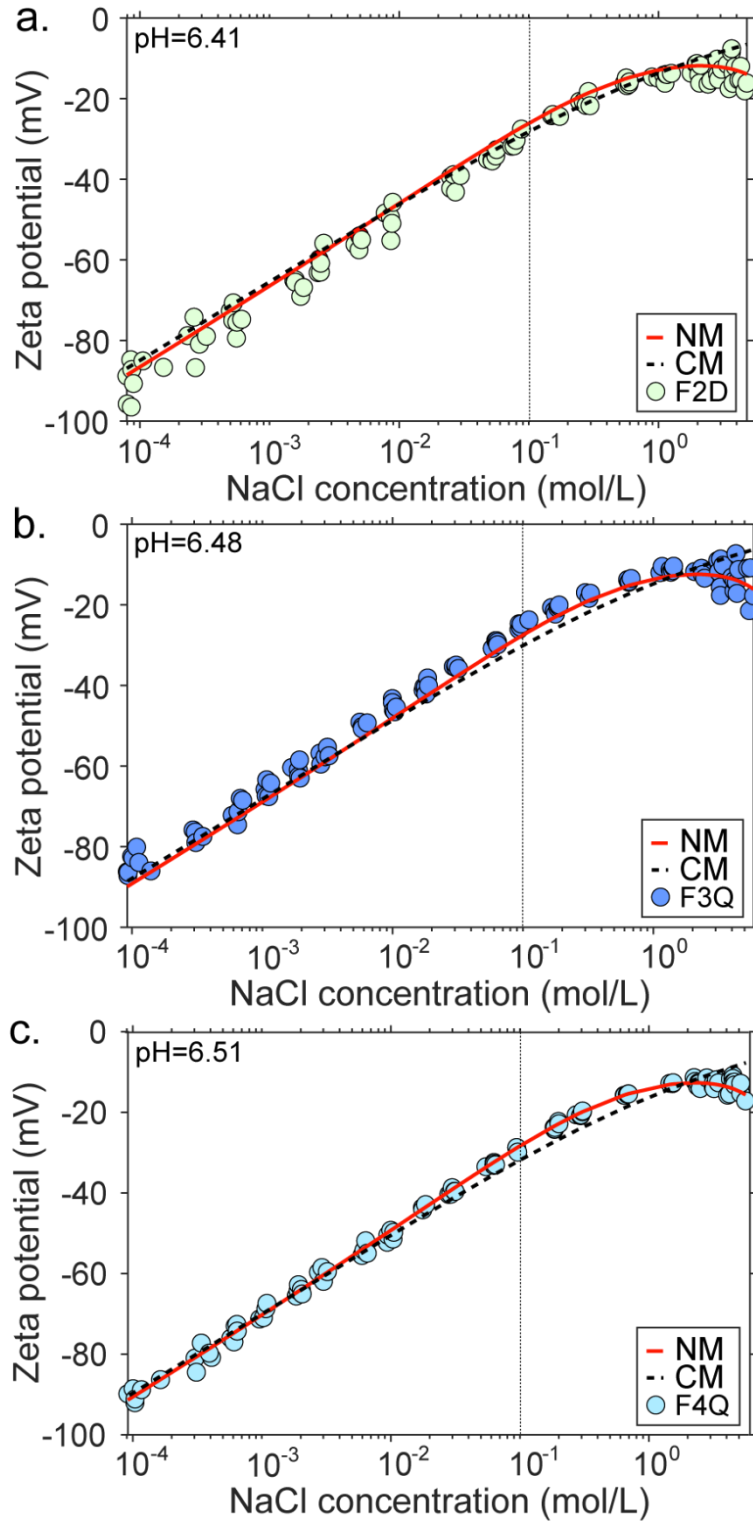
183 *3.1. Considerations of impact of pore space topology and grain roughness on EDL parameters*

184 To test our model, we used the measured zeta potentials of Fontainebleau (F2D, F3Q, F4Q) and
185 Lochaline (L3Q, L4Q) samples in contact with NaCl solutions of increasing salinity obtained by
186 the streaming potential method and reported in Walker and Glover [15] (temperature = 20–25°C).
187 These two rock types were selected as they are known to consist of more than 99% quartz (by
188 weight) [13, 51]. Unlike Fontainebleau and Lochaline samples, zeta potentials of Berea and Boise
189 sandstones reported by Walker and Glover [15] that contained up to 6% feldspar, 2% dolomite,
190 and 8% clays for Berea rocks [52] and up to 13% clays for Boise rocks [53], were excluded from
191 the simulation. Despite the fact that feldspar, dolomite, and clay content in Berea and Boise samples
192 was relatively small, clays are known to line pore walls, thus making these complex minerals a
193 main contributor to the electrochemical processes at the mineral-water interface and causing
194 anomalous or even positive zeta potentials [54, 55]. Therefore, the experimental zeta potential data
195 for Boise and Berea samples were deemed unapplicable for our model that considers only surface
196 complexation reactions on quartz surface.

197 All Fontainebleau and Lochaline samples exhibited a negative zeta potential with its magnitude
198 decreasing with increasing salinity (Figures 3 and 4). The zeta potentials of Lochaline samples
199 were found to be of a larger magnitude than those of Fontainebleau samples. Scanning electron
200 microscopy (SEM) micrographs of the tested samples showed that Fontainebleau rock had sharper-
201 angled grains with larger surface roughness and smaller grains than Lochaline rock (Figure 5 from
202 Walker and Glover [15]). According to Vinogradov et al. [14], pore space topology, grain shape,
203 surface roughness and size, all may influence streaming potential measurements. The authors

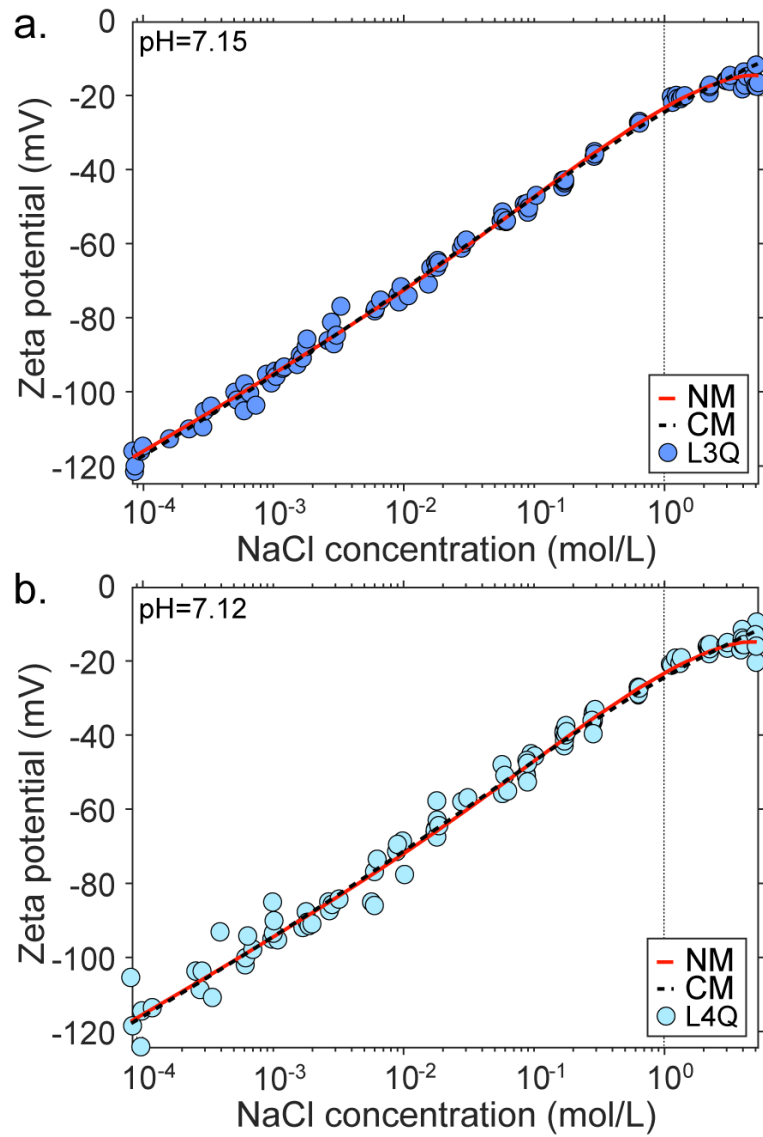
204 suggested that rough rocks with small grains had smaller streaming and zeta potential magnitudes
205 than round, smooth rocks with large grains because existence of sharp grain/pore corners and larger
206 roughness would shift the effective shear plane further away from the mineral surface (read their
207 section 4.2). Alroudhan et al. [56] used the same argument to explain why the zeta potential of
208 colloidal suspensions measured by the electrophoretic mobility method was larger in magnitude
209 than the zeta potential of rocks measured by the streaming potential method (see their Figure 10
210 and read the related discussion in their section 5.2). Schnitzer and Ripperger [57] and Drechsler et
211 al. [58] also showed that increasing surface roughness changes the flow velocity distribution on the
212 solid surface shifting the shear plane further away from the solid surface and decreases the
213 streaming and zeta potential magnitudes. According to these observations, we expected different
214 values of the surface complexation model parameters for Fontainebleau and Lochaline samples.
215 Specifically, for the two tested samples, we allowed different values of the Stern layer capacitance
216 C_1 and the distance d of the shear plane from the OHP (or Stern plane), which are very sensitive
217 to the textural properties of rocks (C_1 depends on the thickness of the Stern layer, equation (2)).

218



219

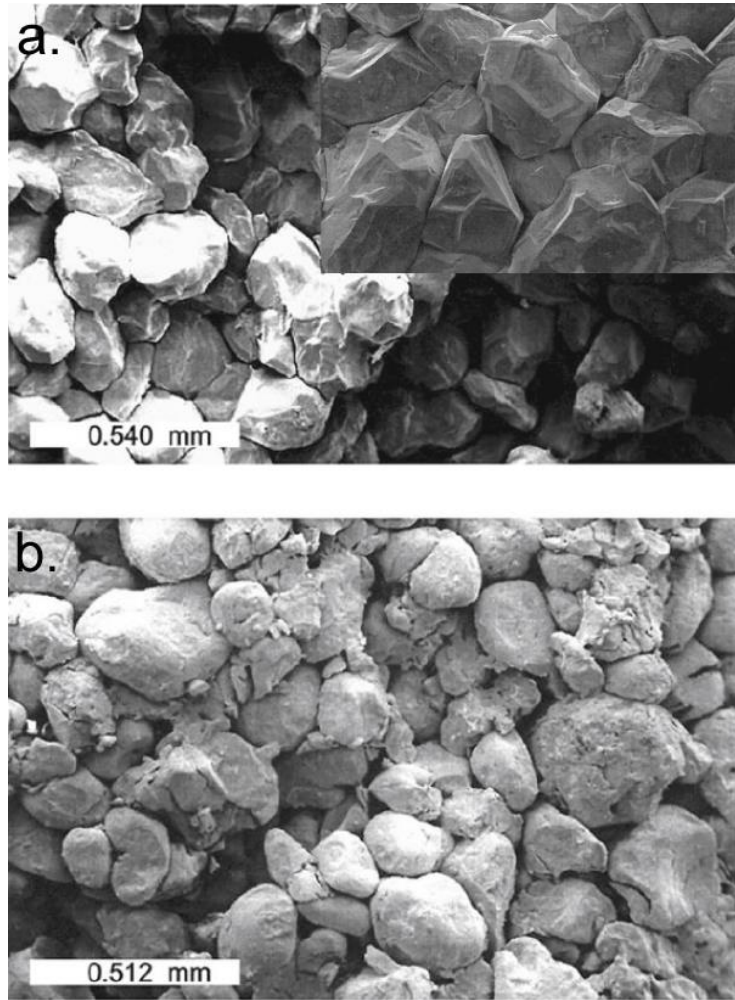
220 **Figure 3.** Zeta potentials of Fontainebleau samples as a function of NaCl concentration. Circle
 221 symbols: experimental zeta potential data with the sample name corresponding to that used by
 222 Walker and Glover [15]; curves: model predictions.



224

225 **Figure 4.** Zeta potentials of Lochaline samples as a function of NaCl concentration. Circle symbols:
 226 experimental zeta potential data with the sample name corresponding to that used by Walker and
 227 Glover [15]; curves: model predictions.

228



229
230 **Figure 5.** SEM micrographs of Fontainebleau (a) and Lochaline (b) rocks (modified from Walker
231 and Glover [15]).

232
233 Figures 3 and 4 demonstrate that below the concentration thresholds of around 0.1 M NaCl
234 (Fontainebleau samples) and 1 M NaCl (Lochaline samples) (denoted by the vertical black dotted
235 lines), the magnitude of the negative zeta potential decreases linearly with increasing salinity. On
236 the other hand, the rate of decrease in the zeta potential magnitude with increasing salinity became
237 smaller above these thresholds, i.e. it became non-linear, and eventually stabilized (or even slightly
238 increased in magnitude) at a zeta potential value of approximately -15 mV for both rock types.

239 Such stabilization of the zeta potential was more apparent for Fontainebleau than for Lochaline
240 samples. These observations were also qualitatively and quantitatively consistent with the data
241 reported by Vinogradov et al. [13], Vinogradov et al. [14] and Walker and Glover [15], who stated
242 that at high salinities, the measured zeta potential stabilized and became equal to -13.01 ± 0.48
243 mV for Fontainebleau samples and to -16.81 ± 0.68 mV for Lochaline samples.

244 Considering that Fontainebleau and Lochaline sandstones did not have the same pore space
245 topology and textural properties, we first optimized separately the parameters of the surface
246 complexation models for these two rock types. That is, a single model was developed for F2D,
247 F3Q, F4Q combined data (Fontainebleau rocks) and a separate model was developed for L3Q, L4Q
248 combined data (Lochaline rocks) to match the simulated zeta potentials to the observed data. We
249 ran the classical model (where the shear plane was assumed to coincide with OHP) denoted by CM
250 with the parameters $\log K_H$, $\log K_{Na}$, and C_1 , and the new model denoted by NM with the
251 parameters $\log K_H$, $\log K_{Na}$, C_1 , and d (the distance of separation between the shear plane and
252 OHP), to investigate the effect of the proposed inward shift of the shear plane on the simulated zeta
253 potential while assigning measured pH values to the respective rock samples as reported by Walker
254 and Glover [15].

255 In parallel, we also used the BSM approach, but for Fontainebleau and Lochaline samples together
256 (all five samples, F2D, F3Q, F4Q, L3Q, L4Q) to develop a unified surface complexation model for
257 quartz in contact with a NaCl aqueous solution, denoted by UNM for the unified new and UCM
258 for the unified classical models.

259

260

261 *3.2. Comparison of the computed to the observed zeta potentials and discussion*

262 Overall, both the NM and CM reproduced well the experimental zeta potential data for the entire
263 salinity range (Figures 3 and 4). According to the surface complexation models, the observed
264 negative zeta potential was due to the presence of the deprotonated silanol sites $>\text{SiO}^-$ at the 0-
265 plane (Figure 2). The optimized values of the equilibrium constant describing protonation of $>\text{SiO}^-$
266 surface sites (K_{H} , reaction (1)) equal to $10^{7.3}$ and $10^{7.2}$ for Fontainebleau and Lochaline samples,
267 respectively, were found to be close or similar to the spectroscopically determined value of $10^{7.2\pm 0.2}$
268 and to the theoretical value of $10^{7.5}$ using Pauling's definition of formal bond valence for silica [19]
269 (Table 1). In addition, our optimized values of K_{H} were found to be similar to the value of $10^{7.2}$
270 determined by Sverjensky [3]. He used a triple layer model (BSM with an additional C_2
271 capacitance between the Stern plane and the external boundary of the diffuse layer) to match
272 surface charge density measurements inferred from acid base potentiometric titration on natural
273 quartz in contact with NaCl solutions. Our models also explained why the zeta potential magnitude
274 of Lochaline samples was larger, for the same salinity, than the zeta potential magnitude of
275 Fontainebleau samples. Indeed, Lochaline samples had higher pH (i.e. less protons in solution)
276 than Fontainebleau samples (7.1 versus 6.5 in average, respectively; Walker and Glover [15]) while
277 having essentially identical $\log K_{\text{H}}$ values (Lochaline had slightly lower $\log K_{\text{H}}$ value), which
278 resulted in Lochaline samples having larger number of deprotonated $>\text{SiO}^-$ sites per nm^2 of the
279 surface and a higher negative surface charge density Q_0 (equation (A5)) (Figure 6).

280

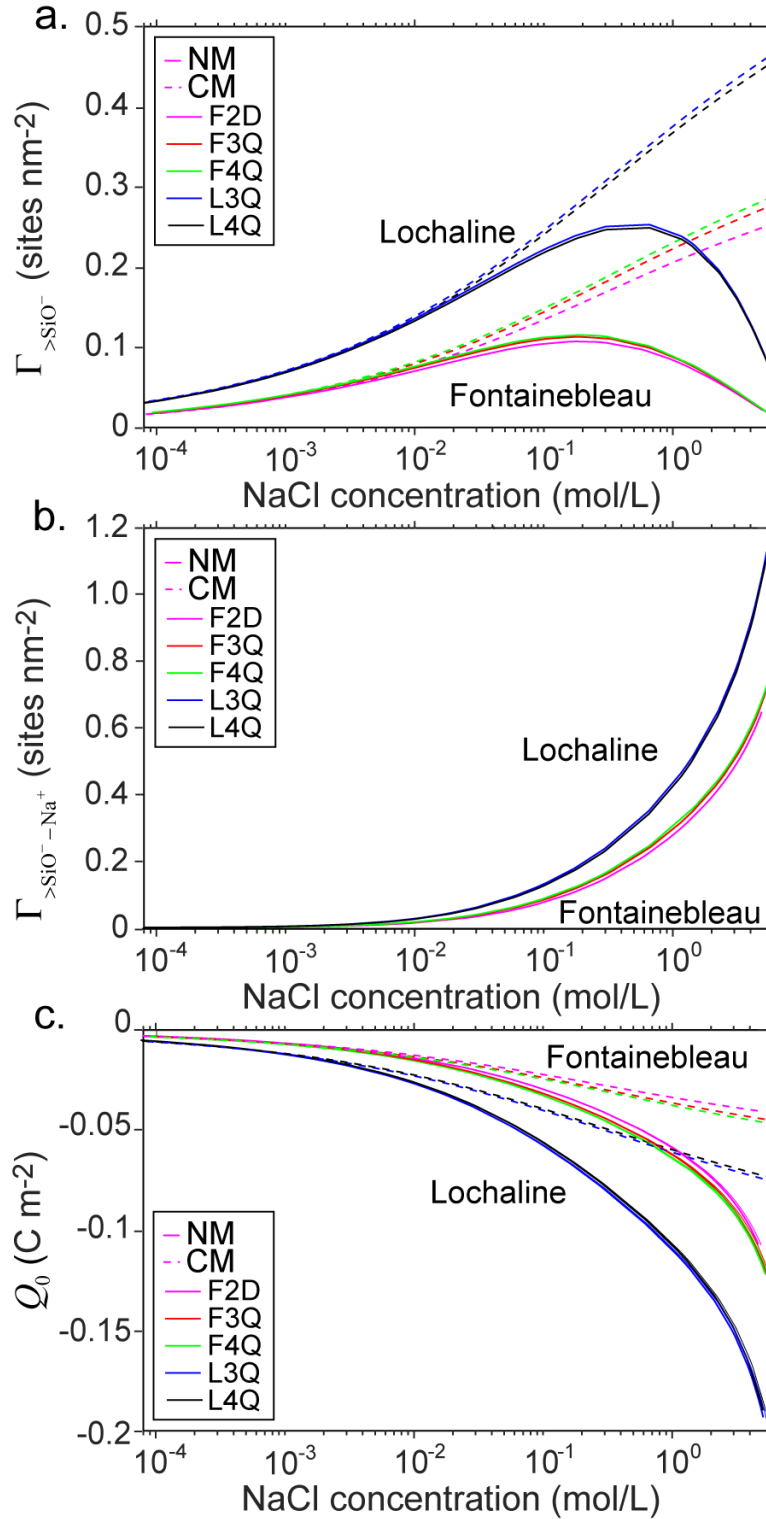
281

282 **Table 1.** BSM parameters and estimated Stern layer thickness for Fontainebleau and Lochaline
 283 sandstones.

Symbols	Range ¹	Fontainebleau		Lochaline	
		CM	NM	CM	NM
$\log K_H$	[4 10]	7.3	7.3	7.2	7.2
$\log K_{Na}$	[-15 5]	-16	0.6	-21	0.1
C_1 (F m ⁻²)	[0.5 5]	3.2	1.3	1.8	2.2
d (Å)	[0 10]	0	0.5	0	0.3
d_{Stern}^2 (Å)		1.2	2.8	2.1	1.7

289 ¹ Hiemstra et al. [19], Kitamura et al. [22], Sonnefeld et al. [59], Sverjensky [3], García et al. [6].

290 ² According to Eq. (2) and fitted C_1 values, considering $\epsilon_1 = 43\epsilon_0$ and $d_{Stern} = x_\beta - x_0$.



291
 292 **Figure 6.** Computed surface site densities of $>\text{SiO}^-$ sites (a), $>\text{SiO}^- - \text{Na}^+$ sites (b), and
 293 respective surface charge densities (c) of Fontainebleau and Lochaline samples as a function of
 294 NaCl concentration. Solid curves correspond to the calculations using the NM, dashed lines

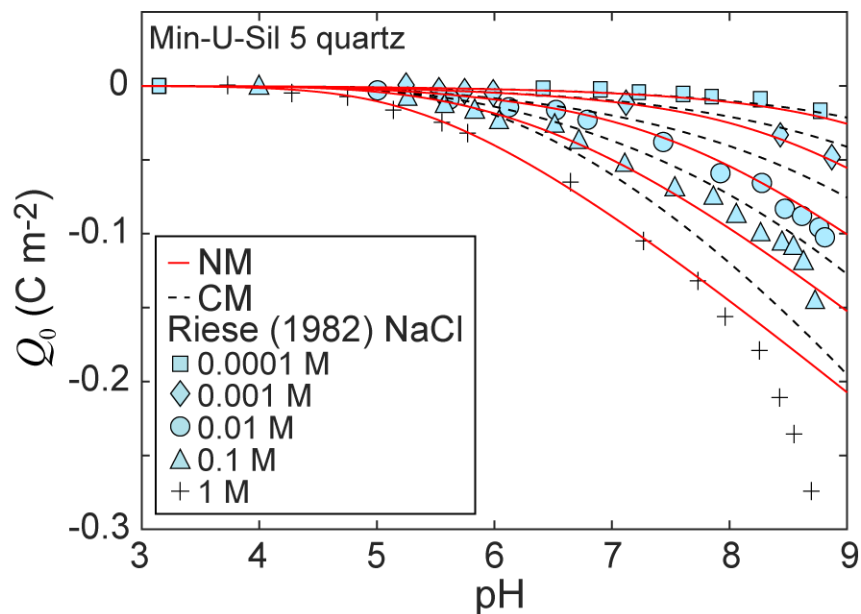
295 correspond to the calculations using the CM. The CM predicted near-zero $> \text{SiO}^- - \text{Na}^+$ surface
296 site densities in the Stern layer (limited at $\cong 0$ sites nm^{-2} in Figure 6b).

297

298 We also found that Lochaline samples had significantly lower $\log K_{\text{Na}}$ values, i.e. weaker sodium
299 adsorption capacity, than Fontainebleau samples (-21 vs -16, respectively, for CM and 0.1 vs 0.6,
300 respectively, for NM, Table 1). This result implies that $> \text{SiO}^- - \text{Na}^+$ surface sites of Lochaline
301 could not counterbalance the negative surface charge density as efficiently as for Fontainebleau
302 samples, and can also explain the larger zeta potential magnitude of Lochaline samples.
303 Interestingly, despite Lochaline samples having lower $\log K_{\text{Na}}$ values than Fontainebleau samples,
304 the models found that Lochaline samples, for the same salinity, had a higher surface site density of
305 adsorbed sodium ion in the Stern layer than Fontainebleau samples due to the higher $> \text{SiO}^-$ surface
306 site density (Figure 6b). The lower $\log K_{\text{Na}}$ values of Lochaline than Fontainebleau samples we
307 found can be explained by Lochaline samples having smoother and larger grains and hence a
308 smaller specific surface area available for sodium adsorption. Sverjensky [3] reported the same
309 observation when comparing two quartz samples with different specific surface area (4.15 and 11.4
310 $\text{m}^2 \text{g}^{-1}$) in contact with NaCl solutions.

311 At the low salinity domain, K_{Na} did not have a noticeable impact on the modelled zeta potential
312 controlled primarily by K_{H} . With the CM, the optimization procedure required a decrease of K_{Na}
313 to extremely low value ($\log K_{\text{Na}} = -16$ or smaller) to fit the high salinity zeta potential
314 measurements (decreasing Na^+ adsorption in the Stern layer results to higher modelled zeta
315 potential magnitude). The K_{Na} values inferred from our CM were extremely low and essentially

316 meant that there was no adsorption of Na^+ at the OHP at all, and everything was controlled solely
 317 by pH. With the NM, the optimization procedure did not require to decrease K_{Na} to extremely low
 318 value to fit the high salinity zeta potential measurements and it found $\log K_{\text{Na}}$ values (0.6 and 0.1
 319 for Fontainebleau and Lochaline samples, respectively) to be of the same order of magnitude as
 320 the value reported by Sverjensky [3] for natural quartz in a contact NaCl solutions ($\log K_{\text{Na}} = 0$).
 321 In addition, and contrary to the CM, our NM was able to reproduce most of the surface charge
 322 density measurements on Min-U-Sil 5 quartz (natural quartz with a mean grain diameter of $5 \mu\text{m}$)
 323 at different pH and NaCl concentrations carried out by Riese [60] (Figure 7).



324
 325 **Figure 7.** Surface charge density of Min-U-Sil 5 quartz as a function of pH and NaCl concentration.
 326 Curves correspond to the predictions. Symbols correspond to the experimental surface charge
 327 density data reported by Riese [60].

328

329 Moreover, the optimized Stern layer capacitance values obtained with our NM were equal to 1.3 F
330 m^{-2} and 2.2 F m^{-2} for Fontainebleau and Lochaline samples, respectively (Table 1), which were
331 closer to the values of 1 F m^{-2} and 2 F m^{-2} reported by Sverjensky [3] and García et al. [6],
332 respectively, for natural quartz in contact with NaCl solution. Conversely, the optimized Stern layer
333 capacitance values obtained with the CM were 3.2 F m^{-2} and 1.8 F m^{-2} for Fontainebleau and
334 Lochaline samples, respectively. Using the optimized Stern layer capacitance values from the NM,
335 equation (2) and $\varepsilon_1 = 43\varepsilon_0$ [3, 39], we found the Stern layer thickness to be comparable to the
336 hydrated radius of sodium ion ($\cong 2 \text{ \AA}$; Leroy et al. [61], Sverjensky [17]). Specifically, the NM
337 predicted Fontainebleau samples to have larger Stern layer thickness (2.8 \AA) than Lochaline
338 samples (1.7 \AA), the results that is explained by sharper and rougher grains of Fontainebleau
339 samples compared to those of Lochaline [15, 62], which push further away the shear plane from
340 the mineral surface and also explain the smaller zeta potential magnitude of Fontainebleau samples.
341 When using the CM, the Stern layer thickness we found for Fontainebleau samples (1.2 \AA) was
342 comparable to the crystallographic radius of sodium ion (1.02 \AA Sverjensky [17]). This result was
343 not realistic for the representation of the quartz/NaCl solution interface, which, according to most
344 studies (e.g., Brown et al. [63]), should contain mostly hydrated sodium ions in the Stern layer,
345 corresponding to a Stern layer thickness at least equal to the hydrated radius of sodium ion. For
346 Lochaline samples, the Stern layer thickness inferred from the CM (2.1 \AA) was comparable to the
347 hydrated radius of sodium ion.

348 Figures 3, 4, 7, the modelling parameters reported in Table 1 and the coefficient of determination
349 values reported in Table 2 clearly demonstrate the importance of considering the location of the
350 shear plane closer to the mineral surface than the OHP. Indeed, as shown in Figures 3 and 4 and
351 reflected by the values of the coefficient of determination at high salinity ($R^2 \geq 0.5$), the

352 stabilization of the zeta potential at high salinity could only be correctly predicted by the NM (red
 353 curves in Figures 3 and 4). The stabilization of the modelled zeta potential at high salinity is
 354 explained by a growing abundance of sodium ions available for adsorption in the Stern layer, and
 355 therefore the decreasing number of $>SiO^-$ sites (Figures 6a and 6b), and importantly by the shear
 356 plane being located slightly closer to the mineral surface than the OHP. Moreover, the NM
 357 reproduced the surface charge density measurements on natural quartz in NaCl solutions reported
 358 in Riese [60] significantly better than the CM (Figure 7) thus independently validating our
 359 assumption on the location of the shear plane.

360

361 **Table 2.** Coefficient of determination values using different BSM parameter values for
 362 Fontainebleau and Lochaline sandstones.

	F2D		F3Q		F4Q		L3Q		L4Q ³⁶³	
	CM	NM	CM	NM	CM	NM	CM	NM	CM	NM ³⁶⁴
R^2	0.97	0.98	0.97	0.99	0.99	1	1	1	0.99	0.99 ³⁶⁵
$R^2 LS^1$	0.96	0.96	0.97	0.97	0.99	0.99	0.99	0.99	0.98	0.98 ³⁶⁷
$R^2 HS^2$	-0.31	0.60	-0.56	0.60	0.12	0.92	-0.03	0.62	0.26	0.50 ³⁶⁸

370

371 ¹ Low salinity, below 0.1 M NaCl (Fontainebleau samples) and 1 M NaCl (Lochaline samples).

372 ² High salinity, above 0.1 M NaCl (Fontainebleau samples) and 1 M NaCl (Lochaline samples).

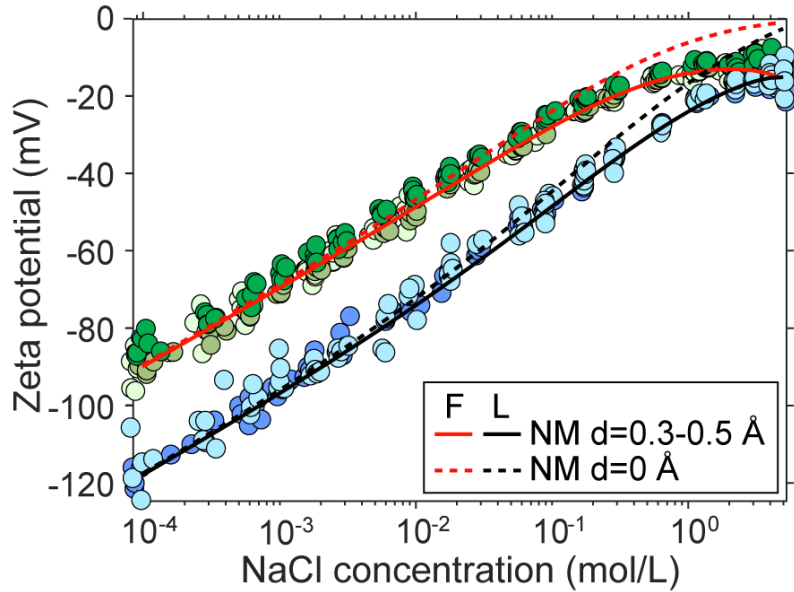
373

374 The measured high salinity zeta potentials were closely matched by our NM, which considers that
 375 the shear plane approaches the mineral surface with a small distance from the OHP ($d = 0.5 \text{ \AA}$ for
 376 Fontainebleau samples and $d = 0.3 \text{ \AA}$ for Lochaline samples; Table 1). Including such a small
 377 distance d between OHP and shear plane increased the computed zeta potential magnitude
 378 compared to CM with a more pronounced impact at high salinity (Figure 8). The effective distance
 379 d used in our NM was significantly smaller than the hydrated radius of Na^+ ($\cong 2 \text{ \AA}$; Leroy et al.

380 [61], Sverjensky [17]), which implied that only some of Na ions were mobilized in the Stern layer,
381 i.e., only a small portion of all ions could move inside the Stern layer. In addition, we found that
382 $d/d_{Stern}(\text{Lochaline}) = d/d_{Stern}(\text{Fontainebleau}) = 0.18$, which implied that regardless of rock type,
383 18% of the, previously considered as immobile, ions in the Stern layer will be flowing. Therefore,
384 the thicker the Stern layer is (and we expect it to become thicker as roughness increases), the larger
385 d will become – exactly as our NM predicted.

386 Moreover, unlike the CM, our NM found that the shear plane of Fontainebleau samples was further
387 away from the mineral surface than the shear plane of Lochaline samples, also explaining why the
388 zeta potential magnitude of Fontainebleau samples was smaller than the zeta potential magnitude
389 of Lochaline samples. Indeed, the total distance of the shear plane from the mineral surface (d_{Stern}
390 $- d$) is larger for Fontainebleau ($2.8-0.5=2.3 \text{ \AA}$) compared with Lochaline ($1.7-0.3=1.4 \text{ \AA}$) samples.
391 This result is consistent with our hypothesis that rougher and sharper Fontainebleau grains (Figure
392 5) lead to expansion of the effective EDL (averaged over large number of grains and pores) further
393 away from the mineral surface (both, the Stern plane and the shear plane).

394



395
 396 **Figure 8.** Computed zeta potential of Fontainebleau (F) and Lochaline (L) samples as a function
 397 of NaCl concentration considering or not the distance d between the OHP and the shear plane.

398
 399 In the classical theory of the electrical double layer, it is assumed that only the mobile excess
 400 counter-ions in the diffuse layer contribute to the measured macroscopic streaming potential [27].
 401 However, the diffuse layer is highly compressed at high salinity, so that there are essentially no
 402 mobile counter-ions available inside it, and such near-zero concentration of mobile counter-ions of
 403 the diffuse layer cannot explain correctly the non-zero zeta potentials in Fontainebleau and
 404 Lochaline sandstones at high salinity. Figure 9 shows the computed thicknesses of the diffuse layer
 405 and of the mobile part of the Stern layer (d), as well as the $\Gamma_{>\text{SiO}^- - \text{Na}^+}$ and $\Gamma_{\text{Na}^+}^d$ surface site density
 406 in the Stern and diffuse layers, respectively. The salinity dependence of the diffuse layer thickness
 407 was evaluated by the Debye length χ :

$$\chi = \sqrt{\frac{\varepsilon_w k_B T}{2e^2 1000 N_A I}}, \quad (5)$$

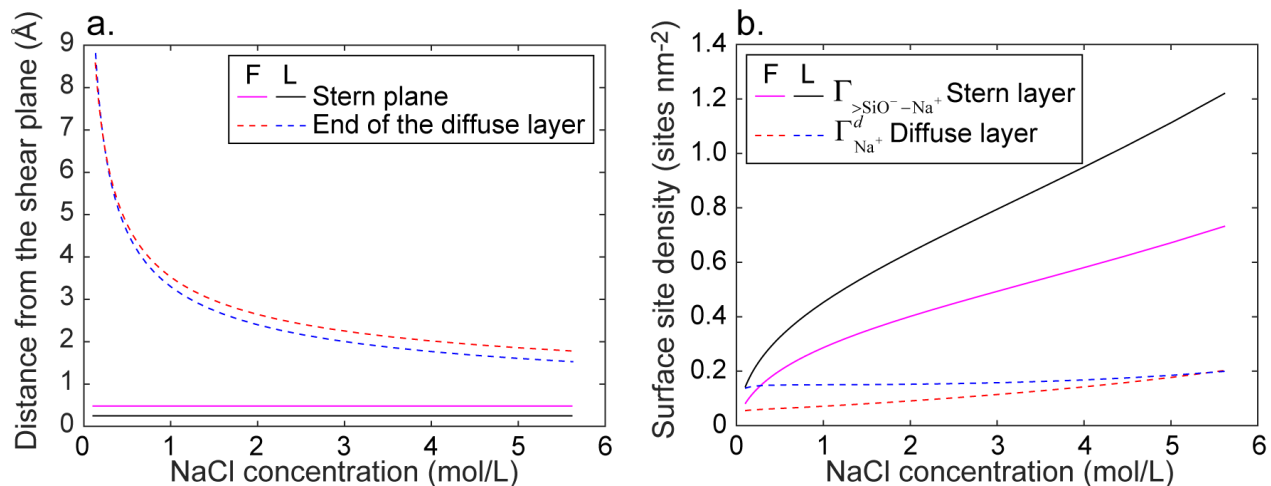
408 where ε_w is the water permittivity (F m^{-1} ; $\varepsilon_w \cong 78.3\varepsilon_0$ at a temperature of 25°C), k_B is the
 409 Boltzmann constant ($\cong 1.381 \times 10^{-23} \text{ J K}^{-1}$), T is the temperature (K), e is the electron charge (\cong
 410 $1.602 \times 10^{-19} \text{ C}$), N_A is the Avogadro number ($\cong 6.022 \times 10^{23} \text{ sites mol}^{-1}$), and I is the ionic strength
 411 (mol L^{-1}). The surface site density of adsorbed Na ion in the diffuse layer, $\Gamma_{\text{Na}^+}^d$, was calculated
 412 using the following equations [23]:

$$\Gamma_{\text{Na}^+}^d = 1000 N_A c_{\text{Na}^+}^\infty \int_{x=0}^{x=\chi} \left\{ \exp[-e\varphi_d(x) / k_B T] - 1 \right\} dx, \quad (6)$$

$$\varphi_d(x) = \frac{4k_B T}{e} \tanh^{-1} \left[\tanh \left(\frac{e\varphi_d}{4k_B T} \right) \exp(-x / \chi) \right], \quad (7)$$

413 where $c_{\text{Na}^+}^\infty$ is the Na^+ concentration (mol L^{-1}) in bulk water (not influenced by the charged surface),
 414 φ_d is the electrical potential at the start of the diffuse layer ($\varphi_\beta = \varphi_d$) and x is the distance from
 415 the OHP (in m).

416



417
 418 **Figure 9.** Computed thickness of the diffuse layer (equal to the Debye length) and of the mobile
 419 part of the Stern layer (a); surface density of $> \text{SiO}^- - \text{Na}^+$ sites in the Stern layer (at OHP) and of
 420 adsorbed Na^+ ions in the diffuse layer (b) as a function of NaCl concentration for Fontainebleau
 421 (F) and Lochaline (L) samples.

422
 423 The computed thickness of the diffuse layer decreases significantly at high salinity to become
 424 comparable to the hydrated radius of sodium ion ($\cong 2 \text{ \AA}$) but it remains considerably larger than
 425 the thickness of the mobile part of the Stern layer (0.5 \AA and 0.3 \AA for Fontainebleau and Lochaline
 426 samples, respectively) (Figure 9a). However, when salinity increases, the computed surface site
 427 density of adsorbed Na^+ ion inside the Stern layer increases considerably more than in the diffuse
 428 layer (Figure 9b), which explains the increasing contribution of the counter-ions in the mobile part
 429 of the Stern layer to the measured streaming potential.

430 Our new surface complexation model applied simultaneously for both Fontainebleau and Lochaline
 431 samples (all five samples together) in NaCl solution (UNM) was able to reproduce the zeta potential
 432 measurements well. Indeed, the values of the coefficient of determination were still close to 1 when
 433 calculated for the entire salinity range (Table 3). The UNM reproduced very well the low salinity

434 measurements, and the quality of match was similar to the results obtained using the unified
 435 classical model, UCM. Across the high salinity domain, the UNM was also found to provide a
 436 better match to the experimental data compared with the UCM (except for L4Q sample at high
 437 salinity). The values of the optimized parameters used in UNM (Table 4) agreed with the values
 438 previously reported in Table 1 for NM, and both sets were consistent with the values reported in
 439 the literature for quartz in NaCl solution. Therefore, our approach is relevant for obtaining a unified
 440 surface complexation model for quartz in a NaCl solution. However, treating different rock samples
 441 separately makes more sense because it accounts for difference in the pore space topology, so we
 442 believe that NM is better and more physically sensible than UNM.

443

444 **Table 3.** Coefficient of determination values using a single set of BSM parameter values for
 445 Fontainebleau and Lochaline sandstones together.

	F2D		F3Q		F4Q		L3Q		L4Q	
	UCM	UNM	UCM	UNM	UCM	UNM	UCM	UNM	UCM	UNM
R^2	0.98	0.99	0.97	0.98	0.99	1	1	1	0.99	0.99
R^2 LS ¹	0.97	0.97	0.95	0.95	0.99	0.99	0.99	0.99	0.98	0.98
R^2 HS ²	-0.45	0.46	-0.60	0.29	0.05	0.79	0.00	0.51	0.21	-0.04

446 ¹ Low salinity, below 0.1 M NaCl (Fontainebleau samples) and 1 M NaCl (Lochaline samples).

447 ² High salinity, above 0.1 M NaCl (Fontainebleau samples) and 1 M NaCl (Lochaline samples).

448

449

450

451

452

453 **Table 4.** BSM parameter values and estimated Stern layer thickness for quartz (combining
 454 Fontainebleau and Lochaline sandstones).

Symbols	Range ¹	UCM	UNM ⁴⁵⁵
$\log K_H$	[4 10]	7.2	7.2
$\log K_{Na}$	[-15 5]	-21	0.1 ⁴⁵⁶
C_1 (F m ⁻²)	[0.5 5]	1.8	2.2
d (Å)	[0 10]	0	0.3 ⁴⁵⁷
d_{Stern}^2 (Å)		2.1	1.7

459 ¹ Hiemstra et al. [19], Kitamura et al. [22], Sonnefeld et al. [59], Sverjensky [3], García et al. [6].

460 ² According to Eq. (2) and fitted C_1 values, considering $\epsilon_1 = 43\epsilon_0$ and $d_{Stern} = x_\beta - x_0$.

461

462 4. Conclusions

463 We developed a basic Stern surface complexation model to explain the zeta potential measurements
 464 on quartz in contact with NaCl solution and describe the concentration dependence of the
 465 electrochemical properties of quartz over a broad salinity range, from around 10⁻⁴ M NaCl up to
 466 around 5.5 M NaCl. These measurements were obtained using the streaming potential method.
 467 Previous surface complexation models considered that the shear plane of quartz in contact with
 468 NaCl solution was located at the Stern plane where sodium counter-ions were preferentially
 469 adsorbed or even further away from the mineral surface. In contrast to previous models, our new
 470 model considered that there could be a non-zero water flow transporting counter-ions within the
 471 Stern layer, i.e. that the shear plane where the zeta potential is defined was located closer to the
 472 mineral surface than the Stern plane.

473 Compared to the classical basic Stern model (BSM considering the zeta potential at the Stern plane),
 474 our new model better reproduced the zeta potential measurements on Fontainebleau and Lochaline
 475 sandstones, especially at high salinity conditions (above 0.1 M NaCl for Fontainebleau samples
 476 and 1 M NaCl for Lochaline samples) where zeta potential appeared to level off to a constant

477 negative value; this was particularly true for Fontainebleau samples. We explained, based on SEM
478 micrograph images and our new model, why Fontainebleau rocks, with sharper-angle grains and
479 larger surface roughness, had smaller in magnitude zeta potential for the same NaCl concentration
480 compared against Lochaline data. The predicted surface charge density of quartz from the new
481 model was also in a better agreement with the experimental data.

482 We found a small distance of the shear plane offset from the Stern plane (0.5 Å for Fontainebleau
483 samples and 0.3 Å for Lochaline samples), i.e., only a small part of the Stern layer (18%
484 independently of Fontainebleau or Lochaline samples) was mobile, confirming that the shear plane
485 was still at a close proximity to the Stern plane. In addition, in our new model, the optimized values
486 of the equilibrium constant describing sodium adsorption in the Stern layer ($10^{0.6}$ for Fontainebleau
487 samples and $10^{0.1}$ for Lochaline samples) were more realistic compared with the classical BSM,
488 which considers essentially no sodium adsorption in the Stern layer to try to match high salinity
489 zeta potential measurements. Using our new model, we found that the Stern layer of Fontainebleau
490 samples is thicker than the Stern layer of Lochaline samples (2.8 Å vs 1.7 Å), and that the shear
491 plane of Fontainebleau samples is further away from the mineral surface (2.3 Å) than the shear
492 plane of Lochaline samples (1.4 Å), in agreement with the pore space topologies given by SEM
493 images. We also explained the increasing contribution of the counter-ions in the mobile part of the
494 Stern layer compared to the contribution of the counter-ions in the diffuse layer to the streaming
495 potential when salinity increases.

496 Our basic Stern surface complexation model with the zeta potential located closer to the mineral
497 surface than the Stern plane can be used to interpret and predict streaming potential measurements
498 and other types of electrokinetic measurements (e.g., electrophoretic mobility) on quartz and other
499 minerals in contact with brines of different chemical compositions and temperatures. Therefore,

500 our zeta potential model, which can be confirmed by laboratory measurements looking phenomena
501 at the microscopic scale (e.g., using microfluidics and spectroscopy methods) and atomistic
502 simulations, may have strong implications for the modelling of the electrochemical properties of
503 minerals in contact with highly saline brines. Our results are of crucial importance for exploring
504 mineral-brine interactions at high salinity levels close to real subsurface conditions.

505

506 **Acknowledgments**

507 The research work of Shuai Li is funded by the National Natural Science Foundation of China
508 (grant no. 41974089) and the Fundamental Research Funds for the Central Universities (China
509 University of Geosciences, Wuhan), China (grant no. CUGGC04). Philippe Leroy acknowledges
510 the internal funding from the French Geological Survey (BRGM) (CHIPPY project no.
511 RP20DEP087) and the support from Francis Claret for his research work as well as the fruitful
512 scientific discussions with Arnault Lassin. The authors also sincerely acknowledge Paul Glover for
513 sending them the SEM micrographs of Fontainebleau and Lochaline rocks.

514

515

516 **Appendix A. Basic Stern surface complexation model**

517 The following two surface complexation reactions were considered for the zeta potential modelling:



518 where K_{H} and K_{Na} (dimensionless) are the associated equilibrium constants, which are written as:

$$K_{\text{H}} = \frac{a_{>\text{SiOH}}}{a_{>\text{SiO}^-} a_{\text{H}^+}} \cong \frac{\Gamma_{>\text{SiOH}}}{\Gamma_{>\text{SiO}^-} a_{\text{H}^+}} = \frac{\Gamma_{>\text{SiOH}}}{\Gamma_{>\text{SiO}^-} a_{\text{H}^+}^{\infty}} \exp\left(\frac{e\varphi_0}{k_{\text{B}}T}\right), \quad (\text{A10})$$

$$K_{\text{Na}} = \frac{a_{>\text{SiO}^- - \text{Na}^+}}{a_{>\text{SiO}^-} a_{\text{Na}^+}} \cong \frac{\Gamma_{>\text{SiO}^- - \text{Na}^+}}{\Gamma_{>\text{SiO}^-} a_{\text{Na}^+}} = \frac{\Gamma_{>\text{SiO}^- - \text{Na}^+}}{\Gamma_{>\text{SiO}^-} a_{\text{Na}^+}^{\infty}} \exp\left(\frac{e\varphi_{\beta}}{k_{\text{B}}T}\right), \quad (\text{A11})$$

519 where a_i is the activity (dimensionless) and Γ_i is the surface site density (sites m^{-2}) of species i , e
 520 is the elementary charge ($\cong 1.602 \times 10^{-19}$ C), φ is the electrical potential (V), k_{B} is the Boltzmann
 521 constant ($\cong 1.381 \times 10^{-23}$ J K^{-1}), and T is the temperature (K). In equations (A3) and (A4), the
 522 superscript “ ∞ ” refers to ion activities in the electroneutral free or bulk electrolyte (not influenced
 523 by the mineral surface), which were computed using Pitzer theory (Appendix B) [61].

524 The following determined system of equations for the surface charge density at the mineral surface,
 525 Q_0 (C m^{-2}), at the β -plane, Q_{β} , and of the diffuse layer, Q_s , was used to compute the electrical
 526 potential distribution at the interface between quartz and bulk NaCl solution as a function of the
 527 equilibrium constants and Stern layer capacitance [20]:

$$Q_0 = -e(\Gamma_{>\text{SiO}^-} + \Gamma_{>\text{SiO}^- - \text{Na}^+}) = -\frac{e\Gamma_s}{A} \left[1 + K_{\text{Na}} a_{\text{Na}^+}^\infty \exp\left(-\frac{e\varphi_\beta}{k_B T}\right) \right], \quad (\text{A12})$$

$$Q_\beta = e\Gamma_{>\text{SiO}^- - \text{Na}^+} = \frac{e\Gamma_s}{A} K_{\text{Na}} a_{\text{Na}^+}^\infty \exp\left(-\frac{e\varphi_\beta}{k_B T}\right), \quad (\text{A13})$$

$$A = 1 + K_{\text{H}} a_{\text{H}^+}^\infty \exp\left(-\frac{e\varphi_0}{k_B T}\right) + K_{\text{Na}} a_{\text{Na}^+}^\infty \exp\left(-\frac{e\varphi_\beta}{k_B T}\right), \quad (\text{A14})$$

$$Q_s = \sqrt{8\varepsilon_w k_B T 1000 N_A I} \sinh\left[-\left(\frac{e\varphi_\beta}{2k_B T}\right)\right], \quad (\text{A15})$$

$$Q_0 + Q_\beta + Q_s = 0, \quad (\text{A16})$$

$$\varphi_0 - \varphi_\beta = \frac{Q_0}{C_1}, \quad (\text{A17})$$

528 where Γ_s is the total surface site density (we took $\Gamma_s = 4.6$ sites nm^{-2} García et al. [6]), I is the
529 molar ionic strength (mol L^{-1}), and φ_0 and φ_β are the electrical potentials at the 0-plane and at the
530 β -plane, respectively (considering $\varphi_\beta = \varphi_d$ for the BSM, where φ_d is the electrical potential at the
531 start of the diffuse layer).

532

533 **Appendix B. Pitzer model for ion activity coefficients in bulk electrolyte**

534

535 The following equations were used to compute ion activity coefficients in bulk electrolyte [61]:

$$a_i^\infty = \gamma_i^\infty \frac{m_i^\infty}{m_0}, \quad (\text{B1})$$

$$m_i^\infty = \frac{1000c_i^\infty}{M_w c_w^\infty}, \quad (\text{B2})$$

$$c_w^\infty = \frac{10^3 - \sum_i c_i^\infty V_i}{V_w}, \quad (\text{B3})$$

536 where γ_i^∞ is the activity coefficient (dimensionless), m_i^∞ is the molality (mol per kilogram of
 537 water, mol kg_w⁻¹, m_0 being the unit molality equal to 1 mol kg_w⁻¹), c_i^∞ is the molar concentration
 538 (M), and V_i is the standard partial molal volume (cm³ mol⁻¹) of ion i in bulk electrolyte. The
 539 quantity $V_i \cong 18.07, 0, -1.13, 17.68$ cm³ mol⁻¹ for H₂O, H⁺, Na⁺ (due to electrostriction) and
 540 Cl⁻, respectively, at a temperature of 25°C. The subscript “w” in equations (B2) and (B3) refers to
 541 water molecules, and M_w refers to the molar mass of water ($\cong 18$ g mol⁻¹).

542 Na⁺ activity coefficient in bulk electrolyte influences modelled Na⁺ adsorption in the Stern plane
 543 ($\Gamma_{>\text{SiO}^- - \text{Na}^+} = K_{\text{Na}} \Gamma_{>\text{SiO}^-} \gamma_{\text{Na}^+}^\infty m_{\text{Na}^+}^\infty / m_0 \exp(-e\phi_\beta / k_B T)$ from equations (A3) and (A4)). According to
 544 Pitzer theory, which is suitable for very saline aqueous solutions (ionic strengths above 0.1 M
 545 Harvie and Weare [64]), the natural logarithm of Na⁺ activity coefficient in NaCl electrolyte is
 546 written as:

$$\ln \gamma_{\text{Na}^+}^\infty = z_{\text{Na}^+}^2 F + m_{\text{Cl}^-}^\infty \left[2B_{\text{Na}^+\text{Cl}^-} + (m_{\text{Na}^+}^\infty + m_{\text{Cl}^-}^\infty) C_{\text{Na}^+\text{Cl}^-} \right] + z_{\text{Na}^+} m_{\text{Na}^+}^\infty m_{\text{Cl}^-}^\infty C_{\text{Na}^+\text{Cl}^-}, \quad (\text{B4})$$

$$F = -A_\phi \left[\frac{\sqrt{I_m}}{1 + b\sqrt{I_m}} + \frac{2}{b} \ln(1 + b\sqrt{I_m}) \right] + m_{\text{Na}^+}^\infty m_{\text{Cl}^-}^\infty B'_{\text{Na}^+\text{Cl}^-}, \quad (\text{B5})$$

$$A_\phi = \frac{1}{3} \sqrt{\frac{2\pi N_A \rho_w}{1000} \left(\frac{e^2}{4\pi \epsilon_w k_B T} \right)^{3/2}}, \quad (\text{B6})$$

$$B'_{\text{Na}^+\text{Cl}^-} = -\frac{2\beta_{\text{Na}^+\text{Cl}^-}^1}{I_m x_1^2} \left[1 - (1 + x_1 + 0.5x_1^2) \exp(-x_1) \right], \quad (\text{B7})$$

$$x_1 = \alpha_1 \sqrt{I_m}, \quad (\text{B8})$$

$$B_{\text{Na}^+\text{Cl}^-} = \beta_{\text{Na}^+\text{Cl}^-}^0 + \frac{2\beta_{\text{Na}^+\text{Cl}^-}^1}{x_1^2} \left[1 - (1 + x_1) \exp(-x_1) \right], \quad (\text{B9})$$

$$C_{\text{Na}^+\text{Cl}^-} = \frac{C_{\phi \text{Na}^+\text{Cl}^-}}{2\sqrt{|z_{\text{Na}^+} z_{\text{Cl}^-}|}}, \quad (\text{B10})$$

547 where z_i is the charge number of ion i , b and α_1 are empirical parameters ($b = 1.2$, $\alpha_1 = 2$ for 1:1
548 and 1:2 electrolytes), I_m is the molal ionic strength (in mol kg_w⁻¹, $I_m = m_{\text{Na}^+}^w$ here), and A_ϕ is the
549 Debye-Hückel coefficient describing long-range electrostatic interaction forces between ions (\cong
550 0.392 at a temperature T of 298 K). The Debye-Hückel coefficient was computed here as a function
551 of the Avogadro number N_A ($\cong 6.022 \times 10^{23}$ sites mol⁻¹), the water volumetric density ρ_w (\cong
552 997×10^3 g m⁻³), and the water permittivity ϵ_w ($\cong 78.3\epsilon_0$ where ϵ_0 is the vacuum permittivity with
553 a value of $\cong 8.854 \times 10^{-12}$ F m⁻¹). The Debye-Hückel coefficient multiplied by the terms in brackets
554 in equation (B5) is enough for computing ion activity coefficient in dilute aqueous solution (ionic

555 strength below 0.1 M). Pitzer and Mayorga [65] considered three additional terms (in equations
556 (B4) and (B5)) to compute ion activity coefficients in concentrated aqueous solutions. The terms
557 $B_{\text{Na}^+\text{Cl}^-}$ and $B'_{\text{Na}^+\text{Cl}^-}$ depend on the ionic strength and describe short-range interaction forces between
558 one cation and one anion (binary system), and the term $C_{\text{Na}^+\text{Cl}^-}$ describes short-range interaction
559 forces between two cations and one anion, and one cation and two anions (ternary system). The
560 Pitzer model for ion activity coefficients in 1:1 aqueous electrolyte such as NaCl depends on three
561 parameters $\beta_{\text{Na}^+\text{Cl}^-}^0$, $\beta_{\text{Na}^+\text{Cl}^-}^1$, and $C_{\phi\text{Na}^+\text{Cl}^-}$. The Pitzer parameter values were adjusted by matching
562 computed to measured osmotic coefficients. According to [Leroy et al. [61]] $\beta_{\text{Na}^+\text{Cl}^-}^0 = 0.0765$,
563 $\beta_{\text{Na}^+\text{Cl}^-}^1 = 0.2664$, and $C_{\phi\text{Na}^+\text{Cl}^-} = 0.00127$.

- 565 [1] Y. Duval, J.A. Mielczarski, O.S. Pokrovsky, E. Mielczarski, J.J. Ehrhardt, Evidence of the existence of three
566 types of species at the quartz-aqueous solution interface at pH 0-10: XPS surface group quantification
567 and surface complexation modeling, *Journal of Physical Chemistry B* 106(11) (2002) 2937-2945,
568 <https://doi.org/10.1021/jp012818s>.
- 569 [2] G. Okay, P. Leroy, A. Ghorbani, P. Cosenza, C. Camerlynck, J. Cabrera, N. Florsch, A. Revil, Spectral
570 induced polarization of clay-sand mixtures: Experiments and modeling, *Geophysics* 79(6) (2014) E353-
571 E375, <https://doi.org/10.1190/Geo2013-0347.1>.
- 572 [3] D.A. Sverjensky, Prediction of surface charge on oxides in salt solutions: Revisions for 1 : 1 (M+L-)
573 electrolytes, *Geochimica Et Cosmochimica Acta* 69(2) (2005) 225-257,
574 <https://doi.org/10.1016/j.gca.2004.05.040>.
- 575 [4] Z. Qi, Y. Wang, H. He, D. Li, X. Xu, Wettability Alteration of the Quartz Surface in the Presence of Metal
576 Cations, *Energy & Fuels* 27(12) (2013) 7354-7359, <https://doi.org/10.1021/ef401928c>.
- 577 [5] F.K. Crundwell, On the Mechanism of the Dissolution of Quartz and Silica in Aqueous Solutions, *ACS*
578 *Omega* 2(3) (2017) 1116-1127, <https://doi.org/10.1021/acsomega.7b00019>.
- 579 [6] D. García, J. Lützenkirchen, V. Petrov, M. Siebentritt, D. Schild, G. Lefèvre, T. Rabung, M. Altmaier, S.
580 Kalmykov, L. Duro, H. Geckeis, Sorption of Eu(III) on quartz at high salt concentrations, *Colloids and*
581 *Surfaces A: Physicochemical and Engineering Aspects* 578 (2019) 123610,
582 <https://doi.org/10.1016/j.colsurfa.2019.123610>.
- 583 [7] A. Revil, P.W.J. Glover, Theory of ionic-surface electrical conduction in porous media, *Phys Rev B* 55(3)
584 (1997) 1757-1773, <https://doi.org/10.1103/PhysRevB.55.1757>.
- 585 [8] M.Z. Jaafar, J. Vinogradov, M.D. Jackson, Measurement of streaming potential coupling coefficient in
586 sandstones saturated with high salinity NaCl brine, *Geophysical Research Letters* 36(21) (2009),
587 <https://doi.org/10.1029/2009gl040549>.
- 588 [9] M. Skold, A. Revil, P. Vaudelet, The pH dependence of spectral induced polarization of silica sands:
589 Experiment and modeling, *Geophysical Research Letters* 38 (2011),
590 <https://doi.org/10.1029/2011GL047748>.
- 591 [10] A. Kemna, A. Binley, G. Cassiani, E. Niederleithinger, A. Revil, L. Slater, K.H. Williams, A.F. Orozco, F.H.
592 Haegel, A. Hordt, S. Kruschwitz, V. Leroux, K. Titov, E. Zimmermann, An overview of the spectral induced
593 polarization method for near-surface applications, *Near Surf Geophys* 10(6) (2012) 453-468,
594 <https://doi.org/10.3997/1873-0604.2012027>.
- 595 [11] A. Revil, M. Karaoulis, T. Johnson, A. Kemna, Review: Some low-frequency electrical methods for
596 subsurface characterization and monitoring in hydrogeology, *Hydrogeology Journal* 20(4) (2012) 617-
597 658, <https://doi.org/10.1007/s10040-011-0819-x>.
- 598 [12] A. Binley, S.S. Hubbard, J.A. Huisman, A. Revil, D.A. Robinson, K. Singha, L.D. Slater, The emergence of
599 hydrogeophysics for improved understanding of subsurface processes over multiple scales, *Water*
600 *Resources Research* 51(6) (2015) 3837-3866, <https://doi.org/10.1002/2015WR017016>.
- 601 [13] J. Vinogradov, M.Z. Jaafar, M.D. Jackson, Measurement of streaming potential coupling coefficient in
602 sandstones saturated with natural and artificial brines at high salinity, *Journal of Geophysical Research*
603 115(B12) (2010), <https://doi.org/10.1029/2010jb007593>.
- 604 [14] J. Vinogradov, M.D. Jackson, M. Chamerois, Zeta potential in sandpicks: Effect of temperature,
605 electrolyte pH, ionic strength and divalent cations, *Colloids and Surfaces A: Physicochemical and*
606 *Engineering Aspects* 553 (2018) 259-271, <https://doi.org/10.1016/j.colsurfa.2018.05.048>.
- 607 [15] E. Walker, P.W.J. Glover, Measurements of the Relationship Between Microstructure, pH, and the
608 Streaming and Zeta Potentials of Sandstones, *Transport Porous Med* 121(1) (2018) 183-206,
609 <https://doi.org/10.1007/s11242-017-0954-5>.

- 610 [16] M. Hidayat, M. Sarmadivaleh, J. Derksen, D. Vega-Maza, S. Iglauer, J. Vinogradov, Zeta potential of
611 CO₂-rich aqueous solutions in contact with intact sandstone sample at temperatures of 23 °C and 40 °C
612 and pressures up to 10.0 MPa, *Journal of Colloid and Interface Science* 607 (2022) 1226-1238,
613 <https://doi.org/10.1016/j.jcis.2021.09.076>.
- 614 [17] D.A. Sverjensky, Interpretation and prediction of triple-layer model capacitances and the structure of
615 the oxide-electrolyte-water interface, *Geochimica Et Cosmochimica Acta* 65(21) (2001) 3643-3655,
616 [https://doi.org/10.1016/S0016-7037\(01\)00709-8](https://doi.org/10.1016/S0016-7037(01)00709-8).
- 617 [18] Z. Brkljača, D. Namjesnik, J. Lützenkirchen, M. Předota, T. Preočanin, Quartz/Aqueous Electrolyte
618 Solution Interface: Molecular Dynamic Simulation and Interfacial Potential Measurements, *The Journal*
619 *of Physical Chemistry C* 122(42) (2018) 24025-24036, <https://doi.org/10.1021/acs.jpcc.8b04035>.
- 620 [19] T. Hiemstra, J.C.M. De Wit, W.H. Van Riemsdijk, Multisite proton adsorption modelling at the
621 solid/solution interface of (hydr)oxides: a new approach. II. Application to various important
622 (hydr)oxides, *Journal of Colloid and Interface Science* 133 (1989) 105-117,
623 [https://doi.org/10.1016/0021-9797\(89\)90285-3](https://doi.org/10.1016/0021-9797(89)90285-3).
- 624 [20] P. Leroy, N. Devau, A. Revil, M. Bizi, Influence of surface conductivity on the apparent zeta potential
625 of amorphous silica nanoparticles, *Journal of Colloid and Interface Science* 410 (2013) 81-93,
626 <https://doi.org/10.1016/j.jcis.2013.08.012>.
- 627 [21] C. Macias-Romero, I. Nahalka, H.I. Okur, S. Roke, Optical imaging of surface chemistry and dynamics
628 in confinement, *Science* 357(6353) (2017) 784-788, <https://doi.org/10.1126/science.aal4346>.
- 629 [22] A. Kitamura, K. Fujiwara, T. Yamamoto, S. Nishikawa, H. Moriyama, Analysis of adsorption behavior of
630 cations onto quartz surface by electrical double-layer model, *J Nucl Sci Technol* 36(12) (1999) 1167-
631 1175, <https://doi.org/10.1080/18811248.1999.9726312>.
- 632 [23] P. Leroy, C. Tournassat, O. Bernard, N. Devau, M. Azaroual, The electrophoretic mobility of
633 montmorillonite. Zeta potential and surface conductivity effects, *Journal of Colloid and Interface*
634 *Science* 451 (2015) 21-39, <https://doi.org/10.1016/j.jcis.2015.03.047>.
- 635 [24] R.J. Hunter, *Zeta Potential in Colloid Science: Principles and Applications*, Academic Press, New York,
636 1981.
- 637 [25] J. Lyklema, M. Minor, On surface conduction and its role in electrokinetics, *Colloids and Surfaces a-*
638 *Physicochemical and Engineering Aspects* 140(1-3) (1998) 33-41, [https://doi.org/10.1016/S0927-](https://doi.org/10.1016/S0927-7757(97)00266-5)
639 [7757\(97\)00266-5](https://doi.org/10.1016/S0927-7757(97)00266-5).
- 640 [26] A. Revil, P.A. Pezard, P.W.J. Glover, Streaming potential in porous media 1. Theory of the zeta potential,
641 *J Geophys Res-Sol Ea* 104(B9) (1999) 20021-20031, <https://doi.org/10.1029/1999jb900089>.
- 642 [27] A. Revil, D. Hermitte, E. Spangenberg, J.J. Cocheme, Electrical properties of zeolitized volcanoclastic
643 materials, *J Geophys Res-Sol Ea* 107(B8) (2002), <https://doi.org/10.1029/2001jb000599>.
- 644 [28] A. Crespy, A. Boleve, A. Revil, Influence of the Dukhin and Reynolds numbers on the apparent zeta
645 potential of granular porous media, *Journal of Colloid and Interface Science* (2007) 188-194,
646 <https://doi.org/10.1016/j.jcis.2006.09.038>.
- 647 [29] S. Li, P. Leroy, F. Heberling, N. Devau, D. Jougnot, C. Chiaberge, Influence of surface conductivity on
648 the apparent zeta potential of calcite, *J. Colloid Interface Sci.* 468 (2016) 262-75,
649 <https://doi.org/10.1016/j.jcis.2016.01.075>.
- 650 [30] P. Leroy, A. Revil, A triple-layer model of the surface electrochemical properties of clay minerals,
651 *Journal of Colloid and Interface Science* (2004) 371-380, <https://doi.org/10.1016/j.jcis.2003.08.007>.
- 652 [31] I.C. Bourg, G. Sposito, Molecular dynamics simulations of the electrical double layer on smectite
653 surfaces contacting concentrated mixed electrolyte (NaCl-CaCl₂) solutions, *Journal of Colloid and*
654 *Interface Science* 360(2) (2011) 701-715, <https://doi.org/10.1016/j.jcis.2011.04.063>.
- 655 [32] H. Zhang, A.A. Hassanali, Y.K. Shin, C. Knight, S.J. Singer, The water-amorphous silica interface: Analysis
656 of the Stern layer and surface conduction, *J Chem Phys* 134(2) (2011),
657 <https://doi.org/10.1063/1.3510536>.

- 658 [33] D. Biriukov, P. Fibich, M. Předota, Zeta Potential Determination from Molecular Simulations, The
659 Journal of Physical Chemistry C 124(5) (2020) 3159-3170, <https://doi.org/10.1021/acs.jpcc.9b11371>.
- 660 [34] M. Předota, M.L. Machesky, D.J. Wesolowski, Molecular Origins of the Zeta Potential, Langmuir 32(40)
661 (2016) 10189-10198, <https://doi.org/10.1021/acs.langmuir.6b02493>.
- 662 [35] P. Leroy, A. Mainault, Exploring the electrical potential inside cylinders beyond the Debye-Hückel
663 approximation: a computer code to solve the Poisson-Boltzmann equation for multivalent electrolytes,
664 Geophys J Int 214(1) (2018) 58-69, <https://doi.org/10.1093/gji/ggy124>.
- 665 [36] J. Westall, H. Hohl, A comparison of electrostatic models for the oxide/solution interface, Advances in
666 Colloid and Interface Science 12(4) (1980) 265-294, [https://doi.org/10.1016/0001-8686\(80\)80012-1](https://doi.org/10.1016/0001-8686(80)80012-1).
- 667 [37] M. Heuser, G. Spagnoli, P. Leroy, N. Klitzsch, H. Stanjek, Electro-osmotic flow in clays and its potential
668 for reducing clogging in mechanical tunnel driving, B Eng Geol Environ 71(4) (2012) 721-733,
669 <https://doi.org/10.1007/s10064-012-0431-x>.
- 670 [38] J. Lyklema, S. Rovillard, J. De Coninck, Electrokinetics: The properties of the stagnant layer unraveled,
671 Langmuir 14(20) (1998) 5659-5663, <https://doi.org/10.1021/la980399t>.
- 672 [39] M.A. Brown, A. Goel, Z. Abbas, Effect of Electrolyte Concentration on the Stern Layer Thickness at a
673 Charged Interface, Angewandte Chemie International Edition 55(11) (2016) 3790-3794,
674 <https://doi.org/10.1002/anie.201512025>.
- 675 [40] D. Lis, E.H.G. Backus, J. Hunger, S.H. Parekh, M. Bonn, Liquid flow along a solid surface reversibly alters
676 interfacial chemistry, Science 344(6188) (2014) 1138-1142, <https://doi.org/10.1126/science.1253793>.
- 677 [41] R. Saini, A. Garg, D.P. Barz, Streaming potential revisited: the influence of convection on the surface
678 conductivity, Langmuir 30(36) (2014) 10950-61, <https://doi.org/10.1021/la501426c>.
- 679 [42] B.L. Werkhoven, J.C. Everts, S. Samin, R. van Roij, Flow-Induced Surface Charge Heterogeneity in
680 Electrokinetics due to Stern-Layer Conductance Coupled to Reaction Kinetics, Physical Review Letters
681 120(26) (2018), <https://doi.org/10.1103/PhysRevLett.120.264502>.
- 682 [43] A. Alizadeh, M. Wang, Flexibility of inactive electrokinetic layer at charged solid-liquid interface in
683 response to bulk ion concentration, Journal of Colloid and Interface Science 534 (2019) 195-204,
684 <https://doi.org/10.1016/j.jcis.2018.09.010>.
- 685 [44] D.E. Yates, S. Levine, T.W. Healy, Site-binding Model of the Electrical Double Layer at the Oxide/Water
686 interface, Journal of the Chemical Society, Faraday Transactions 70 (1974) 1807-1818,
687 <https://doi.org/10.1039/F19747001807>.
- 688 [45] I. Siretanu, D. Ebeling, M.P. Andersson, S.L.S. Stipp, A. Philipse, M.C. Stuart, D. van den Ende, F. Mugele,
689 Direct observation of ionic structure at solid-liquid interfaces: a deep look into the Stern Layer, Scientific
690 reports 4(1) (2014), <https://doi.org/10.1038/srep04956>.
- 691 [46] S.R. Charlton, D.L. Parkhurst, Modules based on the geochemical model PHREEQC for use in scripting
692 and programming languages, Comput Geosci-Uk 37(10) (2011) 1653-1663,
693 <https://doi.org/10.1016/j.cageo.2011.02.005>.
- 694 [47] A. Mainault, Estimation of the electrical potential distribution along metallic casing from surface self-
695 potential profile, J Appl Geophys 129 (2016) 66-78, <https://doi.org/10.1016/j.jappgeo.2016.03.038>.
- 696 [48] P. Leroy, C. Tournassat, M. Bizi, Influence of surface conductivity on the apparent zeta potential of
697 TiO₂ nanoparticles, Journal of Colloid and Interface Science 356(2) (2011) 442-453,
698 <https://doi.org/10.1016/j.jcis.2011.01.016>.
- 699 [49] P. Leroy, D. Jougnot, A. Revil, A. Lassin, M. Azaroual, A double layer model of the gas bubble/water
700 interface, Journal of Colloid and Interface Science 388 (2012) 243-256,
701 <https://doi.org/10.1016/j.jcis.2012.07.029>.
- 702 [50] A. Mendieta, D. Jougnot, P. Leroy, A. Mainault, Spectral Induced Polarization Characterization of
703 Non - Consolidated Clays for Varying Salinities—An Experimental Study, Journal of Geophysical
704 Research: Solid Earth 126(4) (2021), <https://doi.org/10.1029/2020JB021125>.

- 705 [51] B. Lowden, S. Braley, A. Hurst, J. Lewis, Sedimentological studies of the Cretaceous Lochaline
706 Sandstone, NW Scotland, Geological Society, London, Special Publications 62(1) (1992) 159-162,
707 <https://doi.org/10.1144/gsl.sp.1992.062.01.14>.
- 708 [52] P.L. Churcher, P.R. French, J.C. Shaw, L.L. Schramm, Rock Properties of Berea Sandstone, Baker
709 Dolomite, and Indiana Limestone, Society of Petroleum Engineers Journal 21044 (1991) 20-22,
710 <https://doi.org/10.2118/21044-MS>.
- 711 [53] T.-f. Wong, C. David, W. Zhu, The transition from brittle faulting to cataclastic flow in porous
712 sandstones: Mechanical deformation, Journal of Geophysical Research: Solid Earth 102(B2) (1997)
713 3009-3025, <https://doi.org/10.1029/96jb03281>.
- 714 [54] S. Li, H. Collini, M.D. Jackson, Anomalous Zeta Potential Trends in Natural Sandstones, Geophysical
715 Research Letters 45(20) (2018), <https://doi.org/10.1029/2018GL079602>.
- 716 [55] M. Alarouj, H. Collini, M.D. Jackson, Positive Zeta Potential in Sandstones Saturated With Natural
717 Saline Brine, Geophysical Research Letters 48(20) (2021), <https://doi.org/10.1029/2021GL094306>.
- 718 [56] A. Alroudhani, J. Vinogradov, M.D. Jackson, Zeta potential of intact natural limestone: Impact of
719 potential-determining ions Ca, Mg and SO₄, Colloids and Surfaces A: Physicochemical and Engineering
720 Aspects 493 (2016) 83-98, <https://doi.org/10.1016/j.colsurfa.2015.11.068>.
- 721 [57] C. Schnitzer, S. Ripperger, Influence of Surface Roughness on Streaming Potential Method, Chem Eng
722 Technol 31(11) (2008) 1696-1700, <https://doi.org/10.1002/ceat.200800180>.
- 723 [58] A. Drechsler, A. Caspari, A. Snytska, Influence of roughness and capillary size on the zeta potential
724 values obtained by streaming potential measurements, Surf Interface Anal 52(12) (2020) 991-995,
725 <https://doi.org/10.1002/sia.6792>.
- 726 [59] J. Sonnefeld, A. Gobel, W. Vogelsberger, Surface-Charge Density on Spherical Silica Particles in
727 Aqueous Alkali Chloride Solutions .1. Experimental Results, Colloid Polym Sci 273(10) (1995) 926-931,
728 <https://doi.org/10.1007/Bf00660369>.
- 729 [60] A.C. Riese, Adsorption of radium and thorium onto quartz and kaolinite: A comparison of
730 solution/surface equilibrium models, Colorado School of Mines, 1982.
- 731 [61] P. Leroy, A. Lassin, M. Azaroual, L. Andre, Predicting the surface tension of aqueous 1:1 electrolyte
732 solutions at high salinity, Geochimica Et Cosmochimica Acta 74(19) (2010) 5427-5442,
733 <https://doi.org/10.1016/j.gca.2010.06.012>.
- 734 [62] F.A. Saadi, K.-H. Wolf, C.v. Kruijsdijk, Characterization of Fontainebleau Sandstone: Quartz Overgrowth
735 and its Impact on Pore-Throat Framework, Journal of Petroleum & Environmental Biotechnology 08(03)
736 (2017), <https://doi.org/10.4172/2157-7463.1000328>.
- 737 [63] M.A. Brown, Z. Abbas, A. Kleibert, R.G. Green, A. Goel, S. May, T.M. Squires, Determination of Surface
738 Potential and Electrical Double-Layer Structure at the Aqueous Electrolyte-Nanoparticle Interface,
739 Physical Review X 6(1) (2016), <https://doi.org/10.1103/PhysRevX.6.011007>.
- 740 [64] C.E. Harvie, J.H. Weare, The prediction of mineral solubilities in natural waters: the Na-K-Mg-Ca-Cl-
741 SO₄-H₂O system from zero to high concentration at 25 °C, Geochimica Et Cosmochimica Acta 44(7)
742 (1980) 981-997, [https://doi.org/10.1016/0016-7037\(80\)90287-2](https://doi.org/10.1016/0016-7037(80)90287-2).
- 743 [65] K.S. Pitzer, G. Mayorga, Thermodynamics of electrolytes. II. Activity and osmotic coefficients for strong
744 electrolytes with one or both ions univalent, The Journal of Physical Chemistry 77(19) (1973) 2300-
745 2308, <https://doi.org/10.1021/j100621a026>.

746

18 **Abstract**

19 The zeta potential is a measureable electrical potential of paramount importance to understand the
20 electrochemical properties of rocks. However, the zeta potential remains poorly understood
21 because it takes place at the nanoscale of the electrical double layer on the mineral surface.
22 Streaming potential measurements on quartz-rich Fontainebleau and Lochaline sandstones carried
23 out at high salinity (above 0.1 M NaCl) yield surprisingly high zeta potential values, which cannot
24 be correctly reproduced by a traditional surface complexation model considering that the shear
25 plane is located at the beginning of the diffuse layer. We found that placing the shear plane, where
26 the zeta potential is defined, slightly closer to the mineral surface than the Stern plane significantly
27 improves the predictions of the zeta potential and surface charge density of quartz at high salinity
28 as well as the values of the equilibrium constant describing sodium adsorption in the Stern layer.
29 Our results have strong implications for the modelling of the electrochemical properties of minerals
30 in contact with highly saline solutions.

31

32 Key words: zeta potential, quartz, streaming potential, high salinity, shear plane location

33 **1. Introduction**

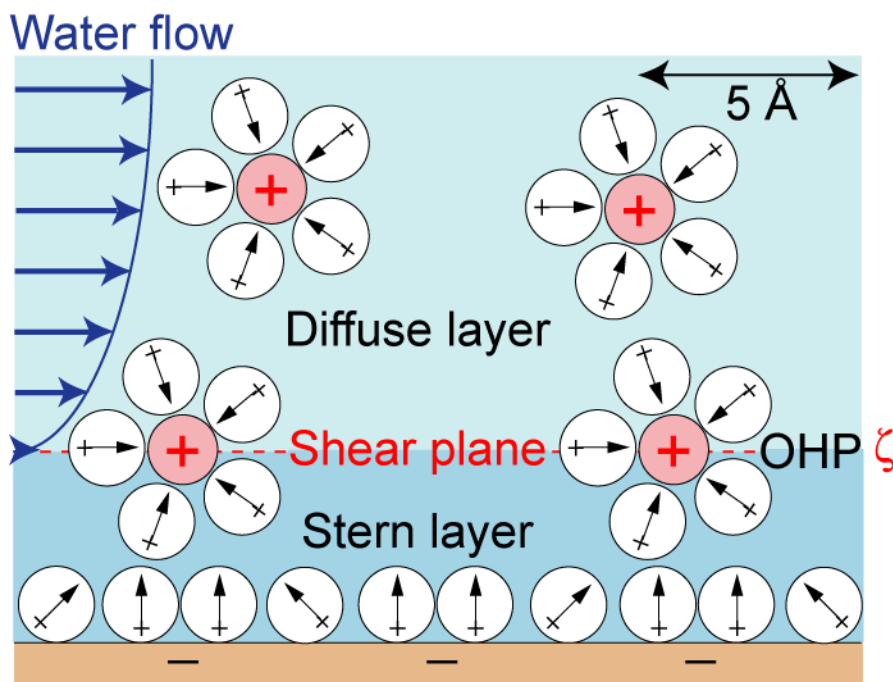
34 Quartz is a mineral that is particularly interesting to study because of its natural abundance and
35 usefulness in the development of new technologies [1]. In contact with water, quartz develops a
36 surface charge attracting counter-ions and repelling co-ions, thus forming the so-called electrical
37 double layer (EDL) usually represented by a “compact” Stern layer and a diffuse layer [2, 3].
38 Investigating the electrochemical properties of quartz is of great interest in many applications in
39 physics, chemistry and Earth sciences because these properties control adsorption and
40 dissolution/precipitation reactions, and wettability on the quartz surface [4-6]. The EDL of quartz
41 is also the source of electrokinetic and geophysical electrical (e.g., self-potential, resistivity,
42 induced polarization) measurements that are used to map for instance geological fluid flows or
43 biogeochemical reactions [7-12]. Studying quartz electrochemical properties notably when quartz
44 is in contact with highly saline brines has a high potential in many geo-environmental and
45 engineering applications including geo-sequestration of CO₂ in deep saline aquifers, and oil and
46 gas exploration and production notably enhanced hydrocarbon recovery [13-17].

47 Exploring the electrochemical properties of quartz is very challenging because of their nanoscopic
48 nature [1, 18, 19]. Indeed, surface complexation reactions between surface sites and ions in the
49 aqueous solution occur at the nm-scale [3, 20-22]. In addition, natural quartz has a low specific
50 surface area (typically below 0.1 m² g⁻¹), which considerably complicates the experimental
51 characterization of its EDL compared to minerals with a large specific surface area such as
52 montmorillonite [2, 3, 23, 24]. Only few methods exist to probe the properties of the EDL on the
53 surface of minerals in contact with brines. Among them, there is the streaming potential method,
54 which implies application of a water pressure difference across the sample while measuring the
55 resulting voltage, the streaming potential, due to the displaced excess counter-ions in the EDL [25-

56 30]. From the measured streaming potential it is possible to obtain some relevant information on
57 the electrochemical properties of minerals through the calculation of the electrokinetic zeta
58 potential (ζ), which is defined as the electrical potential at the shear (or slip) plane [17, 25, 27].
59 The zeta potential determined experimentally can be interpreted in terms of mineral
60 electrochemical properties by matching observed and simulated zeta potential using a relevant
61 surface complexation model [21, 30, 31]. However, this approach relies on the assumption that the
62 exact location of the shear plane from the mineral surface is known, which is obviously not the
63 case because of the lack of experimental information at the molecular level [32-35]. Moreover, the
64 zeta potential is, most of the times, the only physico-chemical quantity available to validate the
65 predictions of electrostatic surface complexation models for low specific surface area minerals
66 such as quartz or calcite [3, 30, 36]. In addition, the zeta potential is inferred from electro-
67 hydrodynamic measurements while surface complexation models rely on electrostatics at
68 thermodynamic equilibrium [25, 35, 37, 38]. Therefore, these limitations contribute to additional
69 uncertainties when investigating mineral electrochemical properties from zeta potential
70 measurements.

71 When water flow relative to the mineral surface takes place, it is widely accepted that the shear
72 plane is located between the “stagnant” Stern layer bounded by the outer Helmholtz plane (OHP)
73 and the diffuse layer because high water viscosity in the Stern layer prevents water flow within it
74 [3, 25, 39] (Figure 1). The Stern layer of silica-based materials such as amorphous silica and quartz
75 in contact with a NaCl solution is traditionally represented by a hydration layer followed by a layer
76 containing hydrated sodium counter-ions [18, 21, 40]. Some molecular dynamic (MD) simulations
77 (e.g., Zhang et al. [33]), spectroscopy measurements (e.g., Lis et al. [41]) and microfluidic studies
78 (e.g., Saini et al. [42] and Werkhoven et al. [43]) have demonstrated that there could be a non-zero

79 flow of water within the Stern layer of silica notably because some counter-ions (such as Na^+) are
80 not stucked to the mineral surface and form outer sphere surface complexes keeping their hydration
81 shell. This implies that there may be some, even weak, water displacement within the Stern layer
82 of silica, and hydrous oxide in general. Therefore, for quartz, the effective shear plane may be
83 located slightly closer to the mineral surface than the outer Helmholtz plane, in agreement with the
84 assumption accepted by most that the shear plane is located at the proximity of the OHP (e.g.,
85 Hunter [25], Sverjensky [3], García et al. [6]).



86
87 **Figure 1.** Sketch showing water flow and ion distribution at the interface between a silica mineral
88 and a NaCl aqueous solution (modified, from Brown et al. [40]). Circles with arrows inside
89 represent water molecules. The shear plane is denoted by the red dashed line. Counter-ions
90 adsorbed as outer sphere complexes form the outer Helmholtz plane (OHP).

91
92 The quartz (0001) crystal face is the most stable plane with the lowest surface energy and is often
93 considered as a “model surface”, convenient for modelling SiO_2 materials and hydrophilic surfaces

94 in general [35]. With the improved accuracy of the streaming potential method, it is now possible
95 to accurately measure extremely small voltages due to the displacement of the ions in the EDL of
96 quartz [14]. Published studies of Jaafar et al. [8], Vinogradov et al. [13], Walker et al. [44], and
97 Walker and Glover [15] observed, that at high salinities (NaCl concentrations above 0.4 M, M
98 means mol L⁻¹), the zeta potential of sandstones appears to level off at a small constant negative
99 value between -30 and -10 mV or even to increase slightly in magnitude (i.e. become more
100 negative) with salinity. They noted that the zeta potential of sandstones stabilizes at a salinity of
101 about 0.4 M NaCl that corresponds to a Debye length characterizing the diffuse layer thickness of
102 approximately 0.47 nm, which is similar to the size of a hydrated sodium ion. This observation led
103 them to suggest that the constant zeta potential of sandstones at high salinities reflected the
104 maximum charge density in the diffuse layer which was reached when the diffuse layer thickness
105 approached the diameter of the counter-ions [45]. However, Jaafar et al. [8], Vinogradov et al. [13],
106 Walker et al. [44], Glover [45], and Walker and Glover [15] did not explicitly explain this behavior
107 through a basic Stern surface complexation model describing their zeta potential measurements on
108 sandstones.

109 In our study, we used a surface complexation model named basic Stern model (BSM) and
110 considered that the shear plane is at the OHP or closer to the mineral surface than the OHP to
111 describe the zeta potential and the electrochemical properties of quartz at varying NaCl
112 concentrations. In our model we described the effective location of the OHP and the shear plane,
113 hence modelling the effective zeta potential. Therefore, the developed surface complexation model
114 accurately replicated the experimental conditions under which the streaming potential
115 measurements on intact rock samples comprising grains of various shape and roughness were
116 conducted. The model predictions were compared to the existing experimental zeta potential data

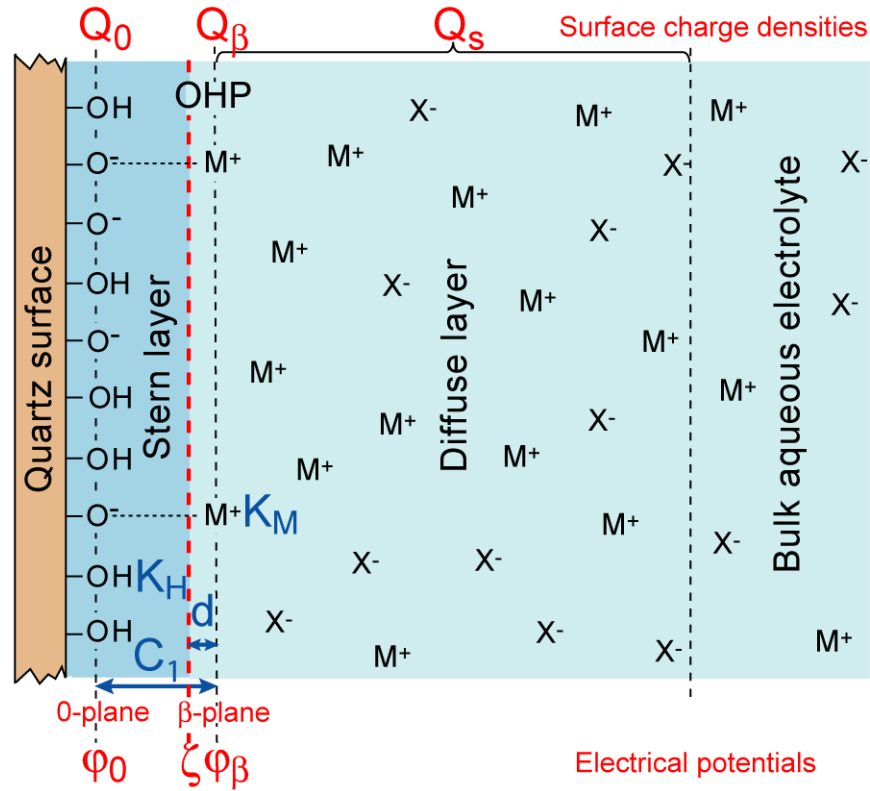
117 measured over a broad salinity range (from around 10^{-4} M NaCl up to around 5.5 M NaCl). The
118 values of the optimized parameters were finally discussed. Our findings shed light on the
119 electrochemical properties of quartz and on the likelihood of non-zero water flow within the Stern
120 layer.

121

122 **2. Theoretical background**

123 *2.1. Surface complexation model for quartz*

124 Our basic Stern model [37, 46] describes proton (H^+) adsorption onto $>SiO^-$ surface sites at the 0-
125 plane (defining the mineral surface) and sodium cation (Na^+) adsorption by these surface sites at
126 the β -plane (Stern plane and OHP) (Figure 2) [3, 6, 20, 21, 23]. The BSM considers that the β -
127 plane coincides with the d -plane defining the start of the diffuse layer. This model only needs one
128 Stern layer capacitance as an input parameter to model the electrical potential distribution between
129 the mineral surface and the Stern plane. Recent studies utilizing atomic force microscopy (AFM)
130 (e.g., Siretanu et al. [47]) and X-ray photoelectron spectroscopy (XPS) (e.g., Brown et al. [40])
131 used the BSM to model the electrochemical properties of amorphous silica in contact with a NaCl
132 aqueous solution and demonstrated that the BSM could accurately reproduce the experimental data.
133 García et al. [6] also used the BSM to match the measured electrochemical properties of quartz in
134 contact with a NaCl aqueous solution thus confirming the validity of the approach.



135
 136 **Figure 2.** Sketch of our basic Stern model to describe the electrochemical properties of the interface
 137 between quartz and a 1:1 electrolyte like NaCl electrolyte (the β -plane coincides with the d -plane).
 138 The model input parameters are shown in blue and the model output parameters, including the zeta
 139 potential (ζ) at the shear plane, are shown in red.

140
 141 In our BSM we used four adjustable parameters, namely the logarithms of the two adsorption
 142 equilibrium constants K_H and K_{Na} , the Stern layer capacitance C_1 ($F\ m^{-2}$), and the distance d
 143 between the shear plane (where the zeta potential is defined) and the β -plane (Figure 2). It should
 144 be noted that we considered that the doubly coordinated surface groups ($>Si_2O^0$) are inert [20] and
 145 that the protonated silanol sites ($>SiOH_2^+$) are not expected to form at close-to-neutral pH of the
 146 streaming potential measurements on sandstones (pH varied between 6.4 and 7.3 Walker and
 147 Glover [15]). Therefore, these surface sites were excluded from the model. In absence of additional

148 measurements, we also did not consider another type of silanol group, hence we made our model
149 as simple as possible in order to decrease the number of optimized parameters. For more
150 information related to our BSM, the reader can refer to Appendixes A and B, and to Leroy et al.
151 [21].

152

153 2.2. Zeta potential computation

154 All calculations were performed by combining the geochemical software IPhreeqc for the surface
155 complexation modelling [48] with an in-house code implemented in Matlab for the calculation of
156 the zeta potential and the optimization procedure [49]. The zeta potential (ζ) defined at the shear
157 plane located at a distance d from the β -plane was determined from the computed φ_0 and φ_β
158 electrical potentials by considering a linear, capacitor-like variation of the electrical potential
159 within the Stern layer [25]

$$\zeta = \varphi_\beta - \left(\frac{\varphi_\beta - \varphi_0}{x_\beta - x_0} \right) d, \quad (1)$$

160 where x is the distance from the mineral surface (defined by the 0-plane, in m). Combining equation
161 (1) with the following equation for the Stern layer capacitance [18]

$$C_1 = \frac{\varepsilon_1}{x_\beta - x_0}, \quad (2)$$

162 where ε_1 is the water permittivity in the Stern layer (F m^{-1} ; we used $\varepsilon_1 = 43\varepsilon_0$, where ε_0 is the
163 vacuum permittivity, in accordance with the study of Sverjensky [3]), we finally obtain an
164 expression for the zeta potential as a function of the modelled electrochemical properties

$$\zeta = \varphi_\beta - (\varphi_\beta - \varphi_0) \frac{C_1}{\varepsilon_1} d. \quad (3)$$

165 We did not consider the presence of a stagnant diffuse layer (also named buffer layer), which
 166 implies that the shear plane is located further away from the mineral surface, as suggested in
 167 Alizadeh and Wang [50]. To the best of our knowledge, the stagnant diffuse layer existence has
 168 never been directly confirmed experimentally. To the contrary, Předota et al. [35], Brkljača et al.
 169 [19], and Biriukov et al. [34] predicted no such stagnant diffuse layer from their molecular dynamic
 170 simulations of the zeta potential of the hydroxylated (110) rutile (TiO₂) and (0001) quartz surfaces.
 171 Furthermore, Leroy and co-workers. Furthermore, Leroy and co-workers (e.g., Leroy et al. [51],
 172 Leroy et al. [52], Leroy et al. [21], Li et al. [30]) attributed the assumption of the presence of a
 173 stagnant diffuse layer in previous studies to the misinterpretation of the zeta potentials from
 174 electrokinetic (e.g., electrophoretic mobility, streaming potential) measurements due to disregard
 175 of surface conductivity effects. Indeed, surface conductivity decreases the magnitude of the
 176 measured electrokinetic signal hence implying smaller apparent zeta potentials, which need to
 177 move away the shear plane from the mineral surface when modelling the zeta potential from a
 178 surface complexation model.

179 The parameters of our surface complexation model ($\log K_H$, $\log K_{Na}$, C_1 , d) were optimized by
 180 minimizing the following cost function [53]:

$$y = 1 - R^2 = \frac{\sum_{i=1}^N (\zeta_{mes}^i - \zeta_{mod}^i)^2}{\sum_{i=1}^N (\zeta_{mes}^i - \langle \zeta_{mes} \rangle)^2}, \quad (4)$$

181 where R^2 is the coefficient of determination, N is the number of zeta potential measurements, ζ_{mes}^i
 182 is the i -th measured zeta potential, $\langle \zeta_{mes} \rangle$ is the arithmetic mean of the measured zeta potentials,

183 and ζ_{mod}^i is the i -th modelled zeta potential. The fitting procedure was realized by using the
184 simulated annealing algorithm to find the global minimum of the cost function (equation (4)), with
185 a refinement using the simplex method at the end of the process [49].

186

187 **3. Comparison with experimental data and discussion**

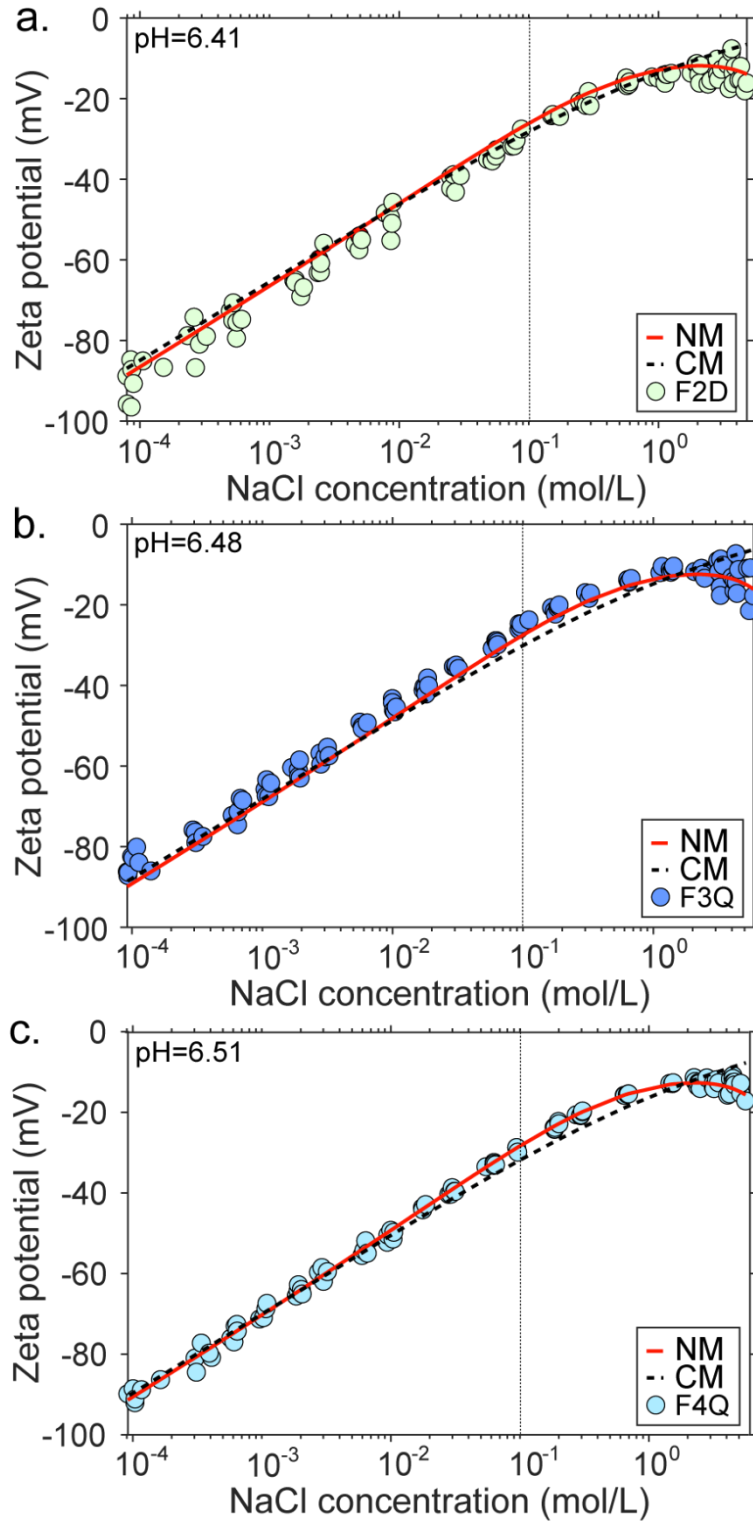
188 *3.1. Considerations of impact of pore space topology and grain roughness on EDL parameters*

189 To test our model, we used the measured zeta potentials of Fontainebleau (F2D, F3Q, F4Q) and
190 Lochaline (L3Q, L4Q) samples in contact with a NaCl aqueous solution of increasing salinity
191 obtained by the streaming potential method and reported in Walker and Glover [15]. These two
192 sample types were selected as they are known to consist of more than 99% quartz (by weight) [13,
193 54]. Unlike Fontainebleau and Lochaline samples, zeta potentials of Berea and Boise sandstones
194 reported by Walker and Glover [15] that contained up to 6% feldspar, 2% dolomite, and 8% clays
195 for Berea rocks [55] and up to 13% clays for Boise rocks [56], were excluded from the simulation.
196 Despite the fact that feldspar, dolomite, and clay content in Berea and Boise samples is relatively
197 small, clays are known to line pore walls, thus making these complex minerals a main contributor
198 to the electrochemical processes at the mineral-water interface and causing anomalous or even
199 positive zeta potentials [57, 58]. Therefore, the experimental zeta potential data for Boise and Berea
200 samples were deemed unapplicable for our model that considers only surface complexation
201 reactions on quartz surface.

202 All Fontainebleau and Lochaline samples exhibit a negative zeta potential with its magnitude
203 decreasing with increasing salinity (Figures 3 and 4). The zeta potentials of Lochaline samples

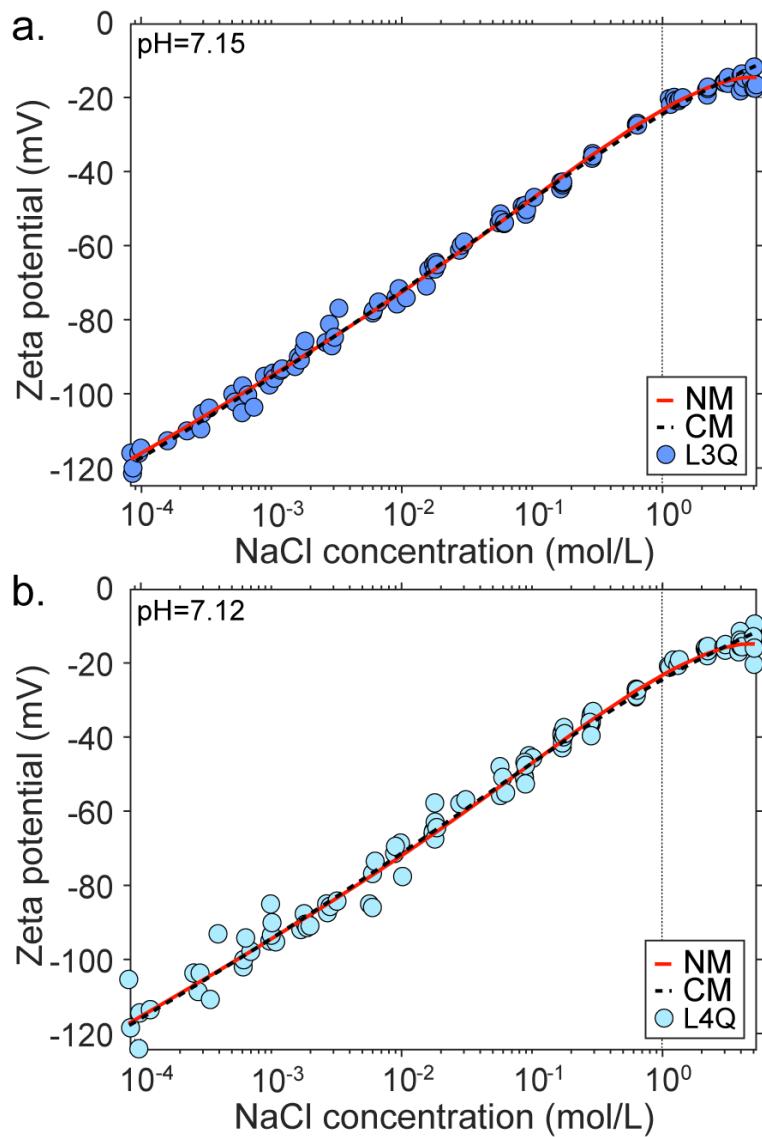
204 were found to be of a larger magnitude than those of Fontainebleau samples. Scanning electron
205 microscopy (SEM) micrographs of the tested samples showed that Fontainebleau rock has sharper-
206 angled grains with larger surface roughness and smaller grains than Lochaline rock (Figure 5 from
207 Walker and Glover [15]). According to Vinogradov et al. [14], pore space topology, grain shape,
208 surface roughness and size influence streaming potential measurements. They considered that
209 rough rocks with small grains have smaller streaming and zeta potential magnitudes than round,
210 smooth rocks with large grains because rock sharp corners and grain roughness would shift the
211 effective shear plane further away from the mineral surface (read their section 4.2). Alroudhan et
212 al. [59] used the same assumption to explain that the zeta potential of colloidal suspensions
213 measured by the electrophoretic mobility method is larger in magnitude than the zeta potential of
214 rocks measured by the streaming potential method (see their Figure 10 and read the related
215 discussion in their section 5.2). Schnitzer and Ripperger [60] and Drechsler et al. [61] showed that
216 increasing surface roughness changes the flow velocity distribution on the solid surface shifting
217 the shear plane further away from the solid surface and decreases the streaming and zeta potential
218 magnitudes. According to these observations, we expected different values of the surface
219 complexation model parameters between Fontainebleau and Lochaline samples, notably for the
220 Stern layer capacitance C_1 and the distance d of the shear plane from the OHP (or Stern plane),
221 which are very sensitive to the textural properties of rocks (C_1 depends on the thickness of the
222 Stern layer, equation (2)).

223



224

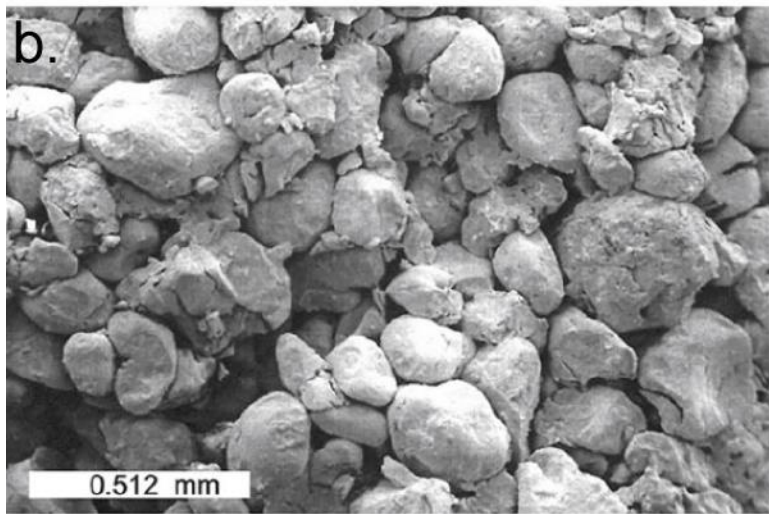
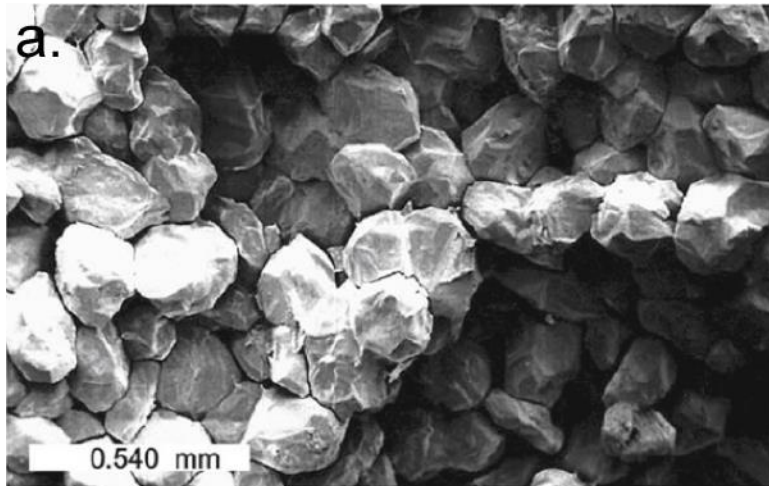
225 **Figure 3.** Zeta potentials of Fontainebleau samples as a function of NaCl concentration. Circle
 226 symbols: experimental zeta potential data with the sample name corresponding to that used by
 227 Walker and Glover [15]; curves: model predictions.



228

229 **Figure 4.** Zeta potentials of Lochaline samples as a function of NaCl concentration. Circle symbols:
 230 experimental zeta potential data with the sample name corresponding to that used by Walker and
 231 Glover [15]; curves: model predictions.

232



233
234 **Figure 5.** SEM micrographs of Fontainebleau (a) and Lochaline (b) rocks (modified from Walker
235 and Glover [15]).

236
237 Figures 3 and 4 demonstrate that below the concentration thresholds of around 0.1 M NaCl
238 (Fontainebleau samples) and 1 M NaCl (Lochaline samples) (denoted by the vertical black dotted
239 lines), the magnitude of the negative zeta potential decreases linearly with increasing salinity.
240 Interestingly, the rate of decrease in the zeta potential magnitude with increasing salinity became
241 smaller above these thresholds, i.e. it became non-linear, and eventually stabilized (or even slightly

242 increased in magnitude) at a zeta potential value of approximately -15 mV for both rock types.
243 Such stabilization of the zeta potential was more apparent for Fontainebleau than for Lochaline
244 samples. These observations were consistent across the data reported by Vinogradov et al. [13],
245 Vinogradov et al. [14] and Walker and Glover [15], who stated that at high salinities, the measured
246 zeta potential stabilized and became equal to -13.01 ± 0.48 mV for Fontainebleau samples and to
247 -16.81 ± 0.68 mV for Lochaline samples.

248 Considering that Fontainebleau and Lochaline sandstones did not have the same pore space
249 topology and textural properties, we first optimized separately the parameters of the surface
250 complexation models for these two rock types. That is, a single model was developed for F2D,
251 F3Q, F4Q combined data (Fontainebleau rocks) and a separate model was developed for L3Q, L4Q
252 combined data (Lochaline rocks) to match simulated to observed zeta potentials. We ran the
253 classical model denoted CM with the parameters $\log K_H$, $\log K_{Na}$, and C_1 , and the new model
254 denoted NM with the parameters $\log K_H$, $\log K_{Na}$, C_1 , and d (the distance of separation between
255 the shear plane and OHP), to investigate the effect of the proposed inward shift of the shear plane
256 on the simulated zeta potential while assigning measured pH values to the respective rock samples
257 as reported by Walker and Glover [15]. We then used the same BSM approach for Fontainebleau
258 and Lochaline samples together (all five samples, F2D, F3Q, F4Q, L3Q, L4Q) to develop a unified
259 surface complexation model for quartz in contact with a NaCl aqueous solution, denoted UNM for
260 unified new model and UCM for unified classical model.

261

262

263

264 *3.2. Comparison of the computed to the observed zeta potentials and discussion*

265 Overall, both the NM and CM reproduced well the experimental zeta potential data for the entire
266 salinity range (Figures 3 and 4, and Tables 1 and 2). To estimate the uncertainties, we fixed
267 two/three of the three/four parameters at their optimal values and then we computed the cost
268 function (i.e., $y=1-R^2$) for the remaining parameter which is allowed to vary. Afterwards, we
269 computed the relative cost function associated to the varying parameter $(y-y_{\text{opt}})/y_{\text{opt}}$, where y_{opt} is
270 the value of the cost function when the three/four parameters are fixed at their optimal values (so
271 the relative cost function associated to the varying parameter is equal to zero for the optimal set of
272 parameters). Finally, we extracted the range of values of the varying parameter for which the
273 relative cost function is less than 0.1. We performed this procedure for the three/four parameters.

274 According to the surface complexation models, the observed negative zeta potential was due to the
275 presence of the deprotonated silanol sites $>\text{SiO}^-$ at the 0-plane (Figure 2). The optimized values of
276 the equilibrium constant describing protonation of $>\text{SiO}^-$ surface sites (K_{H} , reaction (1)) equal to
277 $10^{7.3}$ and $10^{7.2}$ for Fontainebleau and Lochaline samples, respectively, were found to be close or
278 similar to the spectroscopically determined value of $10^{7.2\pm 0.2}$ and to the theoretical value of $10^{7.5}$
279 using Pauling's definition of formal bond valence for silica [20] (Table 1). In addition, our K_{H}
280 optimized values were found to be close or similar to the value of $10^{7.2}$ determined by Sverjensky
281 [3] using a triple layer model (BSM with an additional C_2 capacitance between the Stern plane and
282 the start of the diffuse layer) matching surface charge density measurements inferred from acid
283 base potentiometric titration on natural quartz in contact with a NaCl solution. The models also
284 explained why the zeta potential magnitude of Lochaline samples was larger, for the same salinity,
285 than the zeta potential magnitude of Fontainebleau samples. Indeed, Lochaline samples have higher

286 pH (i.e. less protons in solution) than Fontainebleau samples (7.1 versus 6.5 in average,
 287 respectively Walker and Glover [15]) while having essentially identical $\log K_H$ values, which
 288 resulted in Lochaline samples having larger number of deprotonated $>SiO^-$ sites per nm^2 of surface
 289 and a higher negative surface charge density Q_0 (equation (A5)) than Fontainebleau samples
 290 (Figure 6).

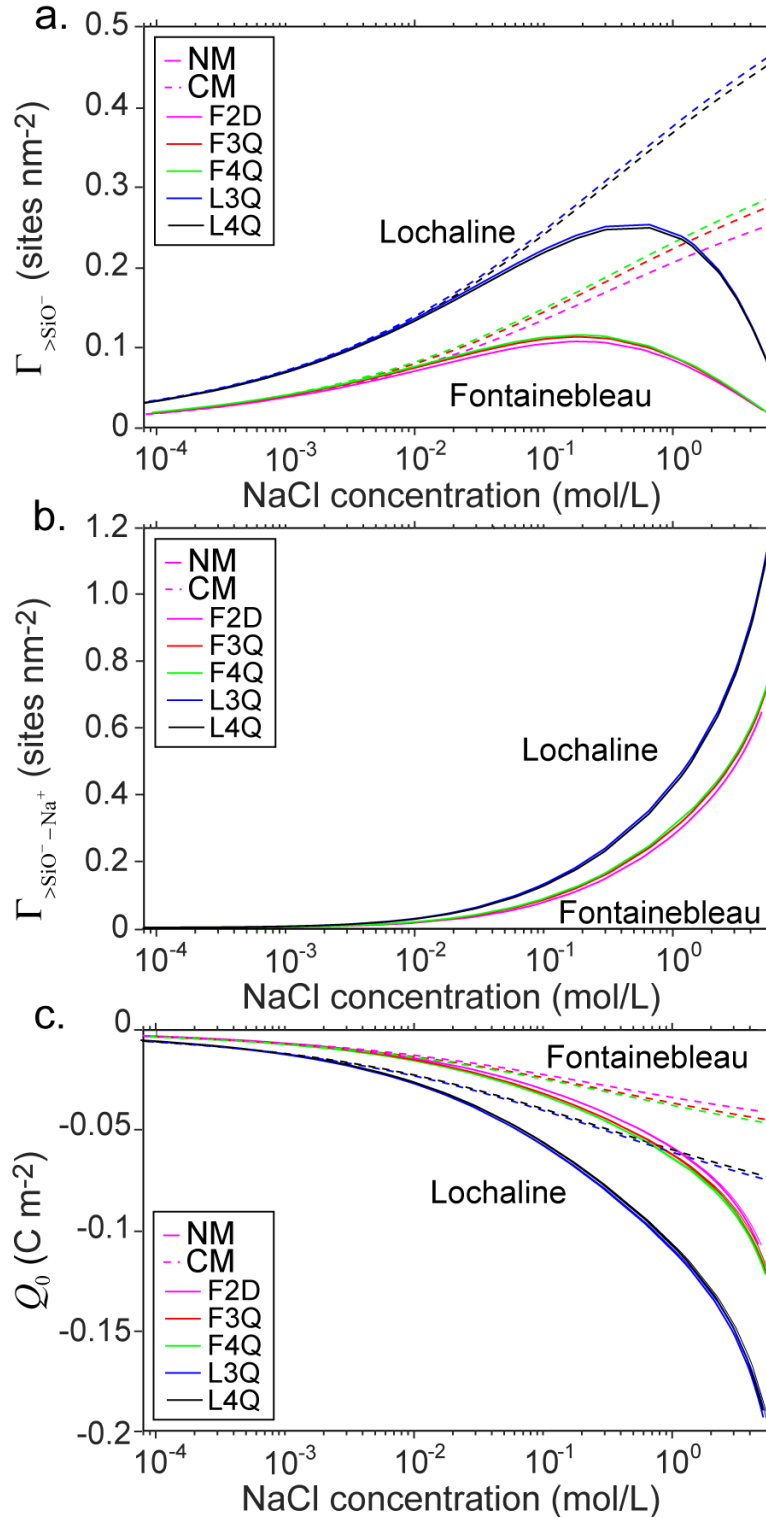
291 **Table 1.** BSM parameter values and estimated Stern layer thickness for Fontainebleau and
 292 Lochaline sandstones.

Symbols	Range ¹	Fontainebleau		Lochaline	
		CM	NM	CM	NM
$\log K_H$	[4 10]	7.32 [7.28 7.36]	7.27 [7.24 7.3]	7.21 [7.18 7.24]	7.24 [7.21 7.27]
$\log K_{Na}$	[-20 5]	-20 [ND ³]	0.58 [0.25 0.83]	-20 [ND ³]	0.13 [-0.1 0.32]
C_1 (F m ⁻²)	[0.5 5]	3.24 [2.01 6.54]	1.34 [1.18 1.51]	1.84 [1.62 2.10]	2.22 [2.01 2.47]
d (Å)	[0 10]	0	0.48 [0.42 0.54]	0	0.25 [0.21 0.28]
d_{Stern}^2 (Å)		1.18 [0.58 1.89]	2.85 [2.52 3.23]	2.07 [1.81 2.35]	1.71 [1.54 1.89]

293
 294 ¹ Hiemstra et al. [20], Kitamura et al. [23], Sonnefeld et al. [62], Sverjensky [3], García et al. [6].

295 ² According to Eq. (2) and fitted C_1 values, considering $\epsilon_1 = 43\epsilon_0$ and $d_{Stern} = x_\beta - x_0$.

296 ³ Not determined.



297

298 **Figure 6.** Computed surface site densities of $> \text{SiO}^-$ sites (a), $> \text{SiO}^- - \text{Na}^+$ sites b), and of surface
 299 charge densities (c) of Fontainebleau and Lochaline samples as a function of NaCl concentration.
 300 Plain line curves correspond to the calculations using the NM, dotted line curves correspond to the

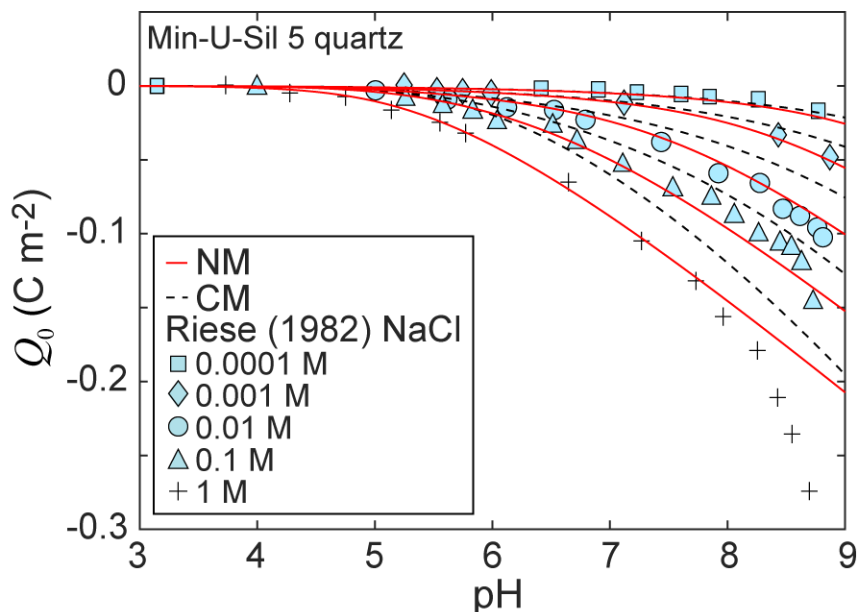
301 calculations using the CM. The CM predicted near-zero surface site densities of adsorbed sodium
302 ion in the Stern layer (limited at $\cong 0$ sites nm^{-2} in Figure 6b).

303

304 We also found that Lochaline samples have significantly lower $\log K_{\text{Na}}$ values, i.e. weaker sodium
305 adsorption capacity, than Fontainebleau samples (-21 vs -16, respectively, for CM and 0.1 vs 0.6,
306 respectively, for NM, Table 1), which could not counterbalance the negative surface charge density
307 as efficiently as for Fontainebleau samples, and can also explain the larger zeta potential magnitude
308 of Lochaline samples. Interestingly, despite Lochaline samples having lower $\log K_{\text{Na}}$ values than
309 Fontainebleau samples, the models found that Lochaline samples, for the same salinity, had a
310 higher surface site density of adsorbed sodium ion in the Stern layer than Fontainebleau samples
311 due to the higher $>\text{SiO}^-$ surface site density (Figure 6b). The lower $\log K_{\text{Na}}$ values of Lochaline
312 than Fontainebleau samples we found can be explained by Lochaline samples having smoother and
313 larger grains and hence a smaller specific surface area than Fontainebleau samples. Sverjensky [3]
314 did the same observation when comparing two quartz with different specific surface area (4.15 and
315 $11.4 \text{ m}^2 \text{ g}^{-1}$) in contact with a NaCl solution. The K_{Na} values inferred from the CM are extremely
316 low and essentially mean that there is no adsorption of Na^+ at the OHP at all and everything is
317 controlled only by pH. With the CM, the optimization procedure decreases K_{Na} to extremely low
318 value to fit the high salinity zeta potential measurements (decreasing Na^+ adsorption in the Stern
319 layer results to higher zeta potential magnitude).

320 With the NM, the optimization procedure doesn't need to decrease K_{Na} to extremely low value to
321 fit the high salinity zeta potential measurements and it found $\log K_{\text{Na}}$ values (0.6 and 0.1 for
322 Fontainebleau and Lochaline samples, respectively) within the same order of magnitude than the

323 value reported by Sverjensky [3] for natural quartz in a contact with a NaCl solution ($\log K_{\text{Na}} = 0$).
 324 In addition, on the contrary to the CM, our NM was able to reproduce most of the surface charge
 325 density measurements on Min-U-Sil 5 quartz (natural quartz with a mean grain diameter of 5 μm)
 326 at different pH and NaCl concentrations carried out by Riese [63] (Figure 7).



327
 328 **Figure 7.** Surface charge density of Min-U-Sil 5 quartz as a function of pH and NaCl concentration.
 329 Curves correspond to the predictions. Symbols correspond to the experimental surface charge
 330 density data reported by Riese [63].

331
 332 With the NM, the optimized Stern layer capacitance values were equal to 1.3 F m^{-2} and 2.2 F m^{-2}
 333 for Fontainebleau and Lochaline samples, respectively (Table 1), which were close to the values
 334 of 1 F m^{-2} and 2 F m^{-2} reported by Sverjensky [3] and García et al. [6], respectively, for natural
 335 quartz in contact with a NaCl solution. With the CM, the optimized Stern layer capacitance values
 336 were equal to 3.2 F m^{-2} and 1.8 F m^{-2} for Fontainebleau and Lochaline samples, respectively. Using
 337 the optimized Stern layer capacitance values from the NM, equation (2) and $\varepsilon_1 = 43\varepsilon_0$ [3, 40], we

338 found a Stern layer thickness comparable to the hydrated radius of sodium ion ($\cong 2 \text{ \AA}$ Leroy et al.
339 [64] Sverjensky [18]), with Fontainebleau samples having larger Stern layer thickness (2.8 \AA) than
340 Lochaline samples (1.7 \AA), which can be explained by Fontainebleau samples having sharper and
341 rougher grains than Lochaline samples [15, 65]. When using the CM, the Stern layer thickness we
342 found for Fontainebleau samples (1.2 \AA) was comparable to the crystallographic radius of sodium
343 ion (1.02 \AA Sverjensky [18]). This result was not realistic regarding the representation of the
344 quartz/NaCl solution interface containing mostly hydrated sodium ions in the Stern layer, which is
345 accepted by most recent models (e.g., Brown et al. [66]). For Lochaline samples, the Stern layer
346 thickness inferred from the CM was comparable to the hydrated radius of sodium ion (2.1 \AA).

347 Figures 3, 4, 7, and the modelling results reported in Table 1 for the parameter values and in Table
348 2 for the coefficient of determination values clearly demonstrate the importance of considering the
349 location of the shear plane to be closer to the mineral surface than the OHP. Indeed, as shown in
350 Figures 3 and 4 and reflected by the values of the coefficient of determination at high salinity
351 reported in Table 2 ($R^2 \geq 0.5$), the stabilization of the zeta potential at high salinity could only be
352 correctly predicted by the NM (red curves in Figures 3 and 4). The stabilization of the modelled
353 zeta potential at high salinity is explained by a growing abundance of sodium ions available for
354 adsorption in the Stern layer, and therefore the decreasing number of $>\text{SiO}^-$ sites (Figures 6a and
355 6b), and importantly by the shear plane being located slightly closer to the mineral surface than the
356 OHP. Moreover, the NM reproduced the surface charge density measurements on natural quartz in
357 a NaCl solution reported in Riese [63] significantly better than the CM (Figure 7) thus
358 independently validating our assumption on the location of the shear plane.

359

360 **Table 2.** Coefficient of determination values using different BSM parameter values for
 361 Fontainebleau and Lochaline sandstones.

	F2D		F3Q		F4Q		L3Q		L4Q	
	CM	NM	CM	NM	CM	NM	CM	NM	CM	NM
365 R^2	0.97	0.98	0.97	0.99	0.99	1	1	1	0.99	1
366 R^2 LS ¹	0.96	0.96	0.97	0.97	0.99	0.99	0.99	0.99	0.98	0.98
367 R^2 HS ²	-0.31	0.60	-0.56	0.60	0.12	0.92	-0.03	0.62	0.26	0.50

369
 370 ¹ Low salinity, below 0.1 M NaCl (Fontainebleau samples) and 1 M NaCl (Lochaline samples).

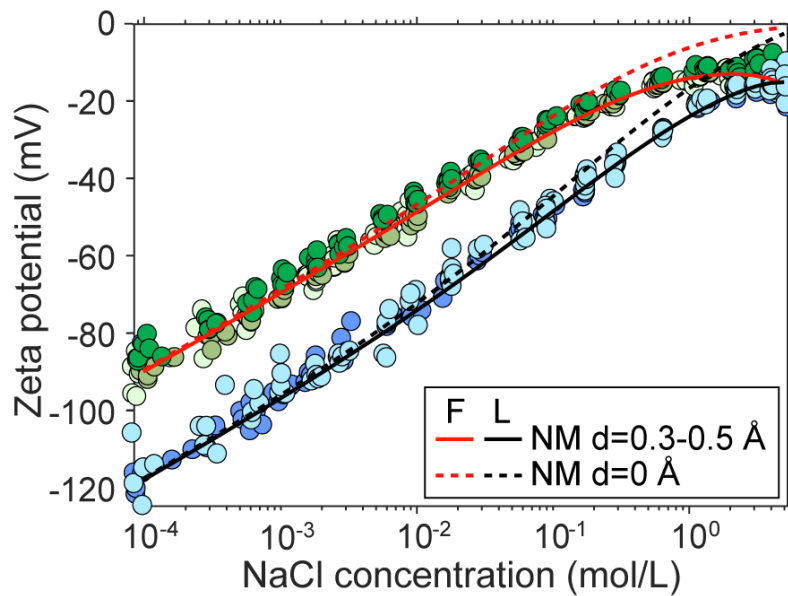
371 ² High salinity, above 0.1 M NaCl (Fontainebleau samples) and 1 M NaCl (Lochaline samples).

372

373 The measured high salinity zeta potentials were closely matched by the BSM considering the shear
 374 plane slightly approaching the mineral surface, i.e. with a very small distance from the OHP ($d =$
 375 0.5 \AA for Fontainebleau samples and $d = 0.3 \text{ \AA}$ for Lochaline samples; Table 1). Including such a
 376 small distance d between OHP and shear plane progressively increases computed zeta potential
 377 magnitude compared to not considering it when salinity increases (Figure 8). The effective distance
 378 d used in our NM was significantly smaller than the hydrated radius of Na^+ ($\cong 2 \text{ \AA}$ Leroy et al. [64]
 379 Sverjensky [18]), which implied that only some of Na ions were mobilized in the Stern layer, i.e.,
 380 only a small portion of all ions could move inside the Stern layer. In addition, d/d_{Stern} (Lochaline)
 381 $= d/d_{\text{Stern}}$ (Fontainebleau) = 0.18. This means that regardless of rock type 18% of the, previously
 382 considered as immobile ions in the Stern layer will be flowing. Then, the thicker the Stern layer is
 383 (and we expect it to become thicker as roughness increases), the larger d will become – exactly as
 384 NM predicts.

385 In addition, unlike the CM, the NM found that the shear plane of Fontainebleau samples is further
 386 away from the mineral surface than the shear plane of Lochaline samples, also explaining why the
 387 zeta potential magnitude of Fontainebleau samples is smaller than the zeta potential magnitude of
 388 Lochaline samples. Indeed, the total distance of the shear plane from the mineral surface ($d_{\text{Stern}} -$

389 d is larger for Fontainebleau ($2.8-0.5=2.3 \text{ \AA}$) compared with Lochaline ($1.7-0.3=1.4 \text{ \AA}$) samples,
 390 which is consistent with our hypothesis that rougher and sharper Fontainebleau grains push EDL
 391 further away from the mineral surface (both, the Stern plane and the shear plane). These findings
 392 were in agreement with the SEM micrographs showing that Fontainebleau rock has sharper-angled
 393 grains with larger surface roughness than Lochaline rock (Figure 5).



394
 395 **Figure 8.** Computed zeta potential of Fontainebleau (F) and Lochaline (L) samples as a function
 396 of NaCl concentration considering or not the distance d between the OHP and the shear plane.

397
 398 In the classical theory of the electrical double layer, it is assumed that only the mobile excess
 399 counter-ions in the diffuse layer contribute to the measured macroscopic streaming potential [28].
 400 However, the diffuse layer is highly compressed at high salinity, so that there are essentially no
 401 mobile counter-ions available inside it, and such near-zero contribution of the diffuse layer cannot
 402 explain correctly the non-zero zeta potentials in Fontainebleau and Lochaline sandstones at high
 403 salinity. Figure 9 shows the computed thicknesses of the diffuse layer and of the mobile part of the

404 Stern layer as well as the surface site density of adsorbed sodium ion in the Stern and diffuse layers,
 405 $\Gamma_{>\text{SiO}^- - \text{Na}^+}$ and $\Gamma_{\text{Na}^+}^d$, respectively. The salinity dependence of the diffuse layer thickness was
 406 evaluated by the Debye length χ :

$$\chi = \sqrt{\frac{\varepsilon_w k_B T}{2e^2 1000 N_A I}}, \quad (5)$$

407 and $\Gamma_{\text{Na}^+}^d$ was calculated using the following equations [24]:

$$\Gamma_{\text{Na}^+}^d = 1000 N_A c_{\text{Na}^+}^\infty \int_{x=0}^{x=\chi} \left\{ \exp[-e\varphi_d(x)/k_B T] - 1 \right\} dx, \quad (6)$$

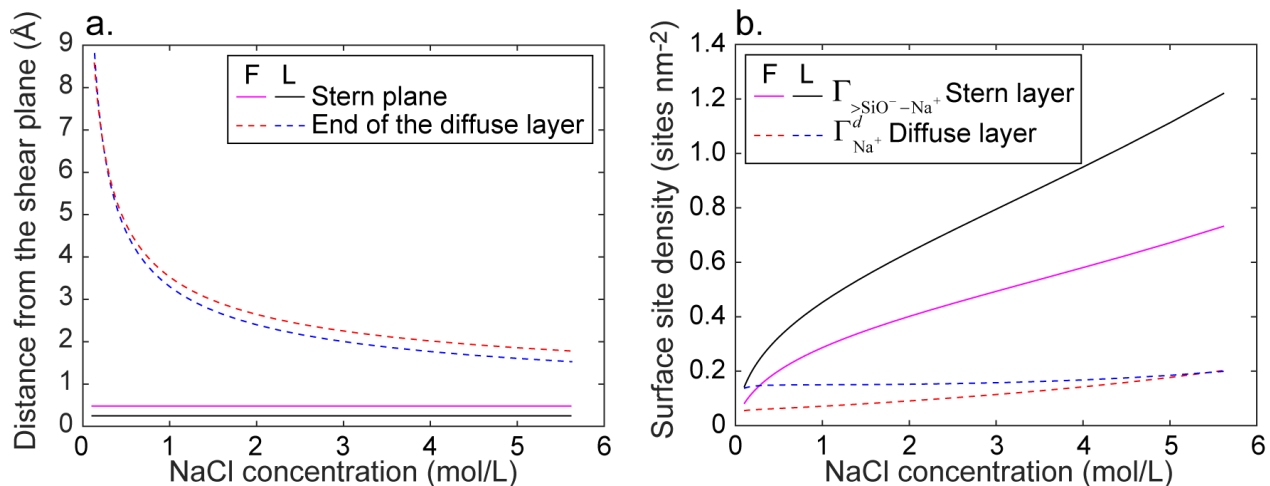
$$\varphi_d(x) = \frac{4k_B T}{e} \tanh^{-1} \left[\tanh \left(\frac{e\varphi_d}{4k_B T} \right) \exp(-x/\chi) \right], \quad (7)$$

408 where φ_d is the electrical potential at the start of the diffuse layer ($\varphi_\beta = \varphi_d$) and x is the position
 409 from the OHP (in m).

410

411

412



413
 414 **Figure 9.** Computed thickness of the diffuse layer (equal to one Debye length) and of the mobile
 415 part of the Stern layer (a) and surface site density of adsorbed Na⁺ ion in the Stern and diffuse
 416 layers (b) as a function of NaCl concentration for Fontainebleau (F) and Lochaline (L) samples.

417
 418 The computed thickness of the diffuse layer decreases significantly at high salinity to become
 419 comparable to the hydrated radius of sodium ion ($\cong 2 \text{ \AA}$) but it remains considerably larger than
 420 the thickness of the mobile part of the Stern layer (0.5 \AA and 0.3 \AA for Fontainebleau and Lochaline
 421 samples, respectively) (Figure 9a). However, when salinity increases, the computed surface site
 422 density of adsorbed Na⁺ ion in the Stern layer increases considerably more than in the diffuse layer
 423 (Figure 9b), which explains the increasing contribution of the counter-ions in the mobile part of
 424 the Stern layer to the measured streaming potential.

425 Our new surface complexation model applied simultaneously for both Fontainebleau and Lochaline
 426 samples (all five samples together) in a NaCl aqueous solution (termed here the unified new model,
 427 UNM) was still able to reproduce the zeta potential measurements well. Indeed, the values of the
 428 coefficient of determination were still close to 1 when calculated for the entire salinity range (Table
 429 3). The UNM reproduced very well the low salinity measurements, and the quality of match was

430 similar to the results obtained using the unified classical model, UCM. Across the high salinity
 431 domain, the UNM was also found to provide a better match to the experimental data compared
 432 with the UCM (except for L4Q sample at high salinity). The values of the optimized parameters
 433 used in UNM (Table 4) agreed with the values previously reported in Table 1, and both sets were
 434 consistent with the values reported in the literature for quartz in a NaCl aqueous solution. Therefore,
 435 our approach is relevant for obtaining a unified surface complexation model for quartz in a NaCl
 436 solution.

437 **Table 3.** Coefficient of determination values using a single set of BSM parameter values for
 438 Fontainebleau and Lochaline sandstones together.

	F2D		F3Q		F4Q		L3Q		L4Q	
	UCM	UNM	UCM	UNM	UCM	UNM	UCM	UNM	UCM	UNM
R^2	0.98	0.99	0.97	0.98	0.99	1	1	1	0.99	0.99
$R^2 LS^1$	0.97	0.97	0.95	0.95	0.99	0.99	0.99	0.99	0.98	0.98
$R^2 HS^2$	-0.45	0.46	-0.60	0.29	0.05	0.79	0.00	0.51	0.21	-0.04

439 ¹Low salinity, below 0.1 M NaCl (Fontainebleau samples) and 1 M NaCl (Lochaline samples).

440 ²High salinity, above 0.1 M NaCl (Fontainebleau samples) and 1 M NaCl (Lochaline samples).

441
 442 **Table 4.** BSM parameter values and estimated Stern layer thickness for quartz (combining
 443 Fontainebleau and Lochaline sandstones).

	Symbols	Range ¹	UCM	UNM
445	$\log K_H$	[4 10]	7.28 [7.24 7.31]	7.31 [7.27 7.34]
	$\log K_{Na}$	[-20 5]	-20 [ND ³]	0.58 [0.27 0.83]
446	C_1 (F m ⁻²)	[0.5 5]	2.26 [1.78 2.96]	3.43 [2.92 4.02]
	d (Å)	[0 10]	0	0.20 [0.17 0.24]
447	d_{Stern}^2 (Å)		1.68 [1.29 2.14]	1.11 [0.95 1.30]

448 ¹ Hiemstra et al. [20], Kitamura et al. [23], Sonnefeld et al. [62], Sverjensky [3], García et al. [6].

449 ² According to Eq. (2) and fitted C_1 values, considering $\epsilon_1 = 43\epsilon_0$ and $d_{Stern} = x_\beta - x_0$.

450 ³ Not determined.

451 **4. Conclusions**

452 We developed a new basic Stern surface complexation model to explain the zeta potential
453 measurements on quartz in contact with NaCl aqueous solutions and to describe the concentration
454 dependence of the electrochemical properties of quartz over a broad salinity range (from around
455 10^{-4} M NaCl up to around 5.5 M NaCl). Previous surface complexation models considered that the
456 shear plane of quartz in contact with a NaCl aqueous solution was located at the Stern plane where
457 sodium counter-ions were preferentially adsorbed or even further away from the mineral surface.
458 In contrast to previous models, our new model considered that there could be some water flow
459 transporting counter-ions within the Stern layer, i.e. that the shear plane where the zeta potential is
460 defined was located closer to the mineral surface than the Stern plane.

461 Compared to the model considering the zeta potential at the Stern plane, our new model better
462 reproduced the zeta potential measurements on Fontainebleau and Lochaline sandstones, especially
463 in high salinity conditions (above 0.1 M NaCl for Fontainebleau samples and 1 M NaCl for
464 Lochaline samples) where zeta potential appeared to level off at a constant negative value. This
465 was particularly true for Fontainebleau samples. We found a small shear plane offset distance from
466 the Stern plane of around 0.3–0.5 Å, i.e. only a small part of the Stern layer was mobile, confirming
467 that the shear plane was still at a close proximity to the Stern plane. In addition, the optimized value
468 of the equilibrium constant describing sodium adsorption in the Stern layer in our new model was
469 more realistic compared with the classical approach considering zero separation distance between
470 the Stern and the shear planes. The predicted surface charge density of quartz of the new model
471 was also in a better agreement with the experimental data. We also explained, based on SEM
472 micrograph images and our new surface complexation model, why Fontainebleau rocks, with

473 sharper-angle grains and larger surface roughness, had smaller in magnitude zeta potential for the
474 same NaCl concentration compared against Lochaline data.

475 Our approach can be used to interpret and even predict streaming potential measurements and other
476 types of electrokinetic measurements (e.g., electrophoretic mobility) on quartz and other minerals
477 in contact with brines of different chemical compositions and temperatures. Therefore, our results,
478 which should be confirmed by laboratory measurements at the microscopic scale (e.g., using
479 microfluidics and spectroscopy methods) and atomistic simulations, may have strong implications
480 for the modelling of the electrochemical properties of minerals in contact with highly saline brines.
481 Our results may be of crucial importance for exploring mineral-brine interactions at high salinity
482 levels close to real subsurface conditions.

483

484 **Acknowledgments**

485 The research work of Shuai Li is funded by the National Natural Science Foundation of China
486 (grant no. 41974089) and the Fundamental Research Funds for the Central Universities (China
487 University of Geosciences, Wuhan), China (grant no. CUGGC04). Philippe Leroy acknowledges
488 the internal funding from the French Geological Survey (BRGM) (CHIPPY project no.
489 RP20DEP087) and the support from Francis Claret for his research work as well as the fruitful
490 scientific discussions with Arnault Lassin. The authors also sincerely acknowledge Paul Glover for
491 sending the SEM micrographs of Fontainebleau and Lochaline rocks and for fruitful discussions.

492

493

494 **Appendix A. Basic Stern surface complexation model**

495 The following two surface complexation reactions were considered for the zeta potential modelling:



496 where K_{H} and K_{Na} (dimensionless) are the associated equilibrium constants, which are written as:

$$K_{\text{H}} = \frac{a_{>\text{SiOH}}}{a_{>\text{SiO}^-} a_{\text{H}^+}} \cong \frac{\Gamma_{>\text{SiOH}}}{\Gamma_{>\text{SiO}^-} a_{\text{H}^+}} = \frac{\Gamma_{>\text{SiOH}}}{\Gamma_{>\text{SiO}^-} a_{\text{H}^+}^{\infty}} \exp\left(\frac{e\varphi_0}{k_{\text{B}}T}\right), \quad (\text{A10})$$

$$K_{\text{Na}} = \frac{a_{>\text{SiO}^- - \text{Na}^+}}{a_{>\text{SiO}^-} a_{\text{Na}^+}} \cong \frac{\Gamma_{>\text{SiO}^- - \text{Na}^+}}{\Gamma_{>\text{SiO}^-} a_{\text{Na}^+}} = \frac{\Gamma_{>\text{SiO}^- - \text{Na}^+}}{\Gamma_{>\text{SiO}^-} a_{\text{Na}^+}^{\infty}} \exp\left(\frac{e\varphi_{\beta}}{k_{\text{B}}T}\right), \quad (\text{A11})$$

497 where a_i is the activity (dimensionless) and Γ_i is the surface site density (sites m^{-2}) of species i , e
 498 is the elementary charge ($\cong 1.602 \times 10^{-19}$ C), φ is the electrical potential (V), k_{B} is the Boltzmann
 499 constant ($\cong 1.381 \times 10^{-23}$ J K^{-1}), and T is the temperature (K). In equations (A3) and (A4), the
 500 superscript “ ∞ ” refers to ion activities in the electroneutral free or bulk electrolyte (not influenced
 501 by the mineral surface), which were computed using Pitzer theory (Appendix B) [64].

502 The following determined system of equations for the surface charge density at the mineral surface,
 503 Q_0 (C m^{-2}), at the β -plane, Q_{β} , and of the diffuse layer, Q_s , was used to compute the electrical
 504 potential distribution at the interface between quartz and bulk NaCl solution as a function of the
 505 equilibrium constants and Stern layer capacitance [21]:

$$Q_0 = -e(\Gamma_{>\text{SiO}^-} + \Gamma_{>\text{SiO}^- - \text{Na}^+}) = -\frac{e\Gamma_s}{A} \left[1 + K_{\text{Na}} a_{\text{Na}^+}^\infty \exp\left(-\frac{e\varphi_\beta}{k_B T}\right) \right], \quad (\text{A12})$$

$$Q_\beta = e\Gamma_{>\text{SiO}^- - \text{Na}^+} = \frac{e\Gamma_s}{A} K_{\text{Na}} a_{\text{Na}^+}^\infty \exp\left(-\frac{e\varphi_\beta}{k_B T}\right), \quad (\text{A13})$$

$$A = 1 + K_{\text{H}} a_{\text{H}^+}^\infty \exp\left(-\frac{e\varphi_0}{k_B T}\right) + K_{\text{Na}} a_{\text{Na}^+}^\infty \exp\left(-\frac{e\varphi_\beta}{k_B T}\right), \quad (\text{A14})$$

$$Q_s = \sqrt{8\varepsilon_w k_B T 1000 N_A I} \sinh\left[-\left(\frac{e\varphi_\beta}{2k_B T}\right)\right], \quad (\text{A15})$$

$$Q_0 + Q_\beta + Q_s = 0, \quad (\text{A16})$$

$$\varphi_0 - \varphi_\beta = \frac{Q_0}{C_1}, \quad (\text{A17})$$

506 where Γ_s is the total surface site density (we took $\Gamma_s = 4.6$ sites nm^{-2} García et al. [6]), I is the
507 molar ionic strength (mol L^{-1}), and φ_0 and φ_β are the electrical potentials at the 0-plane and at the
508 β -plane, respectively (considering $\varphi_\beta = \varphi_d$ for the BSM, where φ_d is the electrical potential at
509 the start of the diffuse layer).

510

511 **Appendix B. Pitzer model for ion activity coefficients in bulk electrolyte**

512

513 The following equations were used to compute ion activity coefficients in bulk electrolyte [64]:

$$a_i^\infty = \gamma_i^\infty \frac{m_i^\infty}{m_0}, \quad (\text{B1})$$

$$m_i^\infty = \frac{1000c_i^\infty}{M_w c_w^\infty}, \quad (\text{B2})$$

$$c_w^\infty = \frac{10^3 - \sum_i c_i^\infty V_i}{V_w}, \quad (\text{B3})$$

514 where γ_i^∞ is the activity coefficient (dimensionless), m_i^∞ is the molality (mol per kilogram of
 515 water, mol kg_w⁻¹, m_0 being the unit molality equal to 1 mol kg_w⁻¹), c_i^∞ is the molar concentration
 516 (M), and V_i is the standard partial molal volume (cm³ mol⁻¹) of ion i in bulk electrolyte. The
 517 quantity $V_i \cong 18.07, 0, -1.13, 17.68$ cm³ mol⁻¹ for H₂O, H⁺, Na⁺ (due to electrostriction) and
 518 Cl⁻, respectively, at a temperature of 25°C. The subscript “w” in equations (B2) and (B3) refers to
 519 water molecules, and M_w refers to the molar mass of water ($\cong 18$ g mol⁻¹).

520 Na⁺ activity coefficient in bulk electrolyte influences modelled Na⁺ adsorption in the Stern plane
 521 ($\Gamma_{>\text{SiO}^- - \text{Na}^+} = K_{\text{Na}} \Gamma_{>\text{SiO}^-} \gamma_{\text{Na}^+}^\infty m_{\text{Na}^+}^\infty / m_0 \exp(-e\phi_\beta / k_B T)$ from equations (A3) and (A4)). According to
 522 Pitzer theory, which is suitable for very saline aqueous solutions (ionic strengths above 0.1 M
 523 Harvie and Weare [67]), the natural logarithm of Na⁺ activity coefficient in NaCl electrolyte is
 524 written as:

$$\ln \gamma_{\text{Na}^+}^{\infty} = z_{\text{Na}^+}^2 F + m_{\text{Cl}^-}^{\infty} \left[2B_{\text{Na}^+\text{Cl}^-} + (m_{\text{Na}^+}^{\infty} + m_{\text{Cl}^-}^{\infty}) C_{\text{Na}^+\text{Cl}^-} \right] + z_{\text{Na}^+} m_{\text{Na}^+}^{\infty} m_{\text{Cl}^-}^{\infty} C_{\text{Na}^+\text{Cl}^-}, \quad (\text{B4})$$

$$F = -A_{\phi} \left[\frac{\sqrt{I_m}}{1 + b\sqrt{I_m}} + \frac{2}{b} \ln(1 + b\sqrt{I_m}) \right] + m_{\text{Na}^+}^{\infty} m_{\text{Cl}^-}^{\infty} B'_{\text{Na}^+\text{Cl}^-}, \quad (\text{B5})$$

$$A_{\phi} = \frac{1}{3} \sqrt{\frac{2\pi N_A \rho_w}{1000}} \left(\frac{e^2}{4\pi \epsilon_w k_B T} \right)^{3/2}, \quad (\text{B6})$$

$$B'_{\text{Na}^+\text{Cl}^-} = -\frac{2\beta_{\text{Na}^+\text{Cl}^-}^1}{I_m x_1^2} \left[1 - (1 + x_1 + 0.5x_1^2) \exp(-x_1) \right], \quad (\text{B7})$$

$$x_1 = \alpha_1 \sqrt{I_m}, \quad (\text{B8})$$

$$B_{\text{Na}^+\text{Cl}^-} = \beta_{\text{Na}^+\text{Cl}^-}^0 + \frac{2\beta_{\text{Na}^+\text{Cl}^-}^1}{x_1^2} \left[1 - (1 + x_1) \exp(-x_1) \right], \quad (\text{B9})$$

$$C_{\text{Na}^+\text{Cl}^-} = \frac{C_{\phi \text{Na}^+\text{Cl}^-}}{2\sqrt{|z_{\text{Na}^+} z_{\text{Cl}^-}|}}, \quad (\text{B10})$$

525 where z_i is the charge number of ion i , b and α_1 are empirical parameters ($b = 1.2$, $\alpha_1 = 2$ for 1:1
526 and 1:2 electrolytes), I_m is the molal ionic strength (in mol kg_w⁻¹, $I_m = m_{\text{Na}^+}^w$ here), and A_{ϕ} is the
527 Debye-Hückel coefficient describing long-range electrostatic interaction forces between ions (\cong
528 0.392 at a temperature T of 298 K). The Debye-Hückel coefficient was computed here as a function
529 of the Avogadro number N_A ($\cong 6.022 \times 10^{23}$ sites mol⁻¹), the water volumetric density ρ_w (\cong
530 997×10^3 g m⁻³), and the water permittivity ϵ_w ($\cong 78.3\epsilon_0$ where ϵ_0 is the vacuum permittivity with
531 a value of $\cong 8.854 \times 10^{-12}$ F m⁻¹). The Debye-Hückel coefficient multiplied by the terms in brackets
532 in equation (B5) is enough for computing ion activity coefficient in dilute aqueous solution (ionic

533 strength below 0.1 M). Pitzer and Mayorga [68] considered three additional terms (in equations
534 (B4) and (B5)) to compute ion activity coefficients in concentrated aqueous solutions. The terms
535 $B_{\text{Na}^+\text{Cl}^-}$ and $B'_{\text{Na}^+\text{Cl}^-}$ depend on the ionic strength and describe short-range interaction forces between
536 one cation and one anion (binary system), and the term $C_{\text{Na}^+\text{Cl}^-}$ describes short-range interaction
537 forces between two cations and one anion, and one cation and two anions (ternary system). The
538 Pitzer model for ion activity coefficients in 1:1 aqueous electrolyte such as NaCl depends on three
539 parameters $\beta_{\text{Na}^+\text{Cl}^-}^0$, $\beta_{\text{Na}^+\text{Cl}^-}^1$, and $C_{\phi\text{Na}^+\text{Cl}^-}$. The Pitzer parameter values were adjusted by matching
540 computed to measured osmotic coefficients. According to [Leroy et al. [64]] $\beta_{\text{Na}^+\text{Cl}^-}^0 = 0.0765$,
541 $\beta_{\text{Na}^+\text{Cl}^-}^1 = 0.2664$, and $C_{\phi\text{Na}^+\text{Cl}^-} = 0.00127$.

542 **References**

- 543 [1] Y. Duval, J.A. Mielczarski, O.S. Pokrovsky, E. Mielczarski, J.J. Ehrhardt, Evidence of the
544 existence of three types of species at the quartz-aqueous solution interface at pH 0-10: XPS
545 surface group quantification and surface complexation modeling, *Journal of Physical Chemistry*
546 *B* 106(11) (2002) 2937-2945, <https://doi.org/10.1021/Jp012818s>.
- 547 [2] G. Okay, P. Leroy, A. Ghorbani, P. Cosenza, C. Camerlynck, J. Cabrera, N. Florsch, A. Revil,
548 Spectral induced polarization of clay-sand mixtures: Experiments and modeling, *Geophysics*
549 79(6) (2014) E353-E375, <https://doi.org/10.1190/Geo2013-0347.1>.
- 550 [3] D.A. Sverjensky, Prediction of surface charge on oxides in salt solutions: Revisions for 1 : 1
551 (M+L-) electrolytes, *Geochimica Et Cosmochimica Acta* 69(2) (2005) 225-257,
552 <https://doi.org/10.1016/j.gca.2004.05.040>.
- 553 [4] Z. Qi, Y. Wang, H. He, D. Li, X. Xu, Wettability Alteration of the Quartz Surface in the
554 Presence of Metal Cations, *Energy & Fuels* 27(12) (2013) 7354-7359,
555 <https://doi.org/10.1021/ef401928c>.
- 556 [5] F.K. Crundwell, On the Mechanism of the Dissolution of Quartz and Silica in Aqueous
557 Solutions, *ACS Omega* 2(3) (2017) 1116-1127, <https://doi.org/10.1021/acsomega.7b00019>.
- 558 [6] D. García, J. Lützenkirchen, V. Petrov, M. Siebentritt, D. Schild, G. Lefèvre, T. Rabung, M.
559 Altmaier, S. Kalmykov, L. Duro, H. Geckeis, Sorption of Eu(III) on quartz at high salt
560 concentrations, *Colloids and Surfaces A: Physicochemical and Engineering Aspects* 578 (2019)
561 123610, <https://doi.org/10.1016/j.colsurfa.2019.123610>.
- 562 [7] A. Revil, P.W.J. Glover, Theory of ionic-surface electrical conduction in porous media, *Phys*
563 *Rev B* 55(3) (1997) 1757-1773, <https://doi.org/10.1103/PhysRevB.55.1757>.
- 564 [8] M.Z. Jaafar, J. Vinogradov, M.D. Jackson, Measurement of streaming potential coupling
565 coefficient in sandstones saturated with high salinity NaCl brine, *Geophysical Research Letters*
566 36(21) (2009), <https://doi.org/10.1029/2009gl040549>.
- 567 [9] M. Skold, A. Revil, P. Vaudelet, The pH dependence of spectral induced polarization of silica
568 sands: Experiment and modeling, *Geophysical Research Letters* 38 (2011),
569 <https://doi.org/10.1029/2011GL047748>.

- 570 [10] A. Kemna, A. Binley, G. Cassiani, E. Niederleithinger, A. Revil, L. Slater, K.H. Williams,
571 A.F. Orozco, F.H. Haegel, A. Hordt, S. Kruschwitz, V. Leroux, K. Titov, E. Zimmermann, An
572 overview of the spectral induced polarization method for near-surface applications, *Near Surf*
573 *Geophys* 10(6) (2012) 453-468, <https://doi.org/10.3997/1873-0604.2012027>.
- 574 [11] A. Revil, M. Karaoulis, T. Johnson, A. Kemna, Review: Some low-frequency electrical
575 methods for subsurface characterization and monitoring in hydrogeology, *Hydrogeology*
576 *Journal* 20(4) (2012) 617-658, <https://doi.org/10.1007/s10040-011-0819-x>.
- 577 [12] A. Binley, S.S. Hubbard, J.A. Huisman, A. Revil, D.A. Robinson, K. Singha, L.D. Slater, The
578 emergence of hydrogeophysics for improved understanding of subsurface processes over
579 multiple scales, *Water Resources Research* 51(6) (2015) 3837-3866,
580 <https://doi.org/10.1002/2015WR017016>.
- 581 [13] J. Vinogradov, M.Z. Jaafar, M.D. Jackson, Measurement of streaming potential coupling
582 coefficient in sandstones saturated with natural and artificial brines at high salinity, *Journal of*
583 *Geophysical Research* 115(B12) (2010), <https://doi.org/10.1029/2010jb007593>.
- 584 [14] J. Vinogradov, M.D. Jackson, M. Chamerois, Zeta potential in sandpacks: Effect of
585 temperature, electrolyte pH, ionic strength and divalent cations, *Colloids and Surfaces A:*
586 *Physicochemical and Engineering Aspects* 553 (2018) 259-271,
587 <https://doi.org/10.1016/j.colsurfa.2018.05.048>.
- 588 [15] E. Walker, P.W.J. Glover, Measurements of the Relationship Between Microstructure, pH,
589 and the Streaming and Zeta Potentials of Sandstones, *Transport Porous Med* 121(1) (2018) 183-
590 206, <https://doi.org/10.1007/s11242-017-0954-5>.
- 591 [16] M. Hidayat, M. Sarmadivaleh, J. Derksen, D. Vega-Maza, S. Iglauer, J. Vinogradov, Zeta
592 potential of CO₂-rich aqueous solutions in contact with intact sandstone sample at temperatures
593 of 23 °C and 40 °C and pressures up to 10.0 MPa, *Journal of Colloid and Interface Science* 607
594 (2022) 1226-1238, <https://doi.org/10.1016/j.jcis.2021.09.076>.
- 595 [17] P.W.J. Glover, *Geophysical Properties of the Near Surface Earth: Electrical Properties*, (2015)
596 89-137, <https://doi.org/10.1016/b978-0-444-53802-4.00189-5>.

- 597 [18] D.A. Sverjensky, Interpretation and prediction of triple-layer model capacitances and the
598 structure of the oxide-electrolyte-water interface, *Geochimica Et Cosmochimica Acta* 65(21)
599 (2001) 3643-3655, [https://doi.org/10.1016/S0016-7037\(01\)00709-8](https://doi.org/10.1016/S0016-7037(01)00709-8).
- 600 [19] Z. Brkljača, D. Namjesnik, J. Lützenkirchen, M. Předota, T. Preočanin, Quartz/Aqueous
601 Electrolyte Solution Interface: Molecular Dynamic Simulation and Interfacial Potential
602 Measurements, *The Journal of Physical Chemistry C* 122(42) (2018) 24025-24036,
603 <https://doi.org/10.1021/acs.jpcc.8b04035>.
- 604 [20] T. Hiemstra, J.C.M. De Wit, W.H. Van Riemsdijk, Multisite proton adsorption modelling at
605 the solid/solution interface of (hydr)oxides: a new approach. II. Application to various important
606 (hydr)oxides, *Journal of Colloid and Interface Science* 133 (1989) 105-117,
607 [https://doi.org/10.1016/0021-9797\(89\)90285-3](https://doi.org/10.1016/0021-9797(89)90285-3).
- 608 [21] P. Leroy, N. Devau, A. Revil, M. Bizi, Influence of surface conductivity on the apparent zeta
609 potential of amorphous silica nanoparticles, *Journal of Colloid and Interface Science* 410 (2013)
610 81-93, <https://doi.org/10.1016/j.jcis.2013.08.012>.
- 611 [22] C. Macias-Romero, I. Nahalka, H.I. Okur, S. Roke, Optical imaging of surface chemistry and
612 dynamics in confinement, *Science* 357(6353) (2017) 784-788,
613 <https://doi.org/10.1126/science.aal4346>.
- 614 [23] A. Kitamura, K. Fujiwara, T. Yamamoto, S. Nishikawa, H. Moriyama, Analysis of adsorption
615 behavior of cations onto quartz surface by electrical double-layer model, *J Nucl Sci Technol*
616 36(12) (1999) 1167-1175, <https://doi.org/10.1080/18811248.1999.9726312>.
- 617 [24] P. Leroy, C. Tournassat, O. Bernard, N. Devau, M. Azaroual, The electrophoretic mobility of
618 montmorillonite. Zeta potential and surface conductivity effects, *Journal of Colloid and*
619 *Interface Science* 451 (2015) 21-39, <https://doi.org/10.1016/j.jcis.2015.03.047>.
- 620 [25] R.J. Hunter, *Zeta Potential in Colloid Science: Principles and Applications*, Academic Press,
621 New York, 1981.
- 622 [26] J. Lyklema, M. Minor, On surface conduction and its role in electrokinetics, *Colloids and*
623 *Surfaces a-Physicochemical and Engineering Aspects* 140(1-3) (1998) 33-41,
624 [https://doi.org/10.1016/S0927-7757\(97\)00266-5](https://doi.org/10.1016/S0927-7757(97)00266-5).

- 625 [27] A. Revil, P.A. Pezard, P.W.J. Glover, Streaming potential in porous media 1. Theory of the
626 zeta potential, *J Geophys Res-Sol Ea* 104(B9) (1999) 20021-20031,
627 <https://doi.org/10.1029/1999jb900089>.
- 628 [28] A. Revil, D. Hermitte, E. Spangenberg, J.J. Cochame, Electrical properties of zeolitized
629 volcanoclastic materials, *J Geophys Res-Sol Ea* 107(B8) (2002),
630 <https://doi.org/10.1029/2001jb000599>.
- 631 [29] A. Crespy, A. Boleve, A. Revil, Influence of the Dukhin and Reynolds numbers on the
632 apparent zeta potential of granular porous media, *Journal of Colloid and Interface Science* (2007)
633 188-194, <https://doi.org/10.1016/j.jcis.2006.09.038>.
- 634 [30] S. Li, P. Leroy, F. Heberling, N. Devau, D. Jougnot, C. Chiaberge, Influence of surface
635 conductivity on the apparent zeta potential of calcite, *J. Colloid Interface Sci.* 468 (2016) 262-
636 75, <https://doi.org/10.1016/j.jcis.2016.01.075>.
- 637 [31] P. Leroy, A. Revil, A triple-layer model of the surface electrochemical properties of clay
638 minerals, *Journal of Colloid and Interface Science* (2004) 371-380,
639 <https://doi.org/10.1016/j.jcis.2003.08.007>.
- 640 [32] I.C. Bourg, G. Sposito, Molecular dynamics simulations of the electrical double layer on
641 smectite surfaces contacting concentrated mixed electrolyte (NaCl-CaCl₂) solutions, *Journal of*
642 *Colloid and Interface Science* 360(2) (2011) 701-715, <https://doi.org/10.1016/j.jcis.2011.04.063>.
- 643 [33] H. Zhang, A.A. Hassanali, Y.K. Shin, C. Knight, S.J. Singer, The water-amorphous silica
644 interface: Analysis of the Stern layer and surface conduction, *J Chem Phys* 134(2) (2011),
645 <https://doi.org/10.1063/1.3510536>.
- 646 [34] D. Biriukov, P. Fibich, M. Předota, Zeta Potential Determination from Molecular Simulations,
647 *The Journal of Physical Chemistry C* 124(5) (2020) 3159-3170,
648 <https://doi.org/10.1021/acs.jpcc.9b11371>.
- 649 [35] M. Předota, M.L. Machesky, D.J. Wesolowski, Molecular Origins of the Zeta Potential,
650 *Langmuir* 32(40) (2016) 10189-10198, <https://doi.org/10.1021/acs.langmuir.6b02493>.
- 651 [36] P. Leroy, A. Maineult, Exploring the electrical potential inside cylinders beyond the Debye-
652 Hückel approximation: a computer code to solve the Poisson-Boltzmann equation for
653 multivalent electrolytes, *Geophys J Int* 214(1) (2018) 58-69, <https://doi.org/10.1093/gji/ggy124>.

- 654 [37] J. Westall, H. Hohl, A comparison of electrostatic models for the oxide/solution interface,
655 Advances in Colloid and Interface Science 12(4) (1980) 265-294, [https://doi.org/10.1016/0001-](https://doi.org/10.1016/0001-8686(80)80012-1)
656 8686(80)80012-1.
- 657 [38] M. Heuser, G. Spagnoli, P. Leroy, N. Klitzsch, H. Stanjek, Electro-osmotic flow in clays and
658 its potential for reducing clogging in mechanical tunnel driving, B Eng Geol Environ 71(4)
659 (2012) 721-733, <https://doi.org/10.1007/s10064-012-0431-x>.
- 660 [39] J. Lyklema, S. Rovillard, J. De Coninck, Electrokinetics: The properties of the stagnant layer
661 unraveled, Langmuir 14(20) (1998) 5659-5663, <https://doi.org/10.1021/la980399t>.
- 662 [40] M.A. Brown, A. Goel, Z. Abbas, Effect of Electrolyte Concentration on the Stern Layer
663 Thickness at a Charged Interface, Angewandte Chemie International Edition 55(11) (2016)
664 3790-3794, <https://doi.org/10.1002/anie.201512025>.
- 665 [41] D. Lis, E.H.G. Backus, J. Hunger, S.H. Parekh, M. Bonn, Liquid flow along a solid surface
666 reversibly alters interfacial chemistry, Science 344(6188) (2014) 1138-1142,
667 <https://doi.org/10.1126/science.1253793>.
- 668 [42] R. Saini, A. Garg, D.P. Barz, Streaming potential revisited: the influence of convection on the
669 surface conductivity, Langmuir 30(36) (2014) 10950-61, <https://doi.org/10.1021/la501426c>.
- 670 [43] B.L. Werkhoven, J.C. Everts, S. Samin, R. van Roij, Flow-Induced Surface Charge
671 Heterogeneity in Electrokinetics due to Stern-Layer Conductance Coupled to Reaction Kinetics,
672 Physical Review Letters 120(26) (2018), <https://doi.org/10.1103/PhysRevLett.120.264502>.
- 673 [44] E. Walker, P.W.J. Glover, J. Ruel, A transient method for measuring the DC streaming
674 potential coefficient of porous and fractured rocks, Journal of Geophysical Research: Solid
675 Earth 119(2) (2014) 957-970, <https://doi.org/10.1002/2013jb010579>.
- 676 [45] P.W.J. Glover, Modelling pH-Dependent and Microstructure-Dependent Streaming Potential
677 Coefficient and Zeta Potential of Porous Sandstones, Transport Porous Med 124(1) (2018) 31-
678 56, <https://doi.org/10.1007/s11242-018-1036-z>.
- 679 [46] D.E. Yates, S. Levine, T.W. Healy, Site-binding Model of the Electrical Double Layer at the
680 Oxide/Water interface, Journal of the Chemical Society, Faraday Transactions 70 (1974) 1807-
681 1818, <https://doi.org/10.1039/F19747001807>.

- 682 [47] I. Siretanu, D. Ebeling, M.P. Andersson, S.L.S. Stipp, A. Philipse, M.C. Stuart, D. van den
683 Ende, F. Mugele, Direct observation of ionic structure at solid-liquid interfaces: a deep look into
684 the Stern Layer, *Scientific reports* 4(1) (2014), <https://doi.org/10.1038/srep04956>.
- 685 [48] S.R. Charlton, D.L. Parkhurst, Modules based on the geochemical model PHREEQC for use
686 in scripting and programming languages, *Comput Geosci-Uk* 37(10) (2011) 1653-1663,
687 <https://doi.org/10.1016/j.cageo.2011.02.005>.
- 688 [49] A. Mainault, Estimation of the electrical potential distribution along metallic casing from
689 surface self-potential profile, *J Appl Geophys* 129 (2016) 66-78,
690 <https://doi.org/10.1016/j.jappgeo.2016.03.038>.
- 691 [50] A. Alizadeh, M. Wang, Flexibility of inactive electrokinetic layer at charged solid-liquid
692 interface in response to bulk ion concentration, *Journal of Colloid and Interface Science* 534
693 (2019) 195-204, <https://doi.org/10.1016/j.jcis.2018.09.010>.
- 694 [51] P. Leroy, C. Tournassat, M. Bizi, Influence of surface conductivity on the apparent zeta
695 potential of TiO₂ nanoparticles, *Journal of Colloid and Interface Science* 356(2) (2011) 442-
696 453, <https://doi.org/10.1016/j.jcis.2011.01.016>.
- 697 [52] P. Leroy, D. Jougnot, A. Revil, A. Lassin, M. Azaroual, A double layer model of the gas
698 bubble/water interface, *Journal of Colloid and Interface Science* 388 (2012) 243-256,
699 <https://doi.org/10.1016/j.jcis.2012.07.029>.
- 700 [53] A. Mendieta, D. Jougnot, P. Leroy, A. Mainault, Spectral Induced Polarization
701 Characterization of Non- Consolidated Clays for Varying Salinities—An Experimental Study,
702 *Journal of Geophysical Research: Solid Earth* 126(4) (2021),
703 <https://doi.org/10.1029/2020JB021125>.
- 704 [54] B. Lowden, S. Braley, A. Hurst, J. Lewis, Sedimentological studies of the Cretaceous
705 Lochaline Sandstone, NW Scotland, Geological Society, London, Special Publications 62(1)
706 (1992) 159-162, <https://doi.org/10.1144/gsl.sp.1992.062.01.14>.
- 707 [55] P.L. Churcher, P.R. French, J.C. Shaw, L.L. Schramm, Rock Properties of Berea Sandstone,
708 Baker Dolomite, and Indiana Limestone, *Society of Petroleum Engineers Journal* 21044 (1991)
709 20-22, <https://doi.org/10.2118/21044-MS>.

- 710 [56] T.-f. Wong, C. David, W. Zhu, The transition from brittle faulting to cataclastic flow in porous
711 sandstones: Mechanical deformation, *Journal of Geophysical Research: Solid Earth* 102(B2)
712 (1997) 3009-3025, <https://doi.org/10.1029/96jb03281>.
- 713 [57] S. Li, H. Collini, M.D. Jackson, Anomalous Zeta Potential Trends in Natural Sandstones,
714 *Geophysical Research Letters* 45(20) (2018), <https://doi.org/10.1029/2018GL079602>.
- 715 [58] M. Alarouj, H. Collini, M.D. Jackson, Positive Zeta Potential in Sandstones Saturated With
716 Natural Saline Brine, *Geophysical Research Letters* 48(20) (2021),
717 <https://doi.org/10.1029/2021GL094306>.
- 718 [59] A. Alroudhan, J. Vinogradov, M.D. Jackson, Zeta potential of intact natural limestone: Impact
719 of potential-determining ions Ca, Mg and SO₄, *Colloids and Surfaces A: Physicochemical and*
720 *Engineering Aspects* 493 (2016) 83-98, <https://doi.org/10.1016/j.colsurfa.2015.11.068>.
- 721 [60] C. Schnitzer, S. Ripperger, Influence of Surface Roughness on Streaming Potential Method,
722 *Chem Eng Technol* 31(11) (2008) 1696-1700, <https://doi.org/10.1002/ceat.200800180>.
- 723 [61] A. Drechsler, A. Caspari, A. Synytska, Influence of roughness and capillary size on the zeta
724 potential values obtained by streaming potential measurements, *Surf Interface Anal* 52(12)
725 (2020) 991-995, <https://doi.org/10.1002/sia.6792>.
- 726 [62] J. Sonnefeld, A. Gobel, W. Vogelsberger, Surface-Charge Density on Spherical Silica
727 Particles in Aqueous Alkali Chloride Solutions .1. Experimental Results, *Colloid Polym Sci*
728 273(10) (1995) 926-931, <https://doi.org/10.1007/Bf00660369>.
- 729 [63] A.C. Riese, Adsorption of radium and thorium onto quartz and kaolinite: A comparison of
730 solution/surface equilibrium models, Colorado School of Mines, 1982.
- 731 [64] P. Leroy, A. Lassin, M. Azaroual, L. Andre, Predicting the surface tension of aqueous 1:1
732 electrolyte solutions at high salinity, *Geochimica Et Cosmochimica Acta* 74(19) (2010) 5427-
733 5442, <https://doi.org/10.1016/j.gca.2010.06.012>.
- 734 [65] F.A. Saadi, K.-H. Wolf, C.v. Kruijsdijk, Characterization of Fontainebleau Sandstone: Quartz
735 Overgrowth and its Impact on Pore-Throat Framework, *Journal of Petroleum & Environmental*
736 *Biotechnology* 08(03) (2017), <https://doi.org/10.4172/2157-7463.1000328>.

- 737 [66] M.A. Brown, Z. Abbas, A. Kleibert, R.G. Green, A. Goel, S. May, T.M. Squires,
738 Determination of Surface Potential and Electrical Double-Layer Structure at the Aqueous
739 Electrolyte-Nanoparticle Interface, *Physical Review X* 6(1) (2016),
740 <https://doi.org/10.1103/PhysRevX.6.011007>.
- 741 [67] C.E. Harvie, J.H. Weare, The prediction of mineral solubilities in natural waters: the Na-K-
742 Mg-Ca-Cl-SO₄-H₂O system from zero to high concentration at 25 °C, *Geochimica Et*
743 *Cosmochimica Acta* 44(7) (1980) 981-997, [https://doi.org/10.1016/0016-7037\(80\)90287-2](https://doi.org/10.1016/0016-7037(80)90287-2).
- 744 [68] K.S. Pitzer, G. Mayorga, Thermodynamics of electrolytes. II. Activity and osmotic
745 coefficients for strong electrolytes with one or both ions univalent, *The Journal of Physical*
746 *Chemistry* 77(19) (1973) 2300–2308, <https://doi.org/10.1021/j100621a026>.
- 747

Declaration of interests

The authors declare that they have no known competing financial interests or personal relationships that could have appeared to influence the work reported in this paper.

The authors declare the following financial interests/personal relationships which may be considered as potential competing interests:

Philippe Leroy: Conceptualization, Methodology, Software, Writing - Original Draft, Validation, Visualization.

Alexis Mainault: Software, Formal analysis.

Shuai Li: Investigation.

Jan Vinogradov: Writing- Reviewing and Editing.

1
2
3
4 **1 The zeta potential of quartz.**

5
6 **2 Surface complexation modelling to elucidate high salinity measurements**

7
8
9
10
11 **3**
12
13
14 **4** Philippe Leroy¹, Alexis Maineult², Shuai Li³, and Jan Vinogradov⁴

15
16
17
18 **5** ¹ BRGM, French Geological Survey, 45100 Orléans, France.

19
20
21 **6** ² Sorbonne Université, CNRS, EPHE, UMR 7619 METIS, 75005 Paris, France.

22
23
24
25
26 **7** ³ Hubei Subsurface Multi-scale Imaging Key Laboratory, Institute of Geophysics and Geomatics,
27
28 **8** China University of Geosciences, Wuhan 430074, China.

29
30
31
32
33
34
35
36
37
38 **9** ⁴ School of Engineering, University of Aberdeen, AB24 3UE, Aberdeen, United Kingdom.

39
40
41
42
43
44
45
46
47
48
49
50
51
52
53
54
55
56
57
58
59
60
61
62
63
64
65
66
67
68
69
70
71
72
73
74
75
76
77
78
79
80
81
82
83
84
85
86
87
88
89
90
91
92
93
94
95
96
97
98
99
100
101
102
103
104
105
106
107
108
109
110
111
112
113
114
115
116
117
118
119
120
121
122
123
124
125
126
127
128
129
130
131
132
133
134
135
136
137
138
139
140
141
142
143
144
145
146
147
148
149
150
151
152
153
154
155
156
157
158
159
160
161
162
163
164
165
166
167
168
169
170
171
172
173
174
175
176
177
178
179
180
181
182
183
184
185
186
187
188
189
190
191
192
193
194
195
196
197
198
199
200
201
202
203
204
205
206
207
208
209
210
211
212
213
214
215
216
217
218
219
220
221
222
223
224
225
226
227
228
229
230
231
232
233
234
235
236
237
238
239
240
241
242
243
244
245
246
247
248
249
250
251
252
253
254
255
256
257
258
259
260
261
262
263
264
265
266
267
268
269
270
271
272
273
274
275
276
277
278
279
280
281
282
283
284
285
286
287
288
289
290
291
292
293
294
295
296
297
298
299
300
301
302
303
304
305
306
307
308
309
310
311
312
313
314
315
316
317
318
319
320
321
322
323
324
325
326
327
328
329
330
331
332
333
334
335
336
337
338
339
340
341
342
343
344
345
346
347
348
349
350
351
352
353
354
355
356
357
358
359
360
361
362
363
364
365
366
367
368
369
370
371
372
373
374
375
376
377
378
379
380
381
382
383
384
385
386
387
388
389
390
391
392
393
394
395
396
397
398
399
400
401
402
403
404
405
406
407
408
409
410
411
412
413
414
415
416
417
418
419
420
421
422
423
424
425
426
427
428
429
430
431
432
433
434
435
436
437
438
439
440
441
442
443
444
445
446
447
448
449
450
451
452
453
454
455
456
457
458
459
460
461
462
463
464
465
466
467
468
469
470
471
472
473
474
475
476
477
478
479
480
481
482
483
484
485
486
487
488
489
490
491
492
493
494
495
496
497
498
499
500
501
502
503
504
505
506
507
508
509
510
511
512
513
514
515
516
517
518
519
520
521
522
523
524
525
526
527
528
529
530
531
532
533
534
535
536
537
538
539
540
541
542
543
544
545
546
547
548
549
550
551
552
553
554
555
556
557
558
559
560
561
562
563
564
565
566
567
568
569
570
571
572
573
574
575
576
577
578
579
580
581
582
583
584
585
586
587
588
589
590
591
592
593
594
595
596
597
598
599
600
601
602
603
604
605
606
607
608
609
610
611
612
613
614
615
616
617
618
619
620
621
622
623
624
625
626
627
628
629
630
631
632
633
634
635
636
637
638
639
640
641
642
643
644
645
646
647
648
649
650
651
652
653
654
655
656
657
658
659
660
661
662
663
664
665
666
667
668
669
670
671
672
673
674
675
676
677
678
679
680
681
682
683
684
685
686
687
688
689
690
691
692
693
694
695
696
697
698
699
700
701
702
703
704
705
706
707
708
709
710
711
712
713
714
715
716
717
718
719
720
721
722
723
724
725
726
727
728
729
730
731
732
733
734
735
736
737
738
739
740
741
742
743
744
745
746
747
748
749
750
751
752
753
754
755
756
757
758
759
760
761
762
763
764
765
766
767
768
769
770
771
772
773
774
775
776
777
778
779
780
781
782
783
784
785
786
787
788
789
790
791
792
793
794
795
796
797
798
799
800
801
802
803
804
805
806
807
808
809
810
811
812
813
814
815
816
817
818
819
820
821
822
823
824
825
826
827
828
829
830
831
832
833
834
835
836
837
838
839
840
841
842
843
844
845
846
847
848
849
850
851
852
853
854
855
856
857
858
859
860
861
862
863
864
865
866
867
868
869
870
871
872
873
874
875
876
877
878
879
880
881
882
883
884
885
886
887
888
889
890
891
892
893
894
895
896
897
898
899
900
901
902
903
904
905
906
907
908
909
910
911
912
913
914
915
916
917
918
919
920
921
922
923
924
925
926
927
928
929
930
931
932
933
934
935
936
937
938
939
940
941
942
943
944
945
946
947
948
949
950
951
952
953
954
955
956
957
958
959
960
961
962
963
964
965
966
967
968
969
970
971
972
973
974
975
976
977
978
979
980
981
982
983
984
985
986
987
988
989
990
991
992
993
994
995
996
997
998
999
1000

11 Corresponding author: Dr. Philippe Leroy (p.leroy@brgm.fr)

12
13
14
15
16
17
18
19
20
21
22
23
24
25
26
27
28
29
30
31
32
33
34
35
36
37
38
39 *17 Intended for publication in Colloids and Surfaces A: Physicochemical and Engineering Aspects*

1
2
3
4
5
6
7
8
9
10
11
12
13
14
15
16
17
18
19
20
21
22
23
24
25
26
27
28
29
30
31
32
33
34
35
36
37
38
39
40
41
42
43
44
45
46
47
48
49
50
51
52
53
54
55
56
57
58
59
60
61
62
63
64
65

18 **Abstract**

19 The zeta potential is a measureable electrical potential of paramount importance to understand the
20 electrochemical properties of rocks. However, the zeta potential remains poorly understood
21 because it takes place at the nanoscale of the electrical double layer on the mineral surface.
22 Streaming potential measurements on quartz-rich Fontainebleau and Lochaline sandstones carried
23 out at high salinity (above 0.1 M NaCl) yield surprisingly high zeta potential values, which cannot
24 be correctly reproduced by a traditional surface complexation model considering that the shear
25 plane is located at the beginning of the diffuse layer. We found that placing the shear plane, where
26 the zeta potential is defined, slightly closer to the mineral surface than the Stern plane significantly
27 improves the predictions of the zeta potential and surface charge density of quartz at high salinity
28 as well as the values of the equilibrium constant describing sodium adsorption in the Stern layer.
29 Our results have strong implications for the modelling of the electrochemical properties of minerals
30 in contact with highly saline solutions.

31
32 Key words: zeta potential, quartz, streaming potential, high salinity, shear plane location

1
2
3
4
5
6
7
8
9
10
11
12
13
14
15
16
17
18
19
20
21
22
23
24
25
26
27
28
29
30
31
32
33
34
35
36
37
38
39
40
41
42
43
44
45
46
47
48
49
50
51
52
53
54
55
56
57
58
59
60
61
62
63
64
65

33 **1. Introduction**

34 Quartz is a mineral that is particularly interesting to study because of its natural abundance and
35 usefulness in the development of new technologies [1]. In contact with water, quartz develops a
36 surface charge attracting counter-ions and repelling co-ions, thus forming the so-called electrical
37 double layer (EDL) usually represented by a “compact” Stern layer and a diffuse layer [2, 3].
38 Investigating the electrochemical properties of quartz is of great interest in many applications in
39 physics, chemistry and Earth sciences because these properties control adsorption and
40 dissolution/precipitation reactions, and wettability on the quartz surface [4-6]. The EDL of quartz
41 is also the source of electrokinetic and geophysical electrical (e.g., self-potential, resistivity,
42 induced polarization) measurements that are used to map for instance geological fluid flows or
43 biogeochemical reactions [7-12]. Studying quartz electrochemical properties notably when quartz
44 is in contact with highly saline brines has a high potential in many geo-environmental and
45 engineering applications including geo-sequestration of CO₂ in deep saline aquifers, and **oil and**
46 **gas exploration and production notably** enhanced hydrocarbon recovery [13-17].

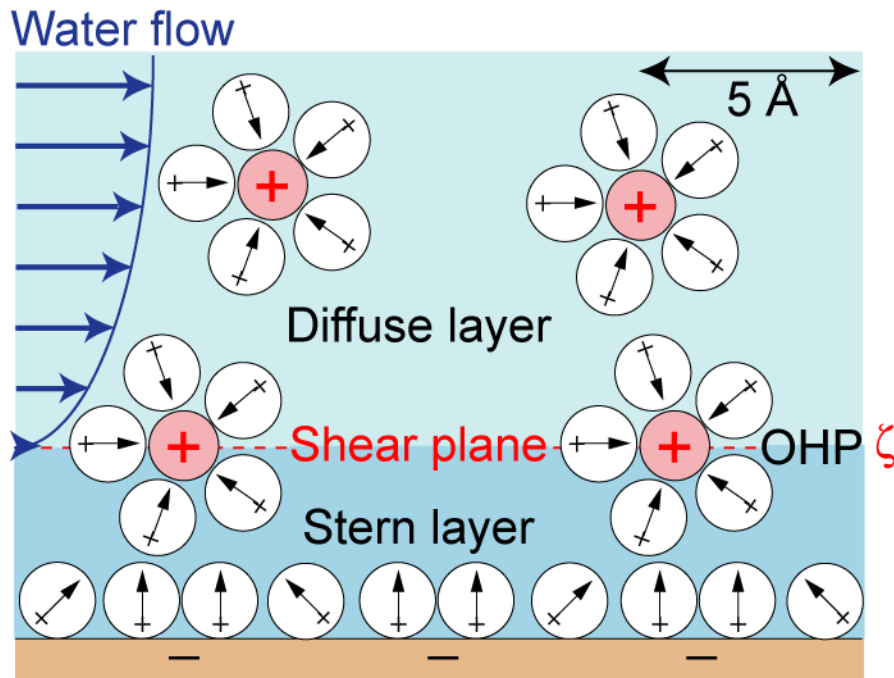
47 Exploring the electrochemical properties of quartz is very challenging because of their nanoscopic
48 nature [1, 18, 19]. Indeed, surface complexation reactions between surface sites and ions in the
49 aqueous solution occur at the nm-scale [3, 20-22]. In addition, natural quartz has a low specific
50 surface area (typically below 0.1 m² g⁻¹), which considerably complicates the experimental
51 characterization of its EDL compared to minerals with a large specific surface area such as
52 montmorillonite [2, 3, 23, 24]. Only few methods exist to probe the properties of the EDL on the
53 surface of minerals in contact with brines. Among them, there is the streaming potential method,
54 which implies application of a water pressure difference across the sample while measuring the
55 resulting voltage, the streaming potential, due to the displaced excess counter-ions in the EDL [25-

1
2
3
4
5
6
7
8
9
10
11
12
13
14
15
16
17
18
19
20
21
22
23
24
25
26
27
28
29
30
31
32
33
34
35
36
37
38
39
40
41
42
43
44
45
46
47
48
49
50
51
52
53
54
55
56
57
58
59
60
61
62
63
64
65

30]. From the measured streaming potential it is possible to obtain some relevant information on the electrochemical properties of minerals through the calculation of the electrokinetic zeta potential (ζ), which is defined as the electrical potential at the shear (or slip) plane [17, 25, 27]. The zeta potential determined experimentally can be interpreted in terms of mineral electrochemical properties by matching observed and simulated zeta potential using a relevant surface complexation model [21, 30, 31]. However, this approach relies on the assumption that the exact location of the shear plane from the mineral surface is known, which is obviously not the case because of the lack of experimental information at the molecular level [32-35]. Moreover, the zeta potential is, most of the times, the only physico-chemical quantity available to validate the predictions of electrostatic surface complexation models for low specific surface area minerals such as quartz or calcite [3, 30, 36]. In addition, the zeta potential is inferred from electrohydrodynamic measurements while surface complexation models rely on electrostatics at thermodynamic equilibrium [25, 35, 37, 38]. Therefore, these limitations contribute to additional uncertainties when investigating mineral electrochemical properties from zeta potential measurements.

When water flow relative to the mineral surface takes place, it is widely accepted that the shear plane is located between the “stagnant” Stern layer bounded by the outer Helmholtz plane (OHP) and the diffuse layer because high water viscosity in the Stern layer prevents water flow within it [3, 25, 39] (Figure 1). The Stern layer of silica-based materials such as amorphous silica and quartz in contact with a NaCl solution is traditionally represented by a hydration layer followed by a layer containing hydrated sodium counter-ions [18, 21, 40]. Some molecular dynamic (MD) simulations (e.g., Zhang et al. [33]), spectroscopy measurements (e.g., Lis et al. [41]) and microfluidic studies (e.g., Saini et al. [42] and Werkhoven et al. [43]) have demonstrated that there could be a non-zero

1
2
3
4 79 flow of water within the Stern layer of silica notably because some counter-ions (such as Na^+) are
5
6 80 not stuck to the mineral surface and form outer sphere surface complexes keeping their hydration
7
8
9 81 shell. This implies that there may be some, even weak, water displacement within the Stern layer
10
11 82 of silica, and hydrous oxide in general. Therefore, for quartz, the effective shear plane may be
12
13
14 83 located slightly closer to the mineral surface than the outer Helmholtz plane, in agreement with the
15
16 84 assumption accepted by most that the shear plane is located at the proximity of the OHP (e.g.,
17
18
19 85 Hunter [25], Sverjensky [3], García et al. [6]).



20
21
22
23
24
25
26
27
28
29
30
31
32
33
34
35
36
37
38
39
40
41
42
43
44 86
45
46 87 **Figure 1.** Sketch showing water flow and ion distribution at the interface between a silica mineral
47
48 88 and a NaCl aqueous solution (modified, from Brown et al. [40]). Circles with arrows inside
49
50 89 represent water molecules. The shear plane is denoted by the red dashed line. Counter-ions
51
52 90 adsorbed as outer sphere complexes form the outer Helmholtz plane (OHP).

53
54 91
55
56
57 92 The quartz (0001) crystal face is the most stable plane with the lowest surface energy and is often
58
59 93 considered as a “model surface”, convenient for modelling SiO_2 materials and hydrophilic surfaces

1
2
3
4
5
6
7
8
9
10
11
12
13
14
15
16
17
18
19
20
21
22
23
24
25
26
27
28
29
30
31
32
33
34
35
36
37
38
39
40
41
42
43
44
45
46
47
48
49
50
51
52
53
54
55
56
57
58
59
60
61
62
63
64
65

94 in general [35]. With the improved accuracy of the streaming potential method, it is now possible
95 to accurately measure extremely small voltages due to the displacement of the ions in the EDL of
96 quartz [14]. Published studies of Jaafar et al. [8], Vinogradov et al. [13], Walker et al. [44], and
97 Walker and Glover [15] observed, that at high salinities (NaCl concentrations above 0.4 M, M
98 means mol L⁻¹), the zeta potential of sandstones appears to level off at a small constant negative
99 value between -30 and -10 mV or even to increase slightly in magnitude (i.e. become more
100 negative) with salinity. They noted that the zeta potential of sandstones stabilizes at a salinity of
101 about 0.4 M NaCl that corresponds to a Debye length characterizing the diffuse layer thickness of
102 approximately 0.47 nm, which is similar to the size of a hydrated sodium ion. This observation led
103 them to suggest that the constant zeta potential of sandstones at high salinities reflected the
104 maximum charge density in the diffuse layer which was reached when the diffuse layer thickness
105 approached the diameter of the counter-ions [45]. However, Jaafar et al. [8], Vinogradov et al. [13],
106 Walker et al. [44], Glover [45], and Walker and Glover [15] did not explicitly explain this behavior
107 through a **basic Stern** surface complexation model describing their zeta potential measurements on
108 sandstones.

109 In our study, we used a surface complexation model named basic Stern model (BSM) and
110 considered that the shear plane is at the OHP or closer to the mineral surface than the OHP to
111 describe the zeta potential and the electrochemical properties of quartz at varying NaCl
112 concentrations. In our model we described the effective location of the OHP and the shear plane,
113 hence modelling the effective zeta potential. Therefore, the developed surface complexation model
114 accurately replicated the experimental conditions under which the streaming potential
115 measurements on intact rock samples comprising grains of various shape and roughness were
116 conducted. The model predictions were compared to the existing experimental zeta potential data

1
2
3
4
5
6
7
8
9
10
11
12
13
14
15
16
17
18
19
20
21
22
23
24
25
26
27
28
29
30
31
32
33
34
35
36
37
38
39
40
41
42
43
44
45
46
47
48
49
50
51
52
53
54
55
56
57
58
59
60
61
62
63
64
65

117 measured over a broad salinity range (from around 10^{-4} M NaCl up to around 5.5 M NaCl). The
118 values of the optimized parameters were finally discussed. Our findings shed light on the
119 electrochemical properties of quartz and on the likelihood of non-zero water flow within the Stern
120 layer.

121

122 **2. Theoretical background**

123 *2.1. Surface complexation model for quartz*

124 Our basic Stern model [37, 46] describes proton (H^+) adsorption onto $>SiO^-$ surface sites at the 0-
125 plane (defining the mineral surface) and sodium cation (Na^+) adsorption by these surface sites at
126 the β -plane (Stern plane and OHP) (Figure 2) [3, 6, 20, 21, 23]. The BSM considers that the β -
127 plane coincides with the d -plane defining the start of the diffuse layer. This model only needs one
128 Stern layer capacitance as an input parameter to model the electrical potential distribution between
129 the mineral surface and the Stern plane. Recent studies utilizing atomic force microscopy (AFM)
130 (e.g., Siretanu et al. [47]) and X-ray photoelectron spectroscopy (XPS) (e.g., Brown et al. [40])
131 used the BSM to model the electrochemical properties of amorphous silica in contact with a NaCl
132 aqueous solution and demonstrated that the BSM could accurately reproduce the experimental data.
133 García et al. [6] also used the BSM to match the measured electrochemical properties of quartz in
134 contact with a NaCl aqueous solution thus confirming the validity of the approach.

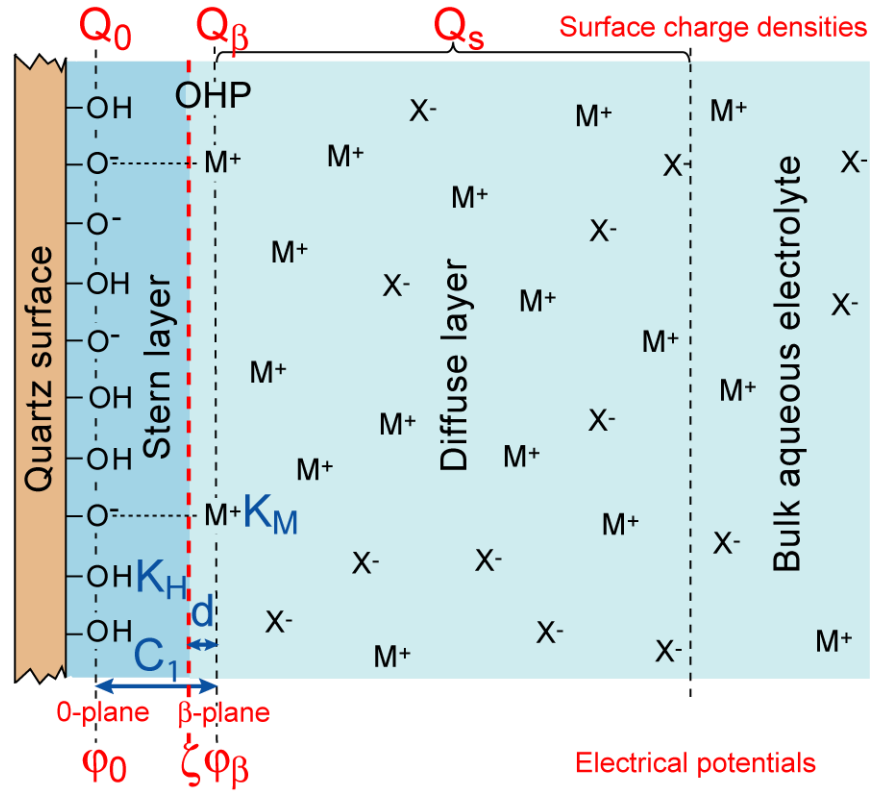


Figure 2. Sketch of our basic Stern model to describe the electrochemical properties of the interface between quartz and a 1:1 electrolyte like NaCl electrolyte (the β -plane coincides with the d -plane). The model input parameters are shown in blue and the model output parameters, including the zeta potential (ζ) at the shear plane, are shown in red.

In our BSM we used four adjustable parameters, namely the logarithms of the two adsorption equilibrium constants K_H and K_{Na} , the Stern layer capacitance C_1 ($F\ m^{-2}$), and the distance d between the shear plane (where the zeta potential is defined) and the β -plane (Figure 2). It should be noted that we considered that the doubly coordinated surface groups ($>Si_2O^0$) are inert [20] and that the protonated silanol sites ($>SiOH_2^+$) are not expected to form at close-to-neutral pH of the streaming potential measurements on sandstones (pH varied between 6.4 and 7.3 Walker and Glover [15]). Therefore, these surface sites were excluded from the model. In absence of additional

1
2
3
4
5
6
7
8
9
10
11
12
13
14
15
16
17
18
19
20
21
22
23
24
25
26
27
28
29
30
31
32
33
34
35
36
37
38
39
40
41
42
43
44
45
46
47
48
49
50
51
52
53
54
55
56
57
58
59
60
61
62
63
64
65

148 measurements, we also did not consider another type of silanol group, hence we made our model
149 as simple as possible in order to decrease the number of optimized parameters. For more
150 information related to our BSM, the reader can refer to Appendixes A and B, and to Leroy et al.
151 [21].

153 2.2. Zeta potential computation

154 All calculations were performed by combining the geochemical software IPhreeqc for the surface
155 complexation modelling [48] with an in-house code implemented in Matlab for the calculation of
156 the zeta potential and the optimization procedure [49]. The zeta potential (ζ) defined at the shear
157 plane located at a distance d from the β -plane was determined from the computed φ_0 and φ_β
158 electrical potentials by considering a linear, capacitor-like variation of the electrical potential
159 within the Stern layer [25]

$$\zeta = \varphi_\beta - \left(\frac{\varphi_\beta - \varphi_0}{x_\beta - x_0} \right) d, \quad (1)$$

160 where x is the distance from the mineral surface (defined by the 0-plane, in m). Combining equation
161 (1) with the following equation for the Stern layer capacitance [18]

$$C_1 = \frac{\varepsilon_1}{x_\beta - x_0}, \quad (2)$$

162 where ε_1 is the water permittivity in the Stern layer (F m^{-1} ; we used $\varepsilon_1 = 43\varepsilon_0$, where ε_0 is the
163 vacuum permittivity, in accordance with the study of Sverjensky [3]), we finally obtain an
164 expression for the zeta potential as a function of the modelled electrochemical properties

$$\zeta = \varphi_\beta - (\varphi_\beta - \varphi_0) \frac{C_1}{\varepsilon_1} d. \quad (3)$$

We did not consider the presence of a stagnant diffuse layer (also named buffer layer), which implies that the shear plane is located further away from the mineral surface, as suggested in Alizadeh and Wang [50]. To the best of our knowledge, the stagnant diffuse layer existence has never been directly confirmed experimentally. To the contrary, Předota et al. [35], Brkljača et al. [19], and Biriukov et al. [34] predicted no such stagnant diffuse layer from their molecular dynamic simulations of the zeta potential of the hydroxylated (110) rutile (TiO₂) and (0001) quartz surfaces. Furthermore, Leroy and co-workers. Furthermore, Leroy and co-workers (e.g., Leroy et al. [51], Leroy et al. [52], Leroy et al. [21], Li et al. [30]) attributed the assumption of the presence of a stagnant diffuse layer in previous studies to the misinterpretation of the zeta potentials from electrokinetic (e.g., electrophoretic mobility, streaming potential) measurements due to disregard of surface conductivity effects. Indeed, surface conductivity decreases the magnitude of the measured electrokinetic signal hence implying smaller apparent zeta potentials, which need to move away the shear plane from the mineral surface when modelling the zeta potential from a surface complexation model.

The parameters of our surface complexation model ($\log K_H$, $\log K_{Na}$, C_1 , d) were optimized by minimizing the following cost function [53]:

$$y = 1 - R^2 = \frac{\sum_{i=1}^N (\zeta_{mes}^i - \zeta_{mod}^i)^2}{\sum_{i=1}^N (\zeta_{mes}^i - \langle \zeta_{mes} \rangle)^2}, \quad (4)$$

where R^2 is the coefficient of determination, N is the number of zeta potential measurements, ζ_{mes}^i is the i -th measured zeta potential, $\langle \zeta_{mes} \rangle$ is the arithmetic mean of the measured zeta potentials,

1
2
3
4 183 and ζ_{mod}^i is the i -th modelled zeta potential. The fitting procedure was realized by using the
5
6
7 184 simulated annealing algorithm to find the global minimum of the cost function (equation (4)), with
8
9
10 185 a refinement using the simplex method at the end of the process [49].
11

16 187 **3. Comparison with experimental data and discussion**

20 188 *3.1. Considerations of impact of pore space topology and grain roughness on EDL parameters*

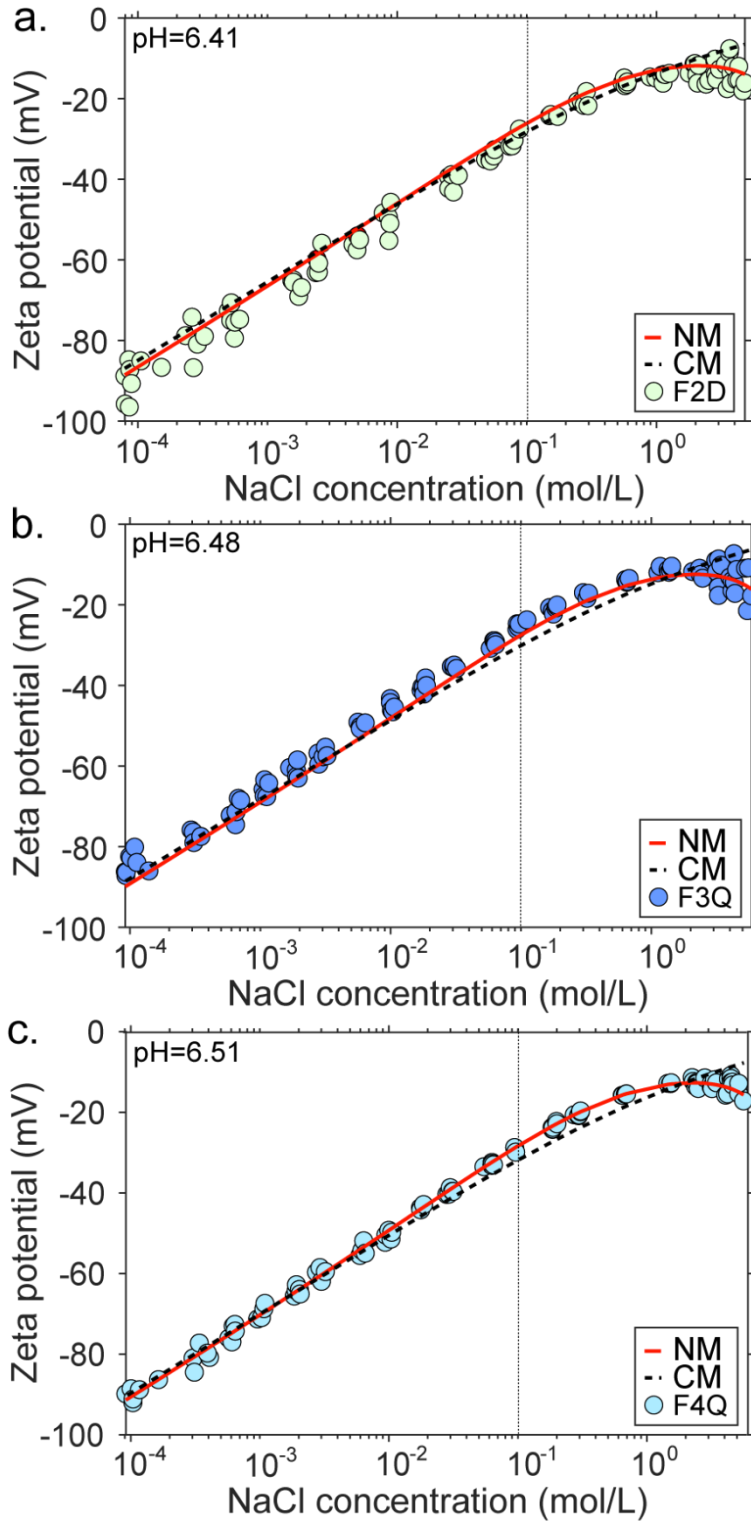
23 189 To test our model, we used the measured zeta potentials of Fontainebleau (F2D, F3Q, F4Q) and
24
25 190 Lochaline (L3Q, L4Q) samples in contact with a NaCl aqueous solution of increasing salinity
26
27
28 191 obtained by the streaming potential method and reported in Walker and Glover [15]. These two
29
30 192 sample types were selected as they are known to consist of more than 99% quartz (by weight) [13,
31
32
33 193 54]. Unlike Fontainebleau and Lochaline samples, zeta potentials of Berea and Boise sandstones
34
35 194 reported by Walker and Glover [15] that contained up to 6% feldspar, 2% dolomite, and 8% clays
36
37
38 195 for Berea rocks [55] and up to 13% clays for Boise rocks [56], were excluded from the simulation.
39
40 196 Despite the fact that feldspar, dolomite, and clay content in Berea and Boise samples is relatively
41
42
43 197 small, clays are known to line pore walls, thus making these complex minerals a main contributor
44
45 198 to the electrochemical processes at the mineral-water interface and causing anomalous or even
46
47
48 199 positive zeta potentials [57, 58]. Therefore, the experimental zeta potential data for Boise and Berea
49
50 200 samples were deemed unapplicable for our model that considers only surface complexation
51
52 201 reactions on quartz surface.
53

55 202 All Fontainebleau and Lochaline samples exhibit a negative zeta potential with its magnitude
56
57
58 203 decreasing with increasing salinity (Figures 3 and 4). The zeta potentials of Lochaline samples
59
60
61
62
63
64
65

1
2
3
4
5
6
7
8
9
10
11
12
13
14
15
16
17
18
19
20
21
22
23
24
25
26
27
28
29
30
31
32
33
34
35
36
37
38
39
40
41
42
43
44
45
46
47
48
49
50
51
52
53
54
55
56
57
58
59
60
61
62
63
64
65

204 were found to be of a larger magnitude than those of Fontainebleau samples. Scanning electron
205 microscopy (SEM) micrographs of the tested samples showed that Fontainebleau rock has sharper-
206 angled grains with larger surface roughness and smaller grains than Lochaline rock (Figure 5 from
Walker and Glover [15]). According to Vinogradov et al. [14], pore space topology, grain shape,
208 surface roughness and size influence streaming potential measurements. They considered that
209 rough rocks with small grains have smaller streaming and zeta potential magnitudes than round,
210 smooth rocks with large grains because rock sharp corners and grain roughness would shift the
211 effective shear plane further away from the mineral surface (read their section 4.2). Alroudhan et
212 al. [59] used the same assumption to explain that the zeta potential of colloidal suspensions
213 measured by the electrophoretic mobility method is larger in magnitude than the zeta potential of
214 rocks measured by the streaming potential method (see their Figure 10 and read the related
215 discussion in their section 5.2). Schnitzer and Ripperger [60] and Drechsler et al. [61] showed that
216 increasing surface roughness changes the flow velocity distribution on the solid surface shifting
217 the shear plane further away from the solid surface and decreases the streaming and zeta potential
218 magnitudes. According to these observations, we expected different values of the surface
219 complexation model parameters between Fontainebleau and Lochaline samples, notably for the
220 Stern layer capacitance C_1 and the distance d of the shear plane from the OHP (or Stern plane),
221 which are very sensitive to the textural properties of rocks (C_1 depends on the thickness of the
222 Stern layer, equation (2)).

1
2
3
4
5
6
7
8
9
10
11
12
13
14
15
16
17
18
19
20
21
22
23
24
25
26
27
28
29
30
31
32
33
34
35
36
37
38
39
40
41
42
43
44
45
46
47
48
49
50
51
52
53
54
55
56
57
58
59
60
61
62
63
64
65

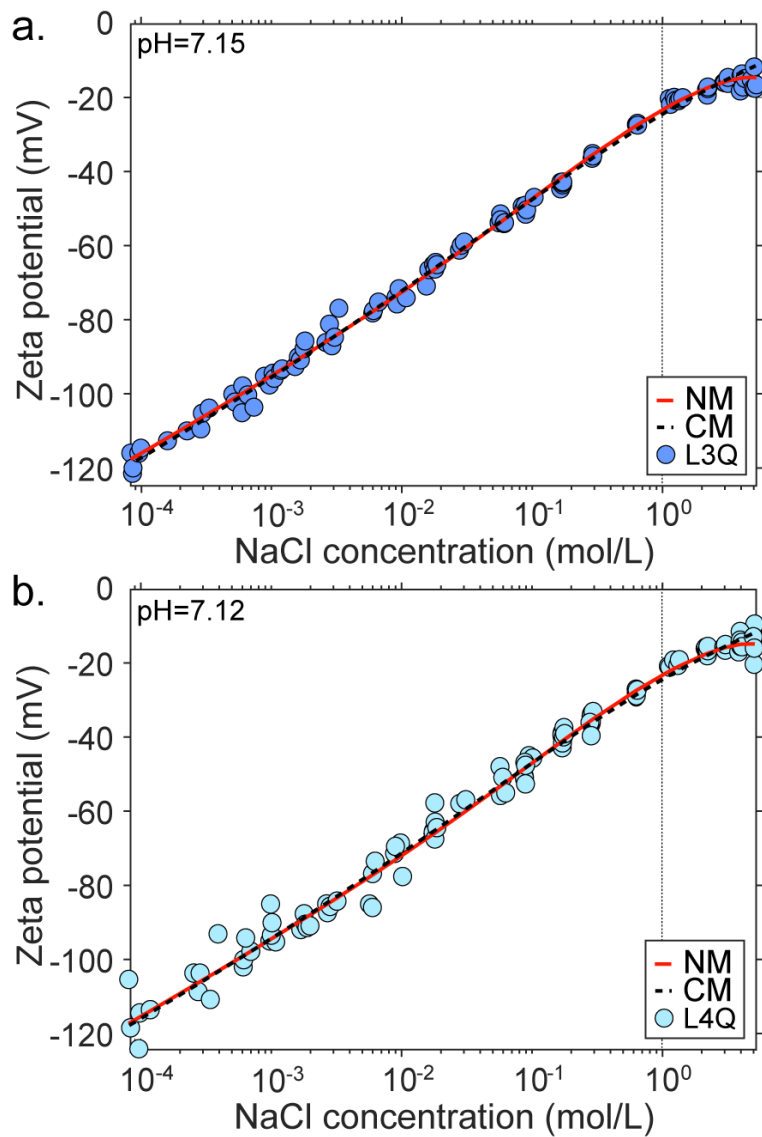


224

225
226
227

Figure 3. Zeta potentials of Fontainebleau samples as a function of NaCl concentration. Circle symbols: experimental zeta potential data with the sample name corresponding to that used by Walker and Glover [15]; curves: model predictions.

1
2
3
4 228
5
6

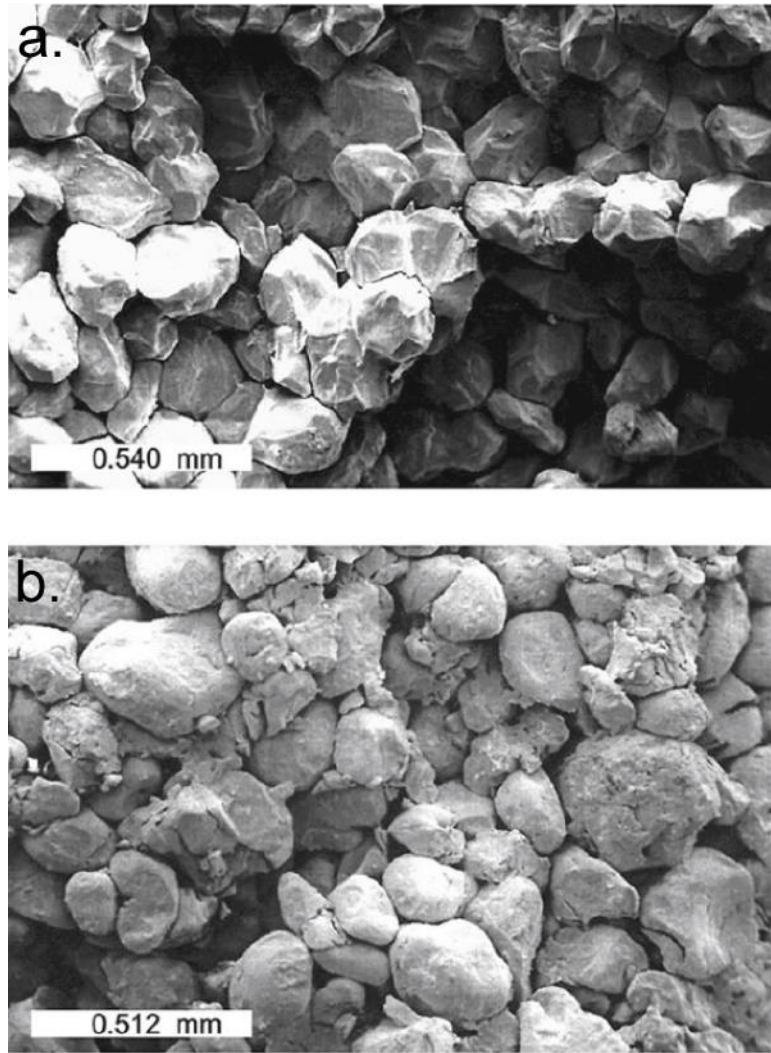


229
230

Figure 4. Zeta potentials of Lochaline samples as a function of NaCl concentration. Circle symbols: experimental zeta potential data with the sample name corresponding to that used by Walker and Glover [15]; curves: model predictions.

233
234
235
236
237
238
239
240
241
242
243
244
245
246
247
248
249
250
251
252
253
254
255
256
257
258
259
260
261
262
263
264
265

1
2
3
4
5
6
7
8
9
10
11
12
13
14
15
16
17
18
19
20
21
22
23
24
25
26
27
28
29
30
31
32
33
34
35
36
37
38
39
40
41
42
43
44
45
46
47
48
49
50
51
52
53
54
55
56
57
58
59
60
61
62
63
64
65



234
235 **Figure 5.** SEM micrographs of Fontainebleau (a) and Lochaline (b) rocks (modified from Walker
236 and Glover [15]).

237
238 Figures 3 and 4 demonstrate that below the concentration thresholds of around 0.1 M NaCl
239 (Fontainebleau samples) and 1 M NaCl (Lochaline samples) (denoted by the vertical black dotted
240 lines), the magnitude of the negative zeta potential decreases linearly with increasing salinity.
241 Interestingly, the rate of decrease in the zeta potential magnitude with increasing salinity became
242 smaller above these thresholds, i.e. it became non-linear, and eventually stabilized (or even slightly

1
2
3
4 243 increased in magnitude) at a zeta potential value of approximately -15 mV for both rock types.
5
6 244 Such stabilization of the zeta potential was more apparent for Fontainebleau than for Lochaline
7
8
9 245 samples. These observations were consistent across the data reported by Vinogradov et al. [13],
10
11 246 Vinogradov et al. [14] and Walker and Glover [15], who stated that at high salinities, the measured
12
13
14 247 zeta potential stabilized and became equal to -13.01 ± 0.48 mV for Fontainebleau samples and to
15
16 248 -16.81 ± 0.68 mV for Lochaline samples.

17
18
19 249 Considering that Fontainebleau and Lochaline sandstones did not have the same pore space
20
21
22 250 topology and textural properties, we first optimized separately the parameters of the surface
23
24 251 complexation models for these two rock types. That is, a single model was developed for F2D,
25
26
27 252 F3Q, F4Q combined data (Fontainebleau rocks) and a separate model was developed for L3Q, L4Q
28
29 253 combined data (Lochaline rocks) to match simulated to observed zeta potentials. We ran the
30
31
32 254 classical model denoted CM with the parameters $\log K_H$, $\log K_{Na}$, and C_1 , and the new model
33
34
35 255 denoted NM with the parameters $\log K_H$, $\log K_{Na}$, C_1 , and d (the distance of separation between
36
37
38 256 the shear plane and OHP), to investigate the effect of the proposed inward shift of the shear plane
39
40 257 on the simulated zeta potential while assigning measured pH values to the respective rock samples
41
42
43 258 as reported by Walker and Glover [15]. We then used the same BSM approach for Fontainebleau
44
45 259 and Lochaline samples together (all five samples, F2D, F3Q, F4Q, L3Q, L4Q) to develop a unified
46
47
48 260 surface complexation model for quartz in contact with a NaCl aqueous solution, denoted UNM for
49
50 261 unified new model and UCM for unified classical model.

51
52
53 262
54
55
56 263
57
58
59
60 264
61
62
63
64
65

1
2
3
4
5
6
7
8
9
10
11
12
13
14
15
16
17
18
19
20
21
22
23
24
25
26
27
28
29
30
31
32
33
34
35
36
37
38
39
40
41
42
43
44
45
46
47
48
49
50
51
52
53
54
55
56
57
58
59
60
61
62
63
64
65

3.2. Comparison of the computed to the observed zeta potentials and discussion

Overall, both the NM and CM reproduced well the experimental zeta potential data for the entire salinity range (Figures 3 and 4, and Tables 1 and 2). To estimate the uncertainties, we fixed two/three of the three/four parameters at their optimal values and then we computed the cost function (i.e., $y=1-R^2$) for the remaining parameter which is allowed to vary. Afterwards, we computed the relative cost function associated to the varying parameter $(y-y_{opt})/y_{opt}$, where y_{opt} is the value of the cost function when the three/four parameters are fixed at their optimal values (so the relative cost function associated to the varying parameter is equal to zero for the optimal set of parameters). Finally, we extracted the range of values of the varying parameter for which the relative cost function is less than 0.1. We performed this procedure for the three/four parameters.

According to the surface complexation models, the observed negative zeta potential was due to the presence of the deprotonated silanol sites $>SiO^-$ at the 0-plane (Figure 2). The optimized values of the equilibrium constant describing protonation of $>SiO^-$ surface sites (K_H , reaction (1)) equal to $10^{7.3}$ and $10^{7.2}$ for Fontainebleau and Lochaline samples, respectively, were found to be close or similar to the spectroscopically determined value of $10^{7.2\pm 0.2}$ and to the theoretical value of $10^{7.5}$ using Pauling's definition of formal bond valence for silica [20] (Table 1). In addition, our K_H optimized values were found to be close or similar to the value of $10^{7.2}$ determined by Sverjensky [3] using a triple layer model (BSM with an additional C_2 capacitance between the Stern plane and the start of the diffuse layer) matching surface charge density measurements inferred from acid base potentiometric titration on natural quartz in contact with a NaCl solution. The models also explained why the zeta potential magnitude of Lochaline samples was larger, for the same salinity, than the zeta potential magnitude of Fontainebleau samples. Indeed, Lochaline samples have higher

1
2
3
4
5
6
7
8
9
10
11
12
13
14
15
16
17
18
19
20
21
22
23
24
25
26
27
28
29
30
31
32
33
34
35
36
37
38
39
40
41
42
43
44
45
46
47
48
49
50
51
52
53
54
55
56
57
58
59
60
61
62
63
64
65

287 pH (i.e. less protons in solution) than Fontainebleau samples (7.1 versus 6.5 in average,
288 respectively Walker and Glover [15]) while having essentially identical $\log K_H$ values, which
289 resulted in Lochaline samples having larger number of deprotonated $>SiO^-$ sites per nm^2 of surface
290 and a higher negative surface charge density Q_0 (equation (A5)) than Fontainebleau samples
291 (Figure 6).

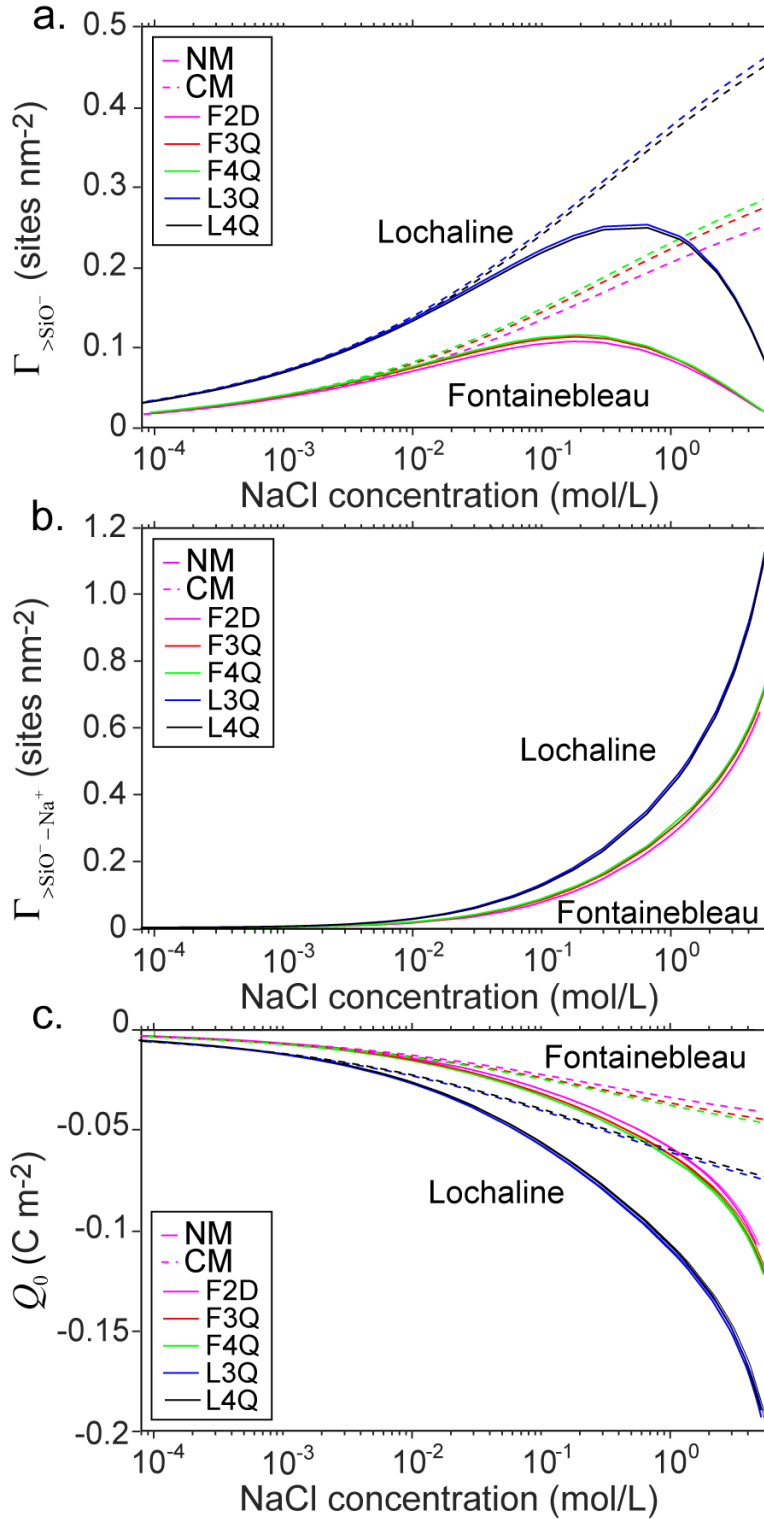
Table 1. BSM parameter values and estimated Stern layer thickness for Fontainebleau and Lochaline sandstones.

Symbols	Range ¹	Fontainebleau		Lochaline	
		CM	NM	CM	NM
$\log K_H$	[4 10]	7.32 [7.28 7.36]	7.27 [7.24 7.3]	7.21 [7.18 7.24]	7.24 [7.21 7.27]
$\log K_{Na}$	[-20 5]	-20 [ND ³]	0.58 [0.25 0.83]	-20 [ND ³]	0.13 [-0.1 0.32]
C_1 (F m ⁻²)	[0.5 5]	3.24 [2.01 6.54]	1.34 [1.18 1.51]	1.84 [1.62 2.10]	2.22 [2.01 2.47]
d (Å)	[0 10]	0	0.48 [0.42 0.54]	0	0.25 [0.21 0.28]
d_{Stern}^2 (Å)		1.18 [0.58 1.89]	2.85 [2.52 3.23]	2.07 [1.81 2.35]	1.71 [1.54 1.89]

¹ Hiemstra et al. [20], Kitamura et al. [23], Sonnefeld et al. [62], Sverjensky [3], García et al. [6].

² According to Eq. (2) and fitted C_1 values, considering $\epsilon_1 = 43\epsilon_0$ and $d_{Stern} = x_\beta - x_0$.

³ Not determined.



298
299 **Figure 6.** Computed surface site densities of $>SiO^-$ sites (a), $>SiO^- - Na^+$ sites b), and of surface
300 charge densities (c) of Fontainebleau and Lochaline samples as a function of NaCl concentration.
301 Plain line curves correspond to the calculations using the NM, dotted line curves correspond to the

1
2
3
4
5
6
7
8
9
10
11
12
13
14
15
16
17
18
19
20
21
22
23
24
25
26
27
28
29
30
31
32
33
34
35
36
37
38
39
40
41
42
43
44
45
46
47
48
49
50
51
52
53
54
55
56
57
58
59
60
61
62
63
64
65

302 calculations using the CM. The CM predicted near-zero surface site densities of adsorbed sodium
303 ion in the Stern layer (limited at $\cong 0$ sites nm^{-2} in Figure 6b).

304
305 We also found that Lochaline samples have significantly lower $\log K_{\text{Na}}$ values, i.e. weaker sodium
306 adsorption capacity, than Fontainebleau samples (-21 vs -16, respectively, for CM and 0.1 vs 0.6,
307 respectively, for NM, Table 1), which could not counterbalance the negative surface charge density
308 as efficiently as for Fontainebleau samples, and can also explain the larger zeta potential magnitude
309 of Lochaline samples. Interestingly, despite Lochaline samples having lower $\log K_{\text{Na}}$ values than
310 Fontainebleau samples, the models found that Lochaline samples, for the same salinity, had a
311 higher surface site density of adsorbed sodium ion in the Stern layer than Fontainebleau samples
312 due to the higher $>\text{SiO}^-$ surface site density (Figure 6b). The lower $\log K_{\text{Na}}$ values of Lochaline
313 than Fontainebleau samples we found can be explained by Lochaline samples having smoother and
314 larger grains and hence a smaller specific surface area than Fontainebleau samples. Sverjensky [3]
315 did the same observation when comparing two quartz with different specific surface area (4.15 and
316 $11.4 \text{ m}^2 \text{ g}^{-1}$) in contact with a NaCl solution. The K_{Na} values inferred from the CM are extremely
317 low and essentially mean that there is no adsorption of Na^+ at the OHP at all and everything is
318 controlled only by pH. With the CM, the optimization procedure decreases K_{Na} to extremely low
319 value to fit the high salinity zeta potential measurements (decreasing Na^+ adsorption in the Stern
320 layer results to higher zeta potential magnitude).

321 With the NM, the optimization procedure doesn't need to decrease K_{Na} to extremely low value to
322 fit the high salinity zeta potential measurements and it found $\log K_{\text{Na}}$ values (0.6 and 0.1 for
323 Fontainebleau and Lochaline samples, respectively) within the same order of magnitude than the

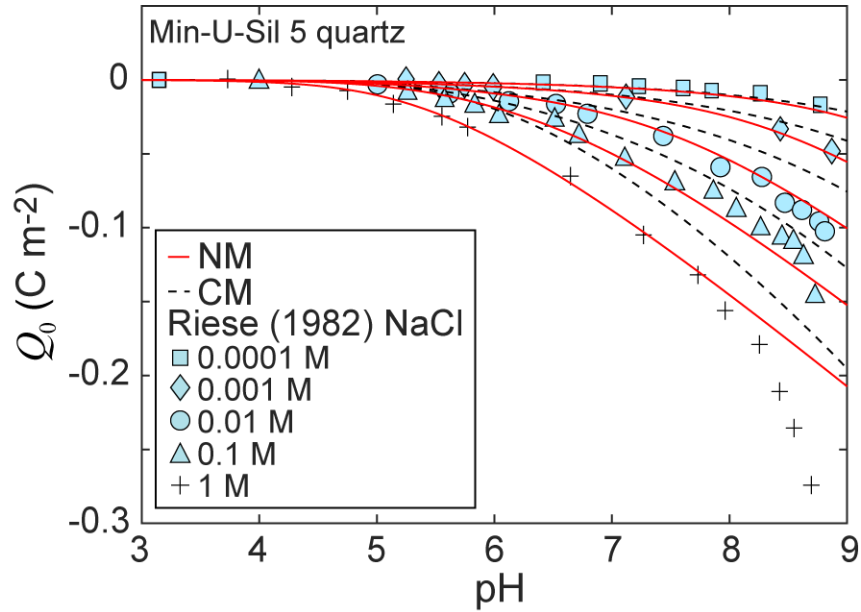


Figure 7. Surface charge density of Min-U-Sil 5 quartz as a function of pH and NaCl concentration. Curves correspond to the predictions. Symbols correspond to the experimental surface charge density data reported by Riese [63].

With the NM, the optimized Stern layer capacitance values were equal to 1.3 F m^{-2} and 2.2 F m^{-2} for Fontainebleau and Lochaline samples, respectively (Table 1), which were close to the values of 1 F m^{-2} and 2 F m^{-2} reported by Sverjensky [3] and García et al. [6], respectively, for natural quartz in contact with a NaCl solution. With the CM, the optimized Stern layer capacitance values were equal to 3.2 F m^{-2} and 1.8 F m^{-2} for Fontainebleau and Lochaline samples, respectively. Using the optimized Stern layer capacitance values from the NM, equation (2) and $\varepsilon_1 = 43\varepsilon_0$ [3, 40], we

1
2
3
4 339 found a Stern layer thickness comparable to the hydrated radius of sodium ion ($\cong 2 \text{ \AA}$ Leroy et al.
5
6
7 340 [64] Sverjensky [18]), with Fontainebleau samples having larger Stern layer thickness (2.8 \AA) than
8
9 341 Lochaline samples (1.7 \AA), which can be explained by Fontainebleau samples having sharper and
10
11 342 rougher grains than Lochaline samples [15, 65]. When using the CM, the Stern layer thickness we
12
13 343 found for Fontainebleau samples (1.2 \AA) was comparable to the crystallographic radius of sodium
14
15 344 ion (1.02 \AA Sverjensky [18]). This result was not realistic regarding the representation of the
16
17 345 quartz/NaCl solution interface containing mostly hydrated sodium ions in the Stern layer, which is
18
19 346 accepted by most recent models (e.g., Brown et al. [66]). For Lochaline samples, the Stern layer
20
21 347 thickness inferred from the CM was comparable to the hydrated radius of sodium ion (2.1 \AA).
22
23
24
25
26
27 348 Figures 3, 4, 7, and the modelling results reported in Table 1 for the parameter values and in Table
28
29 349 2 for the coefficient of determination values clearly demonstrate the importance of considering the
30
31 350 location of the shear plane to be closer to the mineral surface than the OHP. Indeed, as shown in
32
33 351 Figures 3 and 4 and reflected by the values of the coefficient of determination at high salinity
34
35 352 reported in Table 2 ($R^2 \geq 0.5$), the stabilization of the zeta potential at high salinity could only be
36
37 353 correctly predicted by the NM (red curves in Figures 3 and 4). The stabilization of the modelled
38
39 354 zeta potential at high salinity is explained by a growing abundance of sodium ions available for
40
41 355 adsorption in the Stern layer, and therefore the decreasing number of $>\text{SiO}^-$ sites (Figures 6a and
42
43 356 6b), and importantly by the shear plane being located slightly closer to the mineral surface than the
44
45 357 OHP. Moreover, the NM reproduced the surface charge density measurements on natural quartz in
46
47 358 a NaCl solution reported in Riese [63] significantly better than the CM (Figure 7) thus
48
49 359 independently validating our assumption on the location of the shear plane.
50
51
52
53
54
55
56
57
58
59
60
61
62
63
64
65

Table 2. Coefficient of determination values using different BSM parameter values for Fontainebleau and Lochaline sandstones.

	F2D		F3Q		F4Q		L3Q		L4Q	
	CM	NM	CM	NM	CM	NM	CM	NM	CM	NM
R^2	0.97	0.98	0.97	0.99	0.99	1	1	1	0.99	1
R^2 LS ¹	0.96	0.96	0.97	0.97	0.99	0.99	0.99	0.99	0.98	0.98
R^2 HS ²	-0.31	0.60	-0.56	0.60	0.12	0.92	-0.03	0.62	0.26	0.50

¹ Low salinity, below 0.1 M NaCl (Fontainebleau samples) and 1 M NaCl (Lochaline samples).

² High salinity, above 0.1 M NaCl (Fontainebleau samples) and 1 M NaCl (Lochaline samples).

The measured high salinity zeta potentials were closely matched by the BSM considering the shear plane slightly approaching the mineral surface, i.e. with a very small distance from the OHP ($d = 0.5 \text{ \AA}$ for Fontainebleau samples and $d = 0.3 \text{ \AA}$ for Lochaline samples; Table 1). Including such a small distance d between OHP and shear plane progressively increases computed zeta potential magnitude compared to not considering it when salinity increases (Figure 8). The effective distance d used in our NM was significantly smaller than the hydrated radius of Na^+ ($\cong 2 \text{ \AA}$ Leroy et al. [64] Sverjensky [18]), which implied that only some of Na ions were mobilized in the Stern layer, i.e., only a small portion of all ions could move inside the Stern layer. In addition, d/d_{Stern} (Lochaline) = d/d_{Stern} (Fontainebleau) = 0.18. This means that regardless of rock type 18% of the, previously considered as immobile ions in the Stern layer will be flowing. Then, the thicker the Stern layer is (and we expect it to become thicker as roughness increases), the larger d will become – exactly as NM predicts.

In addition, unlike the CM, the NM found that the shear plane of Fontainebleau samples is further away from the mineral surface than the shear plane of Lochaline samples, also explaining why the zeta potential magnitude of Fontainebleau samples is smaller than the zeta potential magnitude of Lochaline samples. Indeed, the total distance of the shear plane from the mineral surface (d_{Stern} –

1
2
3
4
5
6
7
8
9
10
11
12
13
14
15
16
17
18
19
20
21
22
23
24
25
26
27
28
29
30
31
32
33
34
35
36
37
38
39
40
41
42
43
44
45
46
47
48
49
50
51
52
53
54
55
56
57
58
59
60
61
62
63
64
65

d is larger for Fontainebleau ($2.8-0.5=2.3 \text{ \AA}$) compared with Lochaline ($1.7-0.3=1.4 \text{ \AA}$) samples, which is consistent with our hypothesis that rougher and sharper Fontainebleau grains push EDL further away from the mineral surface (both, the Stern plane and the shear plane). These findings were in agreement with the SEM micrographs showing that Fontainebleau rock has sharper-angled grains with larger surface roughness than Lochaline rock (Figure 5).

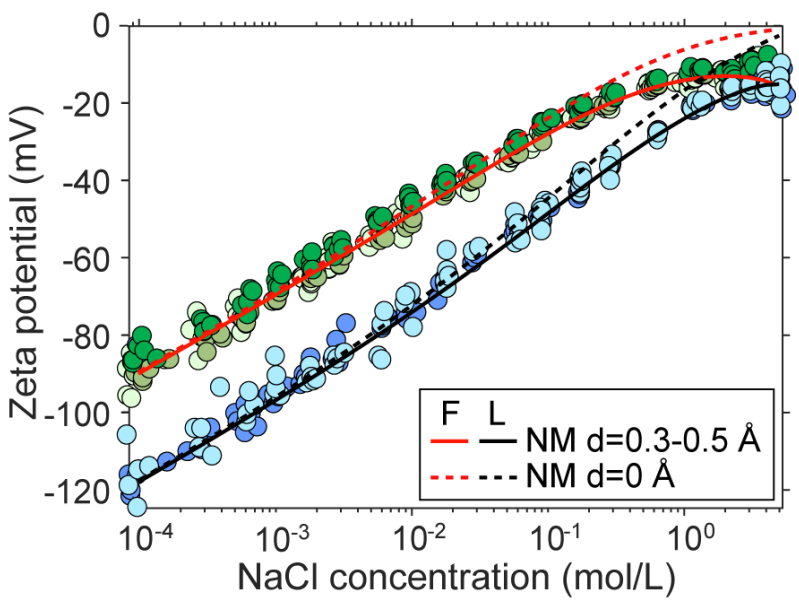


Figure 8. Computed zeta potential of Fontainebleau (F) and Lochaline (L) samples as a function of NaCl concentration considering or not the distance d between the OHP and the shear plane.

In the classical theory of the electrical double layer, it is assumed that only the mobile excess counter-ions in the diffuse layer contribute to the measured macroscopic streaming potential [28]. However, the diffuse layer is highly compressed at high salinity, so that there are essentially no mobile counter-ions available inside it, and such near-zero contribution of the diffuse layer cannot explain correctly the non-zero zeta potentials in Fontainebleau and Lochaline sandstones at high salinity. Figure 9 shows the computed thicknesses of the diffuse layer and of the mobile part of the

1
2
3
4
5
6
7
8
9
10
11
12
13
14
15
16
17
18
19
20
21
22
23
24
25
26
27
28
29
30
31
32
33
34
35
36
37
38
39
40
41
42
43
44
45
46
47
48
49
50
51
52
53
54
55
56
57
58
59
60
61
62
63
64
65

405 Stern layer as well as the surface site density of adsorbed sodium ion in the Stern and diffuse layers,
406 $\Gamma_{>\text{SiO}^- - \text{Na}^+}$ and $\Gamma_{\text{Na}^+}^d$, respectively. The salinity dependence of the diffuse layer thickness was
407 evaluated by the Debye length χ :

$$\chi = \sqrt{\frac{\epsilon_w k_B T}{2e^2 1000 N_A I}}, \quad (5)$$

408 and $\Gamma_{\text{Na}^+}^d$ was calculated using the following equations [24]:

$$\Gamma_{\text{Na}^+}^d = 1000 N_A c_{\text{Na}^+}^\infty \int_{x=0}^{x=\chi} \left\{ \exp[-e\varphi_d(x) / k_B T] - 1 \right\} dx, \quad (6)$$

$$\varphi_d(x) = \frac{4k_B T}{e} \tanh^{-1} \left[\tanh \left(\frac{e\varphi_d}{4k_B T} \right) \exp(-x / \chi) \right], \quad (7)$$

409 where φ_d is the electrical potential at the start of the diffuse layer ($\varphi_\beta = \varphi_d$) and x is the position
410 from the OHP (in m).

411
412
413

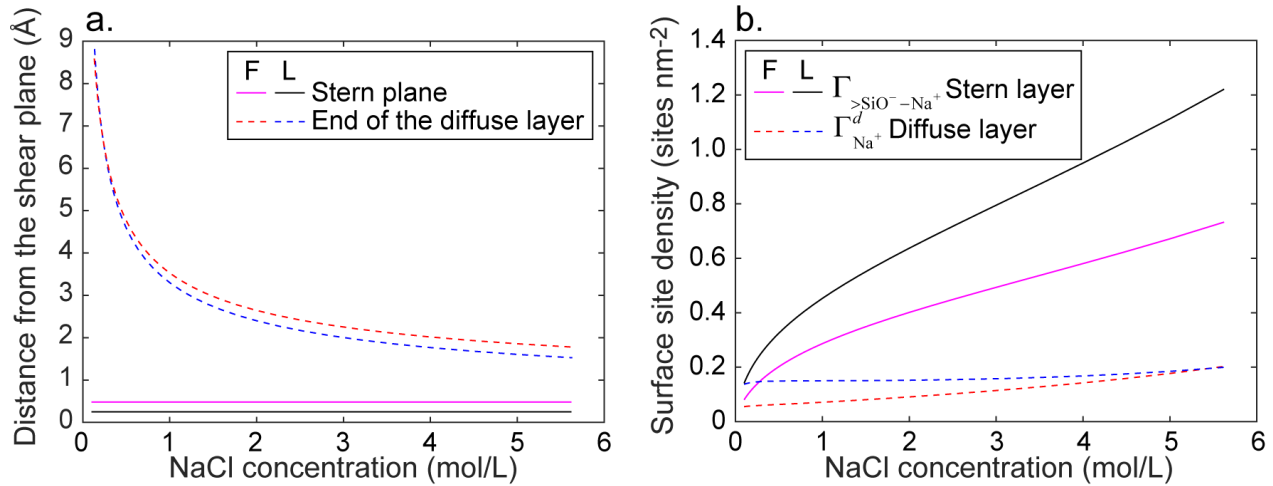


Figure 9. Computed thickness of the diffuse layer (equal to one Debye length) and of the mobile part of the Stern layer (a) and surface site density of adsorbed Na⁺ ion in the Stern and diffuse layers (b) as a function of NaCl concentration for Fontainebleau (F) and Lochaline (L) samples.

The computed thickness of the diffuse layer decreases significantly at high salinity to become comparable to the hydrated radius of sodium ion ($\cong 2 \text{ \AA}$) but it remains considerably larger than the thickness of the mobile part of the Stern layer (0.5 \AA and 0.3 \AA for Fontainebleau and Lochaline samples, respectively) (Figure 9a). However, when salinity increases, the computed surface site density of adsorbed Na⁺ ion in the Stern layer increases considerably more than in the diffuse layer (Figure 9b), which explains the increasing contribution of the counter-ions in the mobile part of the Stern layer to the measured streaming potential.

Our new surface complexation model applied simultaneously for both Fontainebleau and Lochaline samples (all five samples together) in a NaCl aqueous solution (termed here the unified new model, UNM) was still able to reproduce the zeta potential measurements well. Indeed, the values of the coefficient of determination were still close to 1 when calculated for the entire salinity range (Table 3). The UNM reproduced very well the low salinity measurements, and the quality of match was

similar to the results obtained using the unified classical model, UCM. Across the high salinity domain, the UNM was also found to provide a better match to the experimental data compared with the UCM (except for L4Q sample at high salinity). The values of the optimized parameters used in UNM (Table 4) agreed with the values previously reported in Table 1, and both sets were consistent with the values reported in the literature for quartz in a NaCl aqueous solution. Therefore, our approach is relevant for obtaining a unified surface complexation model for quartz in a NaCl solution.

Table 3. Coefficient of determination values using a single set of BSM parameter values for Fontainebleau and Lochaline sandstones together.

	F2D		F3Q		F4Q		L3Q		L4Q	
	UCM	UNM	UCM	UNM	UCM	UNM	UCM	UNM	UCM	UNM
R^2	0.98	0.99	0.97	0.98	0.99	1	1	1	0.99	0.99
$R^2 LS^1$	0.97	0.97	0.95	0.95	0.99	0.99	0.99	0.99	0.98	0.98
$R^2 HS^2$	-0.45	0.46	-0.60	0.29	0.05	0.79	0.00	0.51	0.21	-0.04

¹ Low salinity, below 0.1 M NaCl (Fontainebleau samples) and 1 M NaCl (Lochaline samples).

² High salinity, above 0.1 M NaCl (Fontainebleau samples) and 1 M NaCl (Lochaline samples).

Table 4. BSM parameter values and estimated Stern layer thickness for quartz (combining Fontainebleau and Lochaline sandstones).

Symbols	Range ¹	UCM	UNM
$\log K_H$	[4 10]	7.28 [7.24 7.31]	7.31 [7.27 7.34]
$\log K_{Na}$	[-20 5]	-20 [ND ³]	0.58 [0.27 0.83]
C_1 (F m ⁻²)	[0.5 5]	2.26 [1.78 2.96]	3.43 [2.92 4.02]
d (Å)	[0 10]	0	0.20 [0.17 0.24]
d_{Stern}^2 (Å)		1.68 [1.29 2.14]	1.11 [0.95 1.30]

¹ Hiemstra et al. [20], Kitamura et al. [23], Sonnefeld et al. [62], Sverjensky [3], García et al. [6].

² According to Eq. (2) and fitted C_1 values, considering $\epsilon_1 = 43\epsilon_0$ and $d_{Stern} = x_\beta - x_0$.

³ Not determined.

1
2
3
4
5
6
7
8
9
10
11
12
13
14
15
16
17
18
19
20
21
22
23
24
25
26
27
28
29
30
31
32
33
34
35
36
37
38
39
40
41
42
43
44
45
46
47
48
49
50
51
52
53
54
55
56
57
58
59
60
61
62
63
64
65

4. Conclusions

We developed a new basic Stern surface complexation model to explain the zeta potential measurements on quartz in contact with NaCl aqueous solutions and to describe the concentration dependence of the electrochemical properties of quartz over a broad salinity range (from around 10^{-4} M NaCl up to around 5.5 M NaCl). Previous surface complexation models considered that the shear plane of quartz in contact with a NaCl aqueous solution was located at the Stern plane where sodium counter-ions were preferentially adsorbed or even further away from the mineral surface. In contrast to previous models, our new model considered that there could be some water flow transporting counter-ions within the Stern layer, i.e. that the shear plane where the zeta potential is defined was located closer to the mineral surface than the Stern plane.

Compared to the model considering the zeta potential at the Stern plane, our new model better reproduced the zeta potential measurements on Fontainebleau and Lochaline sandstones, especially in high salinity conditions (above 0.1 M NaCl for Fontainebleau samples and 1 M NaCl for Lochaline samples) where zeta potential appeared to level off at a constant negative value. This was particularly true for Fontainebleau samples. We found a small shear plane offset distance from the Stern plane of around 0.3–0.5 Å, i.e. only a small part of the Stern layer was mobile, confirming that the shear plane was still at a close proximity to the Stern plane. In addition, the optimized value of the equilibrium constant describing sodium adsorption in the Stern layer in our new model was more realistic compared with the classical approach considering zero separation distance between the Stern and the shear planes. The predicted surface charge density of quartz of the new model was also in a better agreement with the experimental data. We also explained, based on SEM micrograph images and our new surface complexation model, why Fontainebleau rocks, with

1
2
3
4 474 sharper-angle grains and larger surface roughness, had smaller in magnitude zeta potential for the
5
6 475 same NaCl concentration compared against Lochaline data.
7
8
9
10 476 Our approach can be used to interpret and even predict streaming potential measurements and other
11
12 477 types of electrokinetic measurements (e.g., electrophoretic mobility) on quartz and other minerals
13
14
15 478 in contact with brines of different chemical compositions and temperatures. Therefore, our results,
16
17 479 which should be confirmed by laboratory measurements at the microscopic scale (e.g., using
18
19
20 480 microfluidics and spectroscopy methods) and atomistic simulations, may have strong implications
21
22 481 for the modelling of the electrochemical properties of minerals in contact with highly saline brines.
23
24
25 482 Our results may be of crucial importance for exploring mineral-brine interactions at high salinity
26
27 483 levels close to real subsurface conditions.
28
29
30 484

31
32
33
34 485 **Acknowledgments**
35
36

37 486 The research work of Shuai Li is funded by the National Natural Science Foundation of China
38
39 487 (grant no. 41974089) and the Fundamental Research Funds for the Central Universities (China
40
41
42 488 University of Geosciences, Wuhan), China (grant no. CUGGC04). Philippe Leroy acknowledges
43
44 489 the internal funding from the French Geological Survey (BRGM) (CHIPPY project no.
45
46
47 490 RP20DEP087) and the support from Francis Claret for his research work as well as the fruitful
48
49 491 scientific discussions with Arnault Lassin. The authors also sincerely acknowledge Paul Glover for
50
51 492 sending the SEM micrographs of Fontainebleau and Lochaline rocks and for fruitful discussions.
52
53
54
55 493
56
57
58 494
59
60
61
62
63
64
65

Appendix A. Basic Stern surface complexation model

The following two surface complexation reactions were considered for the zeta potential modelling:



where K_{H} and K_{Na} (dimensionless) are the associated equilibrium constants, which are written as:

$$K_{\text{H}} = \frac{a_{>\text{SiOH}}}{a_{>\text{SiO}^-} a_{\text{H}^+}} \cong \frac{\Gamma_{>\text{SiOH}}}{\Gamma_{>\text{SiO}^-} a_{\text{H}^+}} = \frac{\Gamma_{>\text{SiOH}}}{\Gamma_{>\text{SiO}^-} a_{\text{H}^+}^{\infty}} \exp\left(\frac{e\varphi_0}{k_{\text{B}}T}\right), \quad (\text{A10})$$

$$K_{\text{Na}} = \frac{a_{>\text{SiO}^- - \text{Na}^+}}{a_{>\text{SiO}^-} a_{\text{Na}^+}} \cong \frac{\Gamma_{>\text{SiO}^- - \text{Na}^+}}{\Gamma_{>\text{SiO}^-} a_{\text{Na}^+}} = \frac{\Gamma_{>\text{SiO}^- - \text{Na}^+}}{\Gamma_{>\text{SiO}^-} a_{\text{Na}^+}^{\infty}} \exp\left(\frac{e\varphi_{\beta}}{k_{\text{B}}T}\right), \quad (\text{A11})$$

where a_i is the activity (dimensionless) and Γ_i is the surface site density (sites m^{-2}) of species i , e is the elementary charge ($\cong 1.602 \times 10^{-19}$ C), φ is the electrical potential (V), k_{B} is the Boltzmann constant ($\cong 1.381 \times 10^{-23}$ J K^{-1}), and T is the temperature (K). In equations (A3) and (A4), the superscript “ ∞ ” refers to ion activities in the electroneutral free or bulk electrolyte (not influenced by the mineral surface), which were computed using Pitzer theory (Appendix B) [64].

The following determined system of equations for the surface charge density at the mineral surface,

Q_0 (C m^{-2}), at the β -plane, Q_{β} , and of the diffuse layer, Q_s , was used to compute the electrical

potential distribution at the interface between quartz and bulk NaCl solution as a function of the

equilibrium constants and Stern layer capacitance [21]:

$$Q_0 = -e(\Gamma_{>\text{SiO}^-} + \Gamma_{>\text{SiO}^- - \text{Na}^+}) = -\frac{e\Gamma_s}{A} \left[1 + K_{\text{Na}} a_{\text{Na}^+}^\infty \exp\left(-\frac{e\varphi_\beta}{k_B T}\right) \right], \quad (\text{A12})$$

$$Q_\beta = e\Gamma_{>\text{SiO}^- - \text{Na}^+} = \frac{e\Gamma_s}{A} K_{\text{Na}} a_{\text{Na}^+}^\infty \exp\left(-\frac{e\varphi_\beta}{k_B T}\right), \quad (\text{A13})$$

$$A = 1 + K_{\text{H}} a_{\text{H}^+}^\infty \exp\left(-\frac{e\varphi_0}{k_B T}\right) + K_{\text{Na}} a_{\text{Na}^+}^\infty \exp\left(-\frac{e\varphi_\beta}{k_B T}\right), \quad (\text{A14})$$

$$Q_s = \sqrt{8\varepsilon_w k_B T 1000 N_A I} \sinh\left[-\left(\frac{e\varphi_\beta}{2k_B T}\right)\right], \quad (\text{A15})$$

$$Q_0 + Q_\beta + Q_s = 0, \quad (\text{A16})$$

$$\varphi_0 - \varphi_\beta = \frac{Q_0}{C_1}, \quad (\text{A17})$$

where Γ_s is the total surface site density (we took $\Gamma_s = 4.6$ sites nm^{-2} García et al. [6]), I is the molar ionic strength (mol L^{-1}), and φ_0 and φ_β are the electrical potentials at the 0-plane and at the β -plane, respectively (considering $\varphi_\beta = \varphi_d$ for the BSM, where φ_d is the electrical potential at the start of the diffuse layer).

1
2
3
4 **512 Appendix B. Pitzer model for ion activity coefficients in bulk electrolyte**

5
6 513

7
8
9 514 The following equations were used to compute ion activity coefficients in bulk electrolyte [64]:

10
11
12
$$a_i^\infty = \gamma_i^\infty \frac{m_i^\infty}{m_0}, \quad (\text{B1})$$

13
14
15
16
17
$$m_i^\infty = \frac{1000c_i^\infty}{M_w c_w^\infty}, \quad (\text{B2})$$

18
19
20
21
22
$$c_w^\infty = \frac{10^3 - \sum_i c_i^\infty V_i}{V_w}, \quad (\text{B3})$$

23
24
25
26
27
28
29 515 where γ_i^∞ is the activity coefficient (dimensionless), m_i^∞ is the molality (mol per kilogram of
30
31
32 516 water, mol kg_w^{-1} , m_0 being the unit molality equal to 1 mol kg_w^{-1}), c_i^∞ is the molar concentration
33
34
35 517 (M), and V_i is the standard partial molal volume ($\text{cm}^3 \text{mol}^{-1}$) of ion i in bulk electrolyte. The
36
37
38 518 quantity $V_i \cong 18.07, 0, -1.13, 17.68 \text{ cm}^3 \text{mol}^{-1}$ for $\text{H}_2\text{O}, \text{H}^+, \text{Na}^+$ (due to electrostriction) and
39
40
41 519 Cl^- , respectively, at a temperature of 25°C. The subscript “w” in equations (B2) and (B3) refers to
42
43 520 water molecules, and M_w refers to the molar mass of water ($\cong 18 \text{ g mol}^{-1}$).

44
45
46
47 521 Na^+ activity coefficient in bulk electrolyte influences modelled Na^+ adsorption in the Stern plane
48
49
50 522 ($\Gamma_{>\text{SiO}^- - \text{Na}^+} = K_{\text{Na}} \Gamma_{>\text{SiO}^-} \gamma_{\text{Na}^+}^\infty m_{\text{Na}^+}^\infty / m_0 \exp(-e\phi_\beta / k_B T)$ from equations (A3) and (A4)). According to
51
52
53 523 Pitzer theory, which is suitable for very saline aqueous solutions (ionic strengths above 0.1 M
54
55 524 Harvie and Weare [67]), the natural logarithm of Na^+ activity coefficient in NaCl electrolyte is
56
57 525 written as:

$$\ln \gamma_{\text{Na}^+}^{\infty} = z_{\text{Na}^+}^2 F + m_{\text{Cl}^-}^{\infty} \left[2B_{\text{Na}^+\text{Cl}^-} + (m_{\text{Na}^+}^{\infty} + m_{\text{Cl}^-}^{\infty}) C_{\text{Na}^+\text{Cl}^-} \right] + z_{\text{Na}^+} m_{\text{Na}^+}^{\infty} m_{\text{Cl}^-}^{\infty} C_{\text{Na}^+\text{Cl}^-}, \quad (\text{B4})$$

$$F = -A_{\phi} \left[\frac{\sqrt{I_m}}{1 + b\sqrt{I_m}} + \frac{2}{b} \ln(1 + b\sqrt{I_m}) \right] + m_{\text{Na}^+}^{\infty} m_{\text{Cl}^-}^{\infty} B'_{\text{Na}^+\text{Cl}^-}, \quad (\text{B5})$$

$$A_{\phi} = \frac{1}{3} \sqrt{\frac{2\pi N_A \rho_w}{1000}} \left(\frac{e^2}{4\pi\epsilon_w k_B T} \right)^{3/2}, \quad (\text{B6})$$

$$B'_{\text{Na}^+\text{Cl}^-} = -\frac{2\beta_{\text{Na}^+\text{Cl}^-}^1}{I_m x_1^2} \left[1 - (1 + x_1 + 0.5x_1^2) \exp(-x_1) \right], \quad (\text{B7})$$

$$x_1 = \alpha_1 \sqrt{I_m}, \quad (\text{B8})$$

$$B_{\text{Na}^+\text{Cl}^-} = \beta_{\text{Na}^+\text{Cl}^-}^0 + \frac{2\beta_{\text{Na}^+\text{Cl}^-}^1}{x_1^2} \left[1 - (1 + x_1) \exp(-x_1) \right], \quad (\text{B9})$$

$$C_{\text{Na}^+\text{Cl}^-} = \frac{C_{\phi \text{Na}^+\text{Cl}^-}}{2\sqrt{|z_{\text{Na}^+} z_{\text{Cl}^-}|}}, \quad (\text{B10})$$

where z_i is the charge number of ion i , b and α_1 are empirical parameters ($b = 1.2$, $\alpha_1 = 2$ for 1:1 and 1:2 electrolytes), I_m is the molal ionic strength (in mol kg_w⁻¹, $I_m = m_{\text{Na}^+}^w$ here), and A_{ϕ} is the Debye-Hückel coefficient describing long-range electrostatic interaction forces between ions ($\cong 0.392$ at a temperature T of 298 K). The Debye-Hückel coefficient was computed here as a function of the Avogadro number N_A ($\cong 6.022 \times 10^{23}$ sites mol⁻¹), the water volumetric density ρ_w ($\cong 997 \times 10^3$ g m⁻³), and the water permittivity ϵ_w ($\cong 78.3\epsilon_0$ where ϵ_0 is the vacuum permittivity with a value of $\cong 8.854 \times 10^{-12}$ F m⁻¹). The Debye-Hückel coefficient multiplied by the terms in brackets in equation (B5) is enough for computing ion activity coefficient in dilute aqueous solution (ionic

1
2
3
4
5
6
7
8
9
10
11
12
13
14
15
16
17
18
19
20
21
22
23
24
25
26
27
28
29
30
31
32
33
34
35
36
37
38
39
40
41
42
43
44
45
46
47
48
49
50
51
52
53
54
55
56
57
58
59
60
61
62
63
64
65

534 strength below 0.1 M). Pitzer and Mayorga [68] considered three additional terms (in equations
535 (B4) and (B5)) to compute ion activity coefficients in concentrated aqueous solutions. The terms
536 $B_{\text{Na}^+\text{Cl}^-}$ and $B'_{\text{Na}^+\text{Cl}^-}$ depend on the ionic strength and describe short-range interaction forces between
537 one cation and one anion (binary system), and the term $C_{\text{Na}^+\text{Cl}^-}$ describes short-range interaction
538 forces between two cations and one anion, and one cation and two anions (ternary system). The
539 Pitzer model for ion activity coefficients in 1:1 aqueous electrolyte such as NaCl depends on three
540 parameters $\beta_{\text{Na}^+\text{Cl}^-}^0$, $\beta_{\text{Na}^+\text{Cl}^-}^1$, and $C_{\phi\text{Na}^+\text{Cl}^-}$. The Pitzer parameter values were adjusted by matching
541 computed to measured osmotic coefficients. According to [Leroy et al. [64]] $\beta_{\text{Na}^+\text{Cl}^-}^0 = 0.0765$,
542 $\beta_{\text{Na}^+\text{Cl}^-}^1 = 0.2664$, and $C_{\phi\text{Na}^+\text{Cl}^-} = 0.00127$.

References

- [1] Y. Duval, J.A. Mielczarski, O.S. Pokrovsky, E. Mielczarski, J.J. Ehrhardt, Evidence of the existence of three types of species at the quartz-aqueous solution interface at pH 0-10: XPS surface group quantification and surface complexation modeling, *Journal of Physical Chemistry B* 106(11) (2002) 2937-2945, <https://doi.org/10.1021/Jp012818s>.
- [2] G. Okay, P. Leroy, A. Ghorbani, P. Cosenza, C. Camerlynck, J. Cabrera, N. Florsch, A. Revil, Spectral induced polarization of clay-sand mixtures: Experiments and modeling, *Geophysics* 79(6) (2014) E353-E375, <https://doi.org/10.1190/Geo2013-0347.1>.
- [3] D.A. Sverjensky, Prediction of surface charge on oxides in salt solutions: Revisions for 1 : 1 (M+L-) electrolytes, *Geochimica Et Cosmochimica Acta* 69(2) (2005) 225-257, <https://doi.org/10.1016/j.gca.2004.05.040>.
- [4] Z. Qi, Y. Wang, H. He, D. Li, X. Xu, Wettability Alteration of the Quartz Surface in the Presence of Metal Cations, *Energy & Fuels* 27(12) (2013) 7354-7359, <https://doi.org/10.1021/ef401928c>.
- [5] F.K. Crundwell, On the Mechanism of the Dissolution of Quartz and Silica in Aqueous Solutions, *ACS Omega* 2(3) (2017) 1116-1127, <https://doi.org/10.1021/acsomega.7b00019>.
- [6] D. García, J. Lützenkirchen, V. Petrov, M. Siebentritt, D. Schild, G. Lefèvre, T. Rabung, M. Altmaier, S. Kalmykov, L. Duro, H. Geckeis, Sorption of Eu(III) on quartz at high salt concentrations, *Colloids and Surfaces A: Physicochemical and Engineering Aspects* 578 (2019) 123610, <https://doi.org/10.1016/j.colsurfa.2019.123610>.
- [7] A. Revil, P.W.J. Glover, Theory of ionic-surface electrical conduction in porous media, *Phys Rev B* 55(3) (1997) 1757-1773, <https://doi.org/10.1103/PhysRevB.55.1757>.
- [8] M.Z. Jaafar, J. Vinogradov, M.D. Jackson, Measurement of streaming potential coupling coefficient in sandstones saturated with high salinity NaCl brine, *Geophysical Research Letters* 36(21) (2009), <https://doi.org/10.1029/2009gl040549>.
- [9] M. Skold, A. Revil, P. Vaudelet, The pH dependence of spectral induced polarization of silica sands: Experiment and modeling, *Geophysical Research Letters* 38 (2011), <https://doi.org/10.1029/2011GL047748>.

1
2
3
4
5
6
7
8
9
10
11
12
13
14
15
16
17
18
19
20
21
22
23
24
25
26
27
28
29
30
31
32
33
34
35
36
37
38
39
40
41
42
43
44
45
46
47
48
49
50
51
52
53
54
55
56
57
58
59
60
61
62
63
64
65

[10] A. Kemna, A. Binley, G. Cassiani, E. Niederleithinger, A. Revil, L. Slater, K.H. Williams, A.F. Orozco, F.H. Haegel, A. Hordt, S. Kruschwitz, V. Leroux, K. Titov, E. Zimmermann, An overview of the spectral induced polarization method for near-surface applications, *Near Surf Geophys* 10(6) (2012) 453-468, <https://doi.org/10.3997/1873-0604.2012027>.

[11] A. Revil, M. Karaoulis, T. Johnson, A. Kemna, Review: Some low-frequency electrical methods for subsurface characterization and monitoring in hydrogeology, *Hydrogeology Journal* 20(4) (2012) 617-658, <https://doi.org/10.1007/s10040-011-0819-x>.

[12] A. Binley, S.S. Hubbard, J.A. Huisman, A. Revil, D.A. Robinson, K. Singha, L.D. Slater, The emergence of hydrogeophysics for improved understanding of subsurface processes over multiple scales, *Water Resources Research* 51(6) (2015) 3837-3866, <https://doi.org/10.1002/2015WR017016>.

[13] J. Vinogradov, M.Z. Jaafar, M.D. Jackson, Measurement of streaming potential coupling coefficient in sandstones saturated with natural and artificial brines at high salinity, *Journal of Geophysical Research* 115(B12) (2010), <https://doi.org/10.1029/2010jb007593>.

[14] J. Vinogradov, M.D. Jackson, M. Chamerois, Zeta potential in sandpacks: Effect of temperature, electrolyte pH, ionic strength and divalent cations, *Colloids and Surfaces A: Physicochemical and Engineering Aspects* 553 (2018) 259-271, <https://doi.org/10.1016/j.colsurfa.2018.05.048>.

[15] E. Walker, P.W.J. Glover, Measurements of the Relationship Between Microstructure, pH, and the Streaming and Zeta Potentials of Sandstones, *Transport Porous Med* 121(1) (2018) 183-206, <https://doi.org/10.1007/s11242-017-0954-5>.

[16] M. Hidayat, M. Sarmadivaleh, J. Derksen, D. Vega-Maza, S. Iglauer, J. Vinogradov, Zeta potential of CO₂-rich aqueous solutions in contact with intact sandstone sample at temperatures of 23 °C and 40 °C and pressures up to 10.0 MPa, *Journal of Colloid and Interface Science* 607 (2022) 1226-1238, <https://doi.org/10.1016/j.jcis.2021.09.076>.

[17] P.W.J. Glover, *Geophysical Properties of the Near Surface Earth: Electrical Properties*, (2015) 89-137, <https://doi.org/10.1016/b978-0-444-53802-4.00189-5>.

- 1
2
3
4 598 [18] D.A. Sverjensky, Interpretation and prediction of triple-layer model capacitances and the
5
6 599 structure of the oxide-electrolyte-water interface, *Geochimica Et Cosmochimica Acta* 65(21)
7
8 600 (2001) 3643-3655, [https://doi.org/10.1016/S0016-7037\(01\)00709-8](https://doi.org/10.1016/S0016-7037(01)00709-8).
9
- 10 601 [19] Z. Brkljača, D. Namjesnik, J. Lützenkirchen, M. Předota, T. Preočanin, Quartz/Aqueous
11
12 602 Electrolyte Solution Interface: Molecular Dynamic Simulation and Interfacial Potential
13
14 603 Measurements, *The Journal of Physical Chemistry C* 122(42) (2018) 24025-24036,
15
16 604 <https://doi.org/10.1021/acs.jpcc.8b04035>.
17
- 18 605 [20] T. Hiemstra, J.C.M. De Wit, W.H. Van Riemsdijk, Multisite proton adsorption modelling at
19
20 606 the solid/solution interface of (hydr)oxides: a new approach. II. Application to various important
21
22 607 (hydr)oxides, *Journal of Colloid and Interface Science* 133 (1989) 105-117,
23
24 608 [https://doi.org/10.1016/0021-9797\(89\)90285-3](https://doi.org/10.1016/0021-9797(89)90285-3).
25
- 26 609 [21] P. Leroy, N. Devau, A. Revil, M. Bizi, Influence of surface conductivity on the apparent zeta
27
28 610 potential of amorphous silica nanoparticles, *Journal of Colloid and Interface Science* 410 (2013)
29
30 611 81-93, <https://doi.org/10.1016/j.jcis.2013.08.012>.
31
- 32 612 [22] C. Macias-Romero, I. Nahalka, H.I. Okur, S. Roke, Optical imaging of surface chemistry and
33
34 613 dynamics in confinement, *Science* 357(6353) (2017) 784-788,
35
36 614 <https://doi.org/10.1126/science.aal4346>.
37
- 38 615 [23] A. Kitamura, K. Fujiwara, T. Yamamoto, S. Nishikawa, H. Moriyama, Analysis of adsorption
39
40 616 behavior of cations onto quartz surface by electrical double-layer model, *J Nucl Sci Technol*
41
42 617 36(12) (1999) 1167-1175, <https://doi.org/10.1080/18811248.1999.9726312>.
43
- 44 618 [24] P. Leroy, C. Tournassat, O. Bernard, N. Devau, M. Azaroual, The electrophoretic mobility of
45
46 619 montmorillonite. Zeta potential and surface conductivity effects, *Journal of Colloid and*
47
48 620 *Interface Science* 451 (2015) 21-39, <https://doi.org/10.1016/j.jcis.2015.03.047>.
49
- 50 621 [25] R.J. Hunter, *Zeta Potential in Colloid Science: Principles and Applications*, Academic Press,
51
52 622 New York, 1981.
53
- 54 623 [26] J. Lyklema, M. Minor, On surface conduction and its role in electrokinetics, *Colloids and*
55
56 624 *Surfaces a-Physicochemical and Engineering Aspects* 140(1-3) (1998) 33-41,
57
58 625 [https://doi.org/10.1016/S0927-7757\(97\)00266-5](https://doi.org/10.1016/S0927-7757(97)00266-5).
59
60
61
62
63
64
65

- 1
2
3
4 626 [27] A. Revil, P.A. Pezard, P.W.J. Glover, Streaming potential in porous media 1. Theory of the
5
6 627 zeta potential, *J Geophys Res-Sol Ea* 104(B9) (1999) 20021-20031,
7
8 628 <https://doi.org/10.1029/1999jb900089>.
9
10 629 [28] A. Revil, D. Hermitte, E. Spangenberg, J.J. Cochame, Electrical properties of zeolitized
11
12 630 volcanoclastic materials, *J Geophys Res-Sol Ea* 107(B8) (2002),
13
14 631 <https://doi.org/10.1029/2001jb000599>.
15
16 632 [29] A. Crespy, A. Boleve, A. Revil, Influence of the Dukhin and Reynolds numbers on the
17
18 633 apparent zeta potential of granular porous media, *Journal of Colloid and Interface Science* (2007)
19
20 634 188-194, <https://doi.org/10.1016/j.jcis.2006.09.038>.
21
22 635 [30] S. Li, P. Leroy, F. Heberling, N. Devau, D. Jougnot, C. Chiaberge, Influence of surface
23
24 636 conductivity on the apparent zeta potential of calcite, *J. Colloid Interface Sci.* 468 (2016) 262-
25
26 637 75, <https://doi.org/10.1016/j.jcis.2016.01.075>.
27
28 638 [31] P. Leroy, A. Revil, A triple-layer model of the surface electrochemical properties of clay
29
30 639 minerals, *Journal of Colloid and Interface Science* (2004) 371-380,
31
32 640 <https://doi.org/10.1016/j.jcis.2003.08.007>.
33
34 641 [32] I.C. Bourg, G. Sposito, Molecular dynamics simulations of the electrical double layer on
35
36 642 smectite surfaces contacting concentrated mixed electrolyte (NaCl-CaCl₂) solutions, *Journal of*
37
38 643 *Colloid and Interface Science* 360(2) (2011) 701-715, <https://doi.org/10.1016/j.jcis.2011.04.063>.
39
40 644 [33] H. Zhang, A.A. Hassanali, Y.K. Shin, C. Knight, S.J. Singer, The water-amorphous silica
41
42 645 interface: Analysis of the Stern layer and surface conduction, *J Chem Phys* 134(2) (2011),
43
44 646 <https://doi.org/10.1063/1.3510536>.
45
46 647 [34] D. Biriukov, P. Fibich, M. Předota, Zeta Potential Determination from Molecular Simulations,
47
48 648 *The Journal of Physical Chemistry C* 124(5) (2020) 3159-3170,
49
50 649 <https://doi.org/10.1021/acs.jpcc.9b11371>.
51
52 650 [35] M. Předota, M.L. Machesky, D.J. Wesolowski, Molecular Origins of the Zeta Potential,
53
54 651 *Langmuir* 32(40) (2016) 10189-10198, <https://doi.org/10.1021/acs.langmuir.6b02493>.
55
56 652 [36] P. Leroy, A. Maineult, Exploring the electrical potential inside cylinders beyond the Debye-
57
58 653 Hückel approximation: a computer code to solve the Poisson-Boltzmann equation for
59
60 654 multivalent electrolytes, *Geophys J Int* 214(1) (2018) 58-69, <https://doi.org/10.1093/gji/ggy124>.
61
62
63
64
65

- 1
2
3
4 655 [37] J. Westall, H. Hohl, A comparison of electrostatic models for the oxide/solution interface,
5
6 656 Advances in Colloid and Interface Science 12(4) (1980) 265-294, <https://doi.org/10.1016/0001->
7
8 657 8686(80)80012-1.
9
- 10 658 [38] M. Heuser, G. Spagnoli, P. Leroy, N. Klitzsch, H. Stanjek, Electro-osmotic flow in clays and
11
12 659 its potential for reducing clogging in mechanical tunnel driving, *B Eng Geol Environ* 71(4)
13
14 660 (2012) 721-733, <https://doi.org/10.1007/s10064-012-0431-x>.
15
- 16 661 [39] J. Lyklema, S. Rovillard, J. De Coninck, Electrokinetics: The properties of the stagnant layer
17
18 662 unraveled, *Langmuir* 14(20) (1998) 5659-5663, <https://doi.org/10.1021/la980399t>.
19
- 20 663 [40] M.A. Brown, A. Goel, Z. Abbas, Effect of Electrolyte Concentration on the Stern Layer
21
22 664 Thickness at a Charged Interface, *Angewandte Chemie International Edition* 55(11) (2016)
23
24 665 3790-3794, <https://doi.org/10.1002/anie.201512025>.
25
- 26 666 [41] D. Lis, E.H.G. Backus, J. Hunger, S.H. Parekh, M. Bonn, Liquid flow along a solid surface
27
28 667 reversibly alters interfacial chemistry, *Science* 344(6188) (2014) 1138-1142,
29
30 668 <https://doi.org/10.1126/science.1253793>.
31
- 32 669 [42] R. Saini, A. Garg, D.P. Barz, Streaming potential revisited: the influence of convection on the
33
34 670 surface conductivity, *Langmuir* 30(36) (2014) 10950-61, <https://doi.org/10.1021/la501426c>.
35
- 36 671 [43] B.L. Werkhoven, J.C. Everts, S. Samin, R. van Roij, Flow-Induced Surface Charge
37
38 672 Heterogeneity in Electrokinetics due to Stern-Layer Conductance Coupled to Reaction Kinetics,
39
40 673 *Physical Review Letters* 120(26) (2018), <https://doi.org/10.1103/PhysRevLett.120.264502>.
41
- 42 674 [44] E. Walker, P.W.J. Glover, J. Ruel, A transient method for measuring the DC streaming
43
44 675 potential coefficient of porous and fractured rocks, *Journal of Geophysical Research: Solid*
45
46 676 *Earth* 119(2) (2014) 957-970, <https://doi.org/10.1002/2013jb010579>.
47
- 48 677 [45] P.W.J. Glover, Modelling pH-Dependent and Microstructure-Dependent Streaming Potential
49
50 678 Coefficient and Zeta Potential of Porous Sandstones, *Transport Porous Med* 124(1) (2018) 31-
51
52 679 56, <https://doi.org/10.1007/s11242-018-1036-z>.
53
- 54 680 [46] D.E. Yates, S. Levine, T.W. Healy, Site-binding Model of the Electrical Double Layer at the
55
56 681 Oxide/Water interface, *Journal of the Chemical Society, Faraday Transactions* 70 (1974) 1807-
57
58 682 1818, <https://doi.org/10.1039/F19747001807>.
59
60
61
62
63
64
65

1
2
3
4
5
6
7
8
9
10
11
12
13
14
15
16
17
18
19
20
21
22
23
24
25
26
27
28
29
30
31
32
33
34
35
36
37
38
39
40
41
42
43
44
45
46
47
48
49
50
51
52
53
54
55
56
57
58
59
60
61
62
63
64
65

[47] I. Siretanu, D. Ebeling, M.P. Andersson, S.L.S. Stipp, A. Philipse, M.C. Stuart, D. van den Ende, F. Mugele, Direct observation of ionic structure at solid-liquid interfaces: a deep look into the Stern Layer, *Scientific reports* 4(1) (2014), <https://doi.org/10.1038/srep04956>.

[48] S.R. Charlton, D.L. Parkhurst, Modules based on the geochemical model PHREEQC for use in scripting and programming languages, *Comput Geosci-Uk* 37(10) (2011) 1653-1663, <https://doi.org/10.1016/j.cageo.2011.02.005>.

[49] A. Mainault, Estimation of the electrical potential distribution along metallic casing from surface self-potential profile, *J Appl Geophys* 129 (2016) 66-78, <https://doi.org/10.1016/j.jappgeo.2016.03.038>.

[50] A. Alizadeh, M. Wang, Flexibility of inactive electrokinetic layer at charged solid-liquid interface in response to bulk ion concentration, *Journal of Colloid and Interface Science* 534 (2019) 195-204, <https://doi.org/10.1016/j.jcis.2018.09.010>.

[51] P. Leroy, C. Tournassat, M. Bizi, Influence of surface conductivity on the apparent zeta potential of TiO₂ nanoparticles, *Journal of Colloid and Interface Science* 356(2) (2011) 442-453, <https://doi.org/10.1016/j.jcis.2011.01.016>.

[52] P. Leroy, D. Jougnot, A. Revil, A. Lassin, M. Azaroual, A double layer model of the gas bubble/water interface, *Journal of Colloid and Interface Science* 388 (2012) 243-256, <https://doi.org/10.1016/j.jcis.2012.07.029>.

[53] A. Mendieta, D. Jougnot, P. Leroy, A. Mainault, Spectral Induced Polarization Characterization of Non- Consolidated Clays for Varying Salinities—An Experimental Study, *Journal of Geophysical Research: Solid Earth* 126(4) (2021), <https://doi.org/10.1029/2020JB021125>.

[54] B. Lowden, S. Braley, A. Hurst, J. Lewis, Sedimentological studies of the Cretaceous Lochaline Sandstone, NW Scotland, Geological Society, London, Special Publications 62(1) (1992) 159-162, <https://doi.org/10.1144/gsl.sp.1992.062.01.14>.

[55] P.L. Churcher, P.R. French, J.C. Shaw, L.L. Schramm, Rock Properties of Berea Sandstone, Baker Dolomite, and Indiana Limestone, *Society of Petroleum Engineers Journal* 21044 (1991) 20-22, <https://doi.org/10.2118/21044-MS>.

1
2
3
4
5
6
7
8
9
10
11
12
13
14
15
16
17
18
19
20
21
22
23
24
25
26
27
28
29
30
31
32
33
34
35
36
37
38
39
40
41
42
43
44
45
46
47
48
49
50
51
52
53
54
55
56
57
58
59
60
61
62
63
64
65

[56] T.-f. Wong, C. David, W. Zhu, The transition from brittle faulting to cataclastic flow in porous sandstones: Mechanical deformation, *Journal of Geophysical Research: Solid Earth* 102(B2) (1997) 3009-3025, <https://doi.org/10.1029/96jb03281>.

[57] S. Li, H. Collini, M.D. Jackson, Anomalous Zeta Potential Trends in Natural Sandstones, *Geophysical Research Letters* 45(20) (2018), <https://doi.org/10.1029/2018GL079602>.

[58] M. Alarouj, H. Collini, M.D. Jackson, Positive Zeta Potential in Sandstones Saturated With Natural Saline Brine, *Geophysical Research Letters* 48(20) (2021), <https://doi.org/10.1029/2021GL094306>.

[59] A. Alroudhan, J. Vinogradov, M.D. Jackson, Zeta potential of intact natural limestone: Impact of potential-determining ions Ca, Mg and SO₄, *Colloids and Surfaces A: Physicochemical and Engineering Aspects* 493 (2016) 83-98, <https://doi.org/10.1016/j.colsurfa.2015.11.068>.

[60] C. Schnitzer, S. Ripperger, Influence of Surface Roughness on Streaming Potential Method, *Chem Eng Technol* 31(11) (2008) 1696-1700, <https://doi.org/10.1002/ceat.200800180>.

[61] A. Drechsler, A. Caspari, A. Synytska, Influence of roughness and capillary size on the zeta potential values obtained by streaming potential measurements, *Surf Interface Anal* 52(12) (2020) 991-995, <https://doi.org/10.1002/sia.6792>.

[62] J. Sonnefeld, A. Gobel, W. Vogelsberger, Surface-Charge Density on Spherical Silica Particles in Aqueous Alkali Chloride Solutions .1. Experimental Results, *Colloid Polym Sci* 273(10) (1995) 926-931, <https://doi.org/10.1007/Bf00660369>.

[63] A.C. Riese, Adsorption of radium and thorium onto quartz and kaolinite: A comparison of solution/surface equilibrium models, *Colorado School of Mines*, 1982.

[64] P. Leroy, A. Lassin, M. Azaroual, L. Andre, Predicting the surface tension of aqueous 1:1 electrolyte solutions at high salinity, *Geochimica Et Cosmochimica Acta* 74(19) (2010) 5427-5442, <https://doi.org/10.1016/j.gca.2010.06.012>.

[65] F.A. Saadi, K.-H. Wolf, C.v. Kruijsdijk, Characterization of Fontainebleau Sandstone: Quartz Overgrowth and its Impact on Pore-Throat Framework, *Journal of Petroleum & Environmental Biotechnology* 08(03) (2017), <https://doi.org/10.4172/2157-7463.1000328>.

1
2
3
4
5
6
7
8
9
10
11
12
13
14
15
16
17
18
19
20
21
22
23
24
25
26
27
28
29
30
31
32
33
34
35
36
37
38
39
40
41
42
43
44
45
46
47
48
49
50
51
52
53
54
55
56
57
58
59
60
61
62
63
64
65

738 [66] M.A. Brown, Z. Abbas, A. Kleibert, R.G. Green, A. Goel, S. May, T.M. Squires,
739 Determination of Surface Potential and Electrical Double-Layer Structure at the Aqueous
740 Electrolyte-Nanoparticle Interface, *Physical Review X* 6(1) (2016),
741 <https://doi.org/10.1103/PhysRevX.6.011007>.

742 [67] C.E. Harvie, J.H. Weare, The prediction of mineral solubilities in natural waters: the Na-K-
743 Mg-Ca-Cl-SO₄-H₂O system from zero to high concentration at 25 °C, *Geochimica Et*
744 *Cosmochimica Acta* 44(7) (1980) 981-997, [https://doi.org/10.1016/0016-7037\(80\)90287-2](https://doi.org/10.1016/0016-7037(80)90287-2).

745 [68] K.S. Pitzer, G. Mayorga, Thermodynamics of electrolytes. II. Activity and osmotic
746 coefficients for strong electrolytes with one or both ions univalent, *The Journal of Physical*
747 *Chemistry* 77(19) (1973) 2300–2308, <https://doi.org/10.1021/j100621a026>.